THE EFFECTS OF AGING AND REMODELING ON BONE QUALITY AND MICRODAMAGE

A Dissertation
Presented to
the Academic Faculty

By

Jessica Marie O'Neal

In Partial Fulfillment
Of the Requirements for the Degree
Doctor of Philosophy in Bioengineering

Georgia Institute of Technology

August, 2011

THE EFFECTS OF AGING AND REMODELING ON BONE QUALITY AND MICRODAMAGE

Approved by:

Dr. Robert Guldberg, Advisor
School of Mechanical Engineering
Georgia Institute of Technology

Dr. Rick Neu
School of Mechanical Engineering
Georgia Institute of Technology

Dr. David Burr
School of Medicine
Indiana University

Dr. Brani Vidakovic
School of Biomedical Engineering
Georgia Institute of Technology

Dr. Ken Gall
School of Mechanical Engineering
Georgia Institute of Technology

Date Approved: May 20, 2011

To Mark.
People often say they couldn't have achieved their goals without the support of their spouse – in this case, it's especially true.

ACKNOWLEDGEMENTS

First and foremost, I have to thank my advisor, Dr. Robert Guldberg, for his guidance throughout my PhD. Thanks Bob, for being open-minded about my ideas, for supporting my direction for this thesis work, and for helping me to develop my independence as a researcher. I'm not sure I would have attained this degree without your flexibility and understanding.

Thank you so much to my committee, Dr. Brani Vidakovic, Dr. David Burr, Dr. Rick Neu, and Dr. Ken Gall. You have all been very supportive and helpful through this process. This thesis work would not be nearly as successful as it has been without your expertise.

Thank you, Tamim and Jason, microdamage group/"Team Awesome." I really can't thank you enough for your help these past 4 years. Tamim, your guidance and suggestions have improved this work tremendously, and it was really good to have someone with your knowledge that I could go to for answers and perspective. Jason, thank you so much for all of your help in developing these protocols/programming/ideas and tolerating all of my complaining/swearing about the microscope work – you are truly a self-less guy. I was very lucky to have you as a desk neighbor, and I'm forever indebted to you for bringing your bhangra dance team to perform at my wedding. You really have the "Indian head shake" down pat!

Thank you, Srin. You taught me from the beginning, and it has been great working with you on this project.

Thank you, Angela, Aqua, and Hazel. Angela, I am so grateful to you for all your help. You are the ultimate problem fixer! I would have been stuck on the very first day without you. Aqua, you really made spending hours/days/weeks in the histology lab tolerable. Thank you for all of your help and patience. I'll miss you. Hazel, I will really miss your excellent sense of humor. Even though the crazy research plans we proposed never materialized, it has always been a lot of fun working with you. I'll leave you to tend to all the microscope problems now. ;)

Thanks Yazdan for all of your help. You are a smart, independent worker, and I know you'll make a great doctor.

Vivian, thank you for dealing with everything that I hate dealing with. It was always fun shooting the breeze with you – I'll miss you.

Joel, Chris, and Brent – not only are you all knowledgeable, you are also fun to be around. You helped make the lab a fun place to work, and I know you all will do well. Ashley, you were an excellent addition to row 3 – thanks for slowing (*way)* down so that I could run with you, and for commiserating with me on the long microscope days. Nick, Alice, Tanu, and Lauren, it was a pleasure working alongside you – you are all intelligent and hard-working, and I know you'll do great.

Thank you, Garcia lab, for really livening up the atmosphere. Ed, you were the best desk neighbor I could have asked for. You're one of the smartest guys I know, and I'm sure you'll do well. Stacie, Rachel, and Chi-Chi, your baked goods were always delicious – thank you for sharing with us! Thank you to everyone else in the lair – it made a big difference in my morale to work with such laid-back, fun-loving people.

Laura and Andrea, thank you guys for all of your help with classes and quals prep. It wasn't much fun, but it was much easier to get through with you guys.

Thanks to all of the IBB staff: Allen, Steve, Floyd, Alyceson, and Chris: all of you are exceptionally friendly and helpful, and it really brightened my day to see you all around the building. Thanks John Graham for your patience and help.

Thank you, Dr. Ed Inscho and Laura Hutcheson. I am very lucky to be in a program with such supportive people. Thanks to everyone at GSHC – you all helped me keep things in perspective, and it was a pleasure learning from you and working with you.

Parul, you've been such an amazing motivator and friend. Thanks for your constant encouragement.

Jack and Paula, Matt and Petra, Grandma and Grandpa Randhan, thank you for being so supportive these past 4 years. I love you all.

Mom, Dad, Christina, Erica, Grandma, and Grandad – you have always been there for me, through good times and bad. I am so, so lucky to have a family like you. Without your strength and support, I could never have achieved so much. I love you all very much.

Finally, to Mark. There aren't enough words to tell you what your support and sacrifice has meant to me. There are very few people that possess the strength, patience, and trust that you have. I thank God everyday for you, and I am so lucky to have you. I love you so much, and I always will.

TABLE OF CONTENTS

LIST OF TABLES

LIST OF FIGURES

LIST OF ABBREVIATIONS

AGEs: Advanced Glycation End-Products

ALN: Alendronate

BMU: Bone Multicellular Unit

BV/TV: Bone Volume/Tissue Volume; Bone Volume Fraction

CI: Confidence Interval

Micro-CT: Micro-Computed Tomography

OPG: Osteoprotegerin

RANK: Receptor for Activator of Nuclear Factor-κβ

RANKL: Receptor for Activator of Nuclear factor-κβ ligand

SERM: Selective Estrogen Receptor Moduluator

SMI: Structural Model Index

SUMMARY

One indication of increasing fragility of bone is the accumulation of microscopic cracks, or microdamage, within the bone matrix. Microdamage accumulates in bone of the elderly, when changes in bone material properties and matrix architecture coupled with a decrease in bone repair mechanisms compromise bone integrity. Although men experience loss of bone mass with age, osteopenic changes in women occur at an earlier age and accelerate when estrogen's bone-protective effects diminish after menopause. Consequently, 3 out of 4 fragility fractures occur in women. To preserve bone mass and reduce fracture risk, therapeutics which alter the morphology of bone are prescribed to at-risk patients. The most commonly prescribed drug to prevent osteoporotic bone fracture is alendronate, a bisphosphonate which increases bone volume fraction by decreasing the rate of bone turnover. However, concerns over adverse effects of prolonged turnover suppression have been reinforced by findings of increased microdamage density with alendronate use.

Microdamage formation is not always pathologic, but extensive accumulation of damage can be an indicator of reduced bone quality. The work in this thesis explores the hypothesis that microdamage in bone of lower quality will form more easily and progress more extensively than in bone of higher quality. The effects of aging, sex, and alendronate treatment on microdamage initiation of linear, diffuse, and severe morphologies were investigated in trabecular bone. With the use of micro-computed tomography at high resolution, estimations of the stress/strain environment of individual trabeculae within the trabecular lattice were obtained with finite element modeling.

Calcium-chelating fluorophores were used to fluorescently label damage in bone, and stress and strain values of trabeculae were linked to observed damage morphologies resulting from mechanical loading. Across all studies, microdamage morphology was highly associated with the stress/strain magnitude on damaged trabeculae. Furthermore, thinner, rod-like trabeculae oriented along the loading axis were most likely to develop severe damage in all studies.

Microdamage initiation stresses and strains were obtained for trabecular bone from older females, older males, and younger females to determine whether thresholds for damage initiation were lower in older females. Results suggest that the stress threshold for damage initiation in older females may indeed be lower compared with younger females, and that normalized strain thresholds for severe damage formation in older males may be decreased compared with older females. Damage propagation was evaluated as a function of age and sex to determine whether damage in older women progressed more extensively than in younger women or men. Results suggest that bone from older individuals had decreased resistance to crack propagation evidenced by an increased number of severely damaged trabeculae which extended in area under cyclic loading; however no sex differences were uncovered. Finally, the stress/strain thresholds for damage initiation were investigated in alendronate-treated bone, and results indicate that a decreased stress threshold was needed to initiate damage formation of a linear and severe morphology after one year of treatment. After three years of treatment, however, micromechanical properties recovered, perhaps due to increased matrix mineralization which increased tissue level stiffness.

CHAPTER 1

INTRODUCTION

1.1 Motivation

Decreased bone mass in aging individuals is a well-established risk factor for osteoporotic fracture. However, loss of bone mass alone cannot account for increased age-related fracture risk, for at a given bone mass, fracture risk is still significantly greater in older individuals than younger individuals. (Hui et al. 1988) It has been proposed that factors related to bone quality are as important as bone density in predicting the risk of fractures. (McCreadie et al. 2000) Bone quality is an imprecise term used to refer to factors other than bone mineral density that influence bone's biomechanical properties. These factors include alterations in extracellular matrix heterogeneity and composition (e.g. collagen and noncollagenous proteins, mineral, and water content), microarchitecture (e.g. trabecular thickness, degree of anisotropy, and structure model index), and remodeling rate. (Hildebrand et al. 1999; Paschalis et al. 2004; Recker et al. 2004; Busse et al. 2009) Accumulation and propagation of microdamage within the bone matrix can also be an indication of increasing fragility, as extensive damage is associated with loss of stiffness and strength. (Schaffler et al. 1989; Burr et al. 1997; Yeh et al. 2001)

Many studies have reported significant increases in microdamage density with age. (Mori et al. 1993; Schaffler et al. 1995; Mori et al. 1997; Norman et al. 1998; Fazzalari et al. 2002; Seeman 2003) While age-related changes in bone structure and composition play a substantial role in promoting microdamage formation, there is also a

breakdown in the microdamage-remodeling feedback loop in aging: the targeted removal and repair of damaged regions is reduced even as the rate of stochastic bone remodeling is increased. (Allen 2008) This results in a structure with decreased bone mass and an increased number of damaged regions. When loss of bone mass reaches a critical level, osteoporosis is diagnosed.

Many therapies are used currently to combat the loss of bone mass, and they can be divided into two broad categories based on whether they stimulate bone formation (teriparatide) or whether they reduce bone resorption (bisphosphonates, selective estrogen receptor modulators, denosumab, strontium ranelate). (Reginster 2011) Of these, bisphosphonates are most commonly prescribed for osteoporosis prevention and treatment. Bisphosphonates' specific action is on osteoclasts, where they inhibit osteoclast recruitment and adhesion, shorten the lifespan of osteoclasts, and inhibit osteoclastic bone resorption. (Fleisch 1998) Their efficacy in fracture prevention has been demonstrated, particularly in sites with large amounts of trabecular bone like the wrist, hip, and vertebrae. (Black et al. 1996; Black et al. 2000) However, concerns about long-term consequences of bone turnover suppression have been corroborated by reports of increased microdamage density with treatment. (Allen et al. 2006; Stepan et al. 2007) Additionally, clinically apparent atypical femoral fractures have been associated with bisphosphonate use, for which microdamage accumulation may play a role. (Shane et al. 2010)

Despite the association of microdamage with adverse biomechanical effects, damage formation is not always pathologic. Studies have shown that crack growth in bone is stable due to the formation of a plastic zone at the crack tip. (Vashishth et al.

1997) This mechanism increases the toughness of bone by allowing for the absorption and dissipation of energy that may otherwise, in more brittle materials, lead to crack extension. (Norman et al. 1995; Vashishth et al. 1997; Zioupos 2001) However it is clear that, if left unrepaired, microdamage accumulation imposes significant adverse effects on the mechanical properties of bone. (Schaffler et al. 1995; Hoshaw et al. 1997; Zioupos 2001; Wang et al. 2004) Moreover, in another study, appreciable damage accumulation was not apparent until bone had lost 15% of its elastic modulus, suggesting that damage accumulation can be an indicator of reduced mechanical properties. (Burr et al. 1998) In order to assess the significance of microdamage in skeletal fragility and traumatic fractures, its mechanisms must be elucidated on a tissue-level scale where the interactions of bone matrix properties, the local biomechanical environment, and trabecular architecture are concurrently examined for their contributions to microdamage formation.

The goal of this work was to demonstrate that changes in bone quality due to aging, sex, and bisphosphonate treatment are reflected in differences in the mechanics of microdamage initiation and propagation in trabecular bone. The *central hypothesis* of this thesis is that microdamage in bone of lower quality will form at decreased stress/strain levels and progress more extensively than in bone of higher quality.

1.2 Specific Aims

This hypothesis is tested in three specific aims:

I. Evaluate Factors Promoting Microdamage Initiation of Different Morphological Types in Human Trabecular Bone as a Function of Age and Gender

Fragility fracture rates are at their highest levels in older women when the bone-protective effects of estrogen diminish after menopause. Estrogen protects bone mass by

inhibiting osteoclastic bone resorption. (Kameda et al. 1997) As the concentration of estrogen falls after menopause, the number of remodeling sites and extent of bone resorption in basic multicellular units increases. (Seeman 2003) This results in fewer and thinner trabeculae, which reduces the strength and stiffness of the structure. Work conducted in this aim investigates whether these changes in trabecular bone lead to a decreased stress/strain threshold for microdamage initiation. The *hypothesis* is that the stress threshold for microdamage initiation will be lower in trabecular bone from older females compared to younger females and older males.

II. Determine the Factors Promoting Microdamage Propagation in Human Trabecular Bone as a Function of Age and Gender

Microdamage density has been shown to increase with age in trabecular bone and is associated with decreased fracture toughness. (Schaffler et al. 1995; Zioupos 2001) Repetitive loading on microdamaged structures can further advance the extent of damage, decreasing stiffness and increasing the risk of overt fracture. (Diab et al. 2005) Extensive studies of crack propagation in cortical bone have been conducted, (Schaffler et al. 1995; Vashishth et al. 1997; Norman et al. 1998; Vashishth et al. 2000; Zioupos 2001; Zioupos 2001) but data in trabecular bone is lacking. (Seeman 2003; Cook et al. 2009) The goal of this aim is to determine whether age and gender-related changes in bone quality lead to increased microdamage propagation in older females. The *hypothesis* is that microdamage propagation in trabecular bone due to increasing age and female gender will show decreased resistance to microdamage propagation than in younger subjects and men.

III. Determine the Effects of Alendronate Administration on Microdamage

Initiation in Canine Trabecular Bone as a Function of Damage Severity, Bisphosphonate Dose, and Treatment Duration

Alendronate is a commonly prescribed therapeutic used to prevent fracture in areas of the skeleton with a large proportion of trabecular bone by reducing bone remodeling, thereby increasing bone mass. Its clinical efficacy in fracture prevention has been well documented. (Black et al. 1996; Black et al. 2000) However, concerns over adverse effects of prolonged turnover suppression have been reinforced by findings of increased microdamage density with alendronate use. (Allen et al. 2006; Stepan et al. 2007) In this aim, the effect of alendronate administration on microdamage initiation is investigated in an animal model after 1 and 3 years of treatment at two clinically relevant doses corresponding to an osteoporotic treatment dose and a Paget's disease treatment dose. The *hypothesis* is that changes in bone quality will be demonstrated by a decreased stress/strain associated with microdamage initiation after one year of treatment, but that further alterations in bone quality will not be observed with increased treatment duration and dose.

1.3 Significance

Fragility fractures are a significant public health concern: in the US, it is estimated that 40% of white women and 13% of white men over 50 will experience a clinically apparent fragility fracture. (Cummings 2002) Fractures also cause significant morbidity associated with chronic pain, reduced mobility, disability, and an increased degree of dependence on others. (Keene et al. 1993) The risk of death related to hip fracture is 2.8%, equivalent to the risk of death from breast cancer in women. (Cummings 1989) These statistics illustrate the great need for research into the mechanisms of bone

fragility fracture.

The work presented in this thesis is *significant* because it investigates the impact of age, sex, and alendronate use on the mechanics of microdamage formation and progression in trabecular bone, three factors which are of particular relevance due to positive associations between damage accumulation and fracture. Since microdamage accumulation has an important effect on bone structural properties like stiffness, strength, and toughness (Schaffler et al. 1995; Hoshaw et al. 1997; Zioupos 2001), an investigation into the factors affecting microdamage initiation and propagation are important in determining the role damage accumulation plays in skeletal fragility and fracture.

The methods detailed in the following chapters are *innovative* in their integration of histology, high resolution micro-computed tomography, and image-based finite element modeling. Furthermore, the *novelty* of solving for trabecular stresses and strains associated with different damage morphologies contributes greatly to the current understanding of factors influencing microdamage formation. Finally, by advancing knowledge in the field by building upon the work of others, results will complement current and future studies on the mechanisms of microdamage formation and progression.

CHAPTER 2

BACKGROUND AND LITERATURE REVIEW

2.1 Bone Function and Structural Hierarchy

2.1.1 Bone Structure at the Apparent Level

Bones can vary widely in form: long bones (ex. femur, humerus) are cylindrical, while short and sesamoid bones (ex. carpels of the hand, patella) are more cuboid. Flat bones (ex. skull, sternum) are flat, while irregular bones don't fit into any of these categories and vary widely in shape (ex. vertebrae, sacrum). Each of these types also varies in their tissue organization depending on their function. Spongy tissue called trabecular (or cancellous) bone is found in the ends of long bones and within flat and irregular bones where material deformation allows for elastic energy dissipation. Dense cortical (or compact) bone is found throughout the skeleton, imparting strength and protection to internal organs.

2.1.2 Bone Structure at the Microstructural Level

The most striking difference between cortical and trabecular bone is in porosity – cortical bone is dense with porosity less than 5%, whereas trabecular bone is much less so, often described as a honeycomb-like structure composed of trabecular struts in the shape of plates or rods with porosity ranging between 50-90% (Figure 2.1*)*. Overall, 80% of bony tissue in the adult human body is cortical and the remaining 20% is trabecular. (Clarke 2008) Cortical and cancellous bone can be further divided into woven and lamellar bone. Woven bone is immature bone formed during growth or healing of bone structures. It is replaced by mature lamellar bone which is more organized and

mineralized than woven bone.

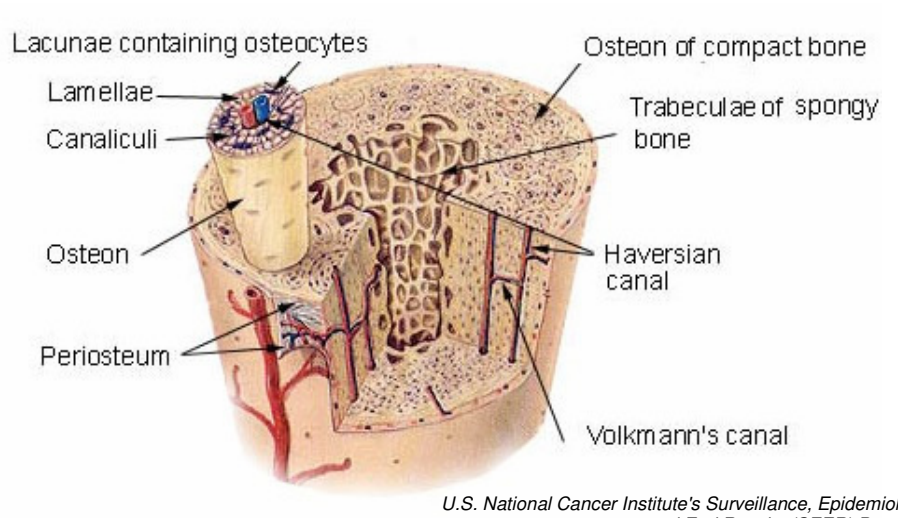

U.S. National Cancer Institute's Surveillance, Epidemiology and End Results (SEER) Program

Figure 2.1. Structural Organization of Bone. Cortical bone is shown to envelope trabecular bone, a common distribution found in long bones and vertebral bodies.

The functional unit of cortical bone is the osteon, also called a Haversian system. The osteon is a cylindrical structure roughly 100 to 300 μm in diameter, the long axis of which is aligned parallel with the major axis of stress. It is created from thin sheets of lamellae which run concentrically around a central cavity (the Haversian canal) where blood vessels and nerves are housed. Cement lines are formed at the periphery of each osteon, and interstitial bone is created from lamellar fragments between intact osteons. Osteons are connected through Volkmann's canals containing blood vessels which run transversely between different Haversian systems.

The functional unit of trabecular bone is known as the hemiosteon, or trabecular packet (approximately 50 μm in thickness), which is organized similarly to the osteon but does not contain vascular channels. Lamellae in the hemiosteon are arranged longitudinally along the trabeculae, rather than concentrically as observed in compact

bone osteons. As in cortical bone, interstitial bone is created from disorganized lamellae between hemiosteons. Lacunae, small cavities housing trapped bone cells called osteocytes, are found in both cortical and trabecular bone.

2.1.3 Bone Structure at the Ultrastructural Level

At the nanoscale, cortical and trabecular bone are identical. Bone is a complex material, comprised of both organic matrix and crystalline salts. The organic matrix of bone is 90 to 95% collagen fibrils which extend along the lines of tensional force, providing much of bone's tensile strength. The remaining organic material is what is termed "ground substance," which includes chondroitin sulfate and hyaluronic acid. These compounds are thought to aid in the deposition of calcium salts. The major crystalline salt found in bone is hydroxyapatite, formed from calcium and phosphate. This material gives bone great compression strength. The organic matrix and crystalline mineral interact intimately; collagen fibrils lie adjacent to hydroxyapatite crystals and bind tightly to it. This prevents shearing due to crystals and collagen slipping out of place. Additionally, adjacent collagen fibrils overlap one another, creating overlapping hydroxyapatite crystals which increase the stability of the structure. Thus, bone material is able to demonstrate great tensile as well as compressive strength (Guyton & Hall, 2006).

2.1.4 Bone Function

Bone serves as the structural foundation of the human body, allowing for muscle attachment, organ and nerve protection, and storage of key physiological ions such as calcium and phosphate. Additionally, bones harbor bone marrow containing vital components of the hematopoietic system like platelets and red and white blood cells.

Bone's material composition accounts for much of its base strength; however, differences in organization between cortical and trabecular bone at the micro-scale result in vastly different mechanical properties. Bone strength is highly dependent on porosity. Its strength, however, is limited by its functional requirements as well. Bone must be dense enough to withstand normal forces, but not so dense as to impede movement or add weight beyond which can be supported by muscle. Bone must also provide rigidity when stressed but act as shock absorbers to withstand repetitive forces. This dual requirement is matched physiologically: the low porosity of cortical bone provides strength in long bone diaphyses, while porous, interconnected trabecular bone accommodates energy absorption in metaphyseal regions and vertebral bodies. Trabeculae are aligned according to stress patterns, but are reinforced by transversely oriented trabeculae to withstand minor assaults in other planes. Thus trabeculae are highly interconnected. Finally, a precise combination of organic and inorganic material provides bone's baseline material strength; imbalance of these components can result in brittle, stiff bones as seen in osteoporosis, or flexible, weak bones seen in osteomalacia. (Turner 2002) The balance achieved between structure and function provides bone with extraordinary capacity to balance sometimes contradictory requirements.

2.2 Cellular Components of Bone

Bone has the important ability to tailor its structure to the loading environment and repair small cracks or fractures. This ability is garnered from cells which live in and around bone tissue. There are three main types of bone cells: osteocytes, osteoclasts, and osteoblasts. Osteoblasts are cells that synthesize all constituents of the unmineralized bone matrix, including collageneous and non-collagenous proteins. Osteoclasts are

multinucleated cells which are formed by the fusion of mononuclear progenitors and are responsible for bone resorption. Osteocytes possess long cytoplasmic processes which extend through a canalicular system to adjacent cells, allowing for rapid communication by exchanging ions and signaling molecules through gap junctions. Because of this elaborate organization, osteocytes are well placed to sense changes in strain and respond to tissue microdamage.

2.2.1 The Bone Remodeling Process

Bone remodeling is a complex process involving coordination between osteoclastic bone resorption and osteoblastic bone formation. It is initiated in response to a variety of conditions, including regulation of mineral concentration, adaptation to changing mechanical environments, and repair of microdamage. Bone remodeling can be targeted towards specific sites, in the case of mechanical adaptation and damage repair, or may be initiated in a non-targeted manner for mineral regulation. (Burr 2002) As much as 30% of bone remodeling may be a result of targeted repair. (Mashiba et al. 2001; Burr 2002)

The bone remodeling process can be understood as a series of progressive stages involving multiple cells within a bone multicellular unit (BMU) coupled by space and time. Osteoclasts within the BMU reabsorb old or damaged bone, a process that takes approximately 3 weeks per site. Osteoblasts then rebuild bone at the site, which takes about 3 to 4 months. (Rodan et al. 2000) There are five stages of the remodeling process: resting, activation, resorption, reversal, and formation. (Hill 1998)

In the resting stage, osteoprogenitor cells line the surface of bone until activation in response to chemical factors. About 80% of cancellous and cortical bone surfaces, and

95% of intracortical surfaces, are inactive at any given time. (Hill 1998) When stimulated, the activation phase begins as osteoclast progenitors differentiate into osteoclasts and attach to the bone surface.

Bone remodeling begins with the osteoclast, which moves to the site to be resorbed, attaches to the bone surface, and forms a ruffled border across which acidic and protease compounds are pumped. Hydrochloric acid is released first, which is effective at dissolving the mineralized components of the matrix. Proteases like cathepsin K and other metalloproteases then digest the organic collagen and other proteins. The osteoclasts then endocytose and digest the degradation products. (Teitelbaum 2000) The cavity that is formed from removal of tissue is called a Howship's lacuna. Osteoclasts then return to a quiescent form or undergo apoptosis. (Schindeler et al. 2008)

The reversal phase follows which lasts approximately 9 days where osteoclasts disappear and macrophage-like cells are seen on the bone surface, perhaps contributing to the stimulation of osteoblasts and also removing debris from the resorption process. (Hill 1998) Once the area has been cleared of degradation products, osteoblasts move in to regenerate the bone matrix. This begins the formation phase.

Osteoblasts move into the resorption pit and begin to lay osteoid, an undermineralized bone matrix scaffold upon which minerals deposit as the matrix matures. Osteoid reaches approximately 70% of its final mineralization after 5 to 10 days, and takes up to 350 days to fully mature. (Fuchs et al. 2008) A period of secondary mineralization follows, which is completed after 30 months. (Bala et al. 2010) The amount of bone removed by osteoclasts compared to the amount regenerated by osteoblasts is referred to as the bone balance. With aging, a net negative bone balance is

seen as more bone is resorbed by osteoclasts than replaced by osteoblasts in the BMU.

Since the behavior of osteoblasts and osteoclasts is coordinated within a resorption pit, remodeling is described as being coupled. Coupling is controlled through paracrine signals secreted by osteoblasts which regulate the differentiation and activation of osteoclasts. In the resting phase, osteoclasts are kept inactive by osteoprotegerin (OPG), a tumor necrosis factor receptor which is secreted by osteoblastic stromal cells. OPG binds to RANKL (receptor for activator of nuclear factor-κβ ligand, also secreted by osteoblasts) and prevents it from binding to its receptor RANK (receptor for activator of nuclear factor-κβ) on osteoclastic progenitor cells, which is required for osteoclastic stimulation. Osteoblastic stromal cells then control bone resorption by increasing the expression of RANKL and decreasing the expression of OPG. (Robling et al. 2006)

2.2.2 Aging, Remodeling, and Osteoporosis

The rate of bone remodeling increases in late mid-life as the concentration of sex hormones declines. (Khosla et al. 1998; Riggs et al. 1998; Recker et al. 2004) One would expect that the increased rate of bone turnover would mean that microdamage density was low, but this is not the case. It is well documented that microdamage accumulates with age, suggesting that targeted remodeling repair mechanisms are compromised with aging even as stochastic remodeling is ramped up. (Schaffler et al. 1995; Allen 2008) This may result if signaling mechanisms are compromised, which is plausible considering that osteocyte numbers also decline with age. (Mori et al. 1997; Vashishth et al. 2000) Low bone mineral density has also been shown to be a factor in microdamage formation, and it is possible that repair mechanisms cannot keep up with increased damage formation. (Stepan et al. 2007) This increased rate of remodeling may be the most

significant factor in predicting fracture risk, even more so than bone mineral density values. (Cummings 2002; Heaney 2003; Recker et al. 2004) Remodeling can produce transient weakness because, not only does the removal of old bony material locally weaken bone, but also new osteoid is less stiff than mature matrix. (Recker et al. 2004)

When bone mineral density declines to a point that is 2.5 standard deviations lower than the average peak bone mass for a woman at age 30, osteoporosis is diagnosed. This disease is associated with an increased risk of fracture, especially in areas with high amounts of trabecular bone like the hip, wrist, and spine. It occurs due to an increase in remodeling rates coupled with a negative bone balance at the BMU. (Compston 2002) There are some who suggest that osteoporosis is at the extreme of a continuous spectrum of increased remodeling rates and bone loss that occurs normally with aging and does not have a separate mechanism itself. (Keaveny et al. 2002) Currently, no causative agent has been identified that distinguishes the mechanism for osteoporosis development (excluding drug-induced forms) from age-related bone loss mechanisms.

2.2.3 Drugs which Modulate the Bone Remodeling Process

A variety of therapies exist which target cells within the bone remodeling process to modulate the rate and amount of bone formation. Generally, they can be divided into two groups: stimulators of bone formation and inhibitors of bone resorption.

2.2.3.1 Stimulators of Bone Formation

In some instances, the loss of bone mass is so great that slowing bone resorption is not enough – new bone formation must also be stimulated. For these cases, drugs which target the osteoblast are prescribed. Parathyroid hormone (PTH) and its recombinant form, teriparatide, stimulate bone formation by increasing the number and

activity of osteoblasts. (Dobnig et al. 1995) Intermittent dosing of PTH has been shown to increase vertebral and femoral neck bone density. (Dobnig et al. 1995; Lane et al. 1998) There is also evidence that treatment with teriparatide reduces microdamage accumulation in the iliac crest of patients previously treated with alendronate. (Dobnig et al. 2009)

Strontium ranelate is a new drug that has been shown to reduce the risk of vertebral and nonvertebral fractures in women with post-menopausal osteoporosis. (Meunier et al. 2004; Reginster et al. 2005; Roux et al. 2006) Its mechanism of action is still under investigation; while some have shown anabolic effects of bone formation, (Reginster et al. 2005; Caverzasio 2008) others have not. (Fuchs et al. 2008; Ma et al. 2011)

2.2.3.2 Inhibitors of Bone Resorption

Many bone diseases are caused by an increase in the rate and/or amount of bone reabsorbed by osteoclasts. For these diseases, drugs which slow the bone resorption phase of bone remodeling equalize the balance between resorption and formation and stabilize bone mass. The cellular target is the osteoclast, and these drugs work either by preventing their differentiation from precursors or inducing apoptosis of the cells directly.

Estrogens and selective estrogen receptor modulators (SERMs) work through this first mechanism, inhibiting osteoclastic differentiation. Raloxifene, a commonly used drug within the class of SERMs, has been shown to reduce the risk of vertebral fracture by 40%, despite increasing bone density by only 3 to 4%. (Delmas et al. 1997; Cummings et al. 1999; Ettinger et al. 1999) Bisphosphonates work through the second mechanism, inducing apoptosis of osteoclasts.

2.2.3.3 Bisphosphonates

Bisphosphonates are pyrophosphate analogs, containing a phosphate-carbon-phosphate (P-C-P) backbone that gives them affinity for bone and renders them resistant to enzymatic degradation. (Grey et al. 2006) Of all therapeutics available, they are the most effective inhibitors of bone resorption, achieving this result by inhibiting the enzyme farnesyl diphosphate synthase in the mevalonate pathway of cholesterol synthesis within the osteoclast. (Luckman et al. 1998; Fisher et al. 1999) This induces osteoclasts to undergo programmed cell death (apotose), resulting in reduced bone resorption, lower bone turnover, and a positive bone balance. (Rodan et al. 2000) Side chains added to the P-C-P backbone modulate the characteristics of the bisphosphonate and have generated a large number of therapeutics. (Figure 2.2) The addition of nitrogen in the alkyl chain increases the antiresorptive potency of the drugs from between 100 to 10000x that of non-nitrogen containing bisphosphonates. (Russell et al. 1999)

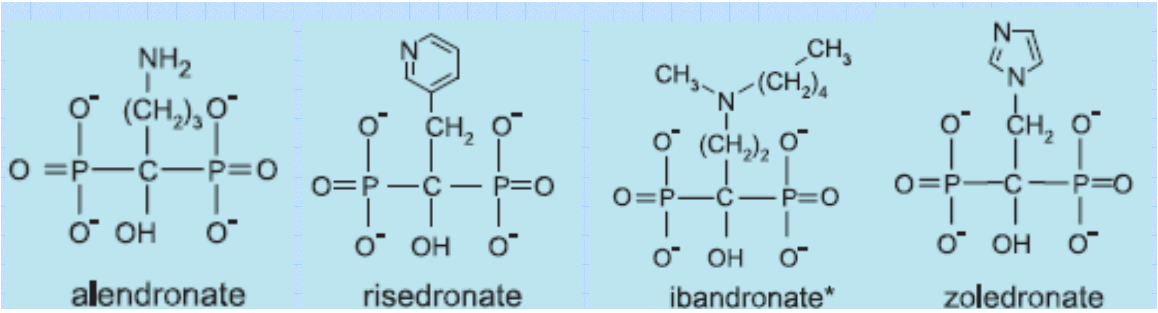

Figure 2.2 Chemical Structures of Some Commonly Prescribed Bisphosphonates (Rodan et al. 2000) In order of increasing potency: alendronate (Fosamax), risedronate (Actonel), ibandronate (Boniva), and zoledronate (Reclast).

Alendronate was the first inhibitor of bone resorption to show a significant reduction in the number of fractures of the spine, wrist, and hip. (Liberman et al. 1995;

Black et al. 1996) Alendronate has been shown to increase bone density in the vertebrae, femoral neck and trochanter, iliac crest, and wrist. (Black et al. 1996; Seeman 1999; Recker et al. 2005) It also improves bone microarchitecture by increasing trabecular thickness, decreasing trabecular spacing, and decreasing anisotropy. (Hu et al. 2002; Recker et al. 2005) Investigations of its effects on bone composition reveal increased degree and uniformity of bone matrix mineralization and increased collagen crosslinking, all of which can increase strength and stiffness of bone. (Roschger et al. 2001) These changes account for its effectiveness in reducing the risk of bone fracture.

While alendronate's efficacy in reducing fractures is well proven, it is also associated with a number of side effects. Two side effects in particular, osteonecrosis of the jaw and atypical femoral subtrochanteric fractures, are thought to occur due to an oversuppression of bone turnover, which increases the brittleness of the bone material. (Goh et al. 2007; Wynn 2007; Neviaser et al. 2008; Bocanegra-Perez et al. 2009) While these side effects cause substantial morbidity, they are rare: a recent study in Danish women reported 100 atypical subtrochanteric fractures per 100,000 patients on long-term alendronate treatment (Abrahamsen et al. 2009) and less than one incident of osteonecrosis of the jaw per 14,200 patient treatment-years. (Grbic et al. 2010) However, the use of bisphosphonates in diseases like cancer has shown an increased risk for these side effects. (Bamias et al. 2005)

Another sub-clinical side effect of bisphosphonate use is the accumulation of microdamage. (Allen et al. 2006; Stepan et al. 2007) The link between bisphosphonate use and microdamage accumulation is discussed in more depth in section 2.4.1.

2.3 Trabecular Bone Mechanical Properties

The mechanical properties of trabecular bone can be examined at the structural level with trabecular bone samples large enough for continuum assumptions to be valid (no smaller than 3 to 5 intertrabecular lengths), or can be determined at the tissue level for individual trabeculae. (Harrigan et al. 1988) Accurately defining properties like tissue and apparent-level stiffness, ultimate strength, and toughness are important to the work developed in this thesis because finite element models in particular rely on the input of properties which dictate how a material will behave under loading. Furthermore, in order to fully appreciate the consequences of how aging and bisphosphonate use affect bone fragility, one must have a basic understanding of the mechanical properties of healthy tissue.

2.3.1 Apparent and Tissue-Level Strength and Stiffness of Trabecular Bone

Trabecular bone is viscoelastic and exhibits properties of a transversely isotropic cellular solid in healthy young adults. (Linde et al. 1990; Linde 1994) Its viscoelasticity results from its organization as a composite, consisting of an inorganic mineral phase and an organic (mostly) collagenous phase. Bone has asymmetric tissue properties, exhibiting greater strength in compression than in tension. (Keaveny et al. 1997; Niebur et al. 2000) Trabecular bone strength in standard specimens has been reported between 2.4 and 5.8 MPa. (Linde et al. 1992) Stiffness values for trabecular bone structure have been reported between 78 to over 1000 MPa, though typical values are closer to the upper portion of this range. (Linde et al. 1992)

The typical stress/strain curve of trabecular bone in uniaxial loading is similar to that of a ductile metal, with an initial linear elastic region up to a strain yield ranging from 0.7 to 1.4% (Linde 1994), followed by non-linear plastic deformation with

substantial post-yield behavior. Early studies conducted in trabecular bone detected a non-linear 'toe-in' region, but work by Keaveny et al demonstrated that this region was erroneous, reflecting end-effects rather than true tissue behavior. (Keaveny et al. 1997) Beyond yield, there is a non-linear increase in stress until the ultimate stress is reached. Further increases in strain beyond the failure point results in a stress plateau as trabeculae are fractured up until all pores are filled with fractured bone and stresses again increase. This point occurs after 30-70% strain depending on the porosity of the trabecular structure. (Hayes et al. 1976)

The mechanical properties of the trabecular bone structure vary widely among individuals and between anatomical sites. While differences in bone volume fraction have a large effect on the variability of trabecular bone mechanical properties, accounting for up to 83% of the variability in the vertebrae and 92% of the variability in the proximal femur, other factors such as trabecular architectural organization and bone material composition also affect the mechanical response. (McCalden et al. 1997; Morgan et al. 2001; Keaveny et al. 2002) Alterations in trabecular orientation and anisotropy have also been shown to influence variability in stiffness measures, especially in multi-axial testing. (Hodgskinson et al. 1990; Goulet et al. 1994) Additionally, the degree of mineralization and collagen cross-linking affects not only stiffness, but also non-linear properties of bone as well. (Currey 1984; Wang et al. 2002) Though studies vary widely in their reports of trabecular bone strength and elastic modulus, it is generally accepted that the stiffness of trabecular bone is 20 to 30% less than that of cortical bone. (Kuhn et al. 1989; Choi et al. 1992)

While trabecular bone shows a wide distribution in strength, yield strains remain fairly constant. Studies have shown that they vary little with differences in density and are isotropic. (Turner 1989; Keaveny et al. 1994) Yield strains are higher in compression than tension and are similar within anatomic sites but can vary between sites. (Kopperdahl et al. 1998; Morgan et al. 2001) This implies that, if the elastic properties of samples are known, then strength can be estimated based on yield strains. (Keaveny 2001)

Tissue-level properties are more difficult to determine, and values have been reported using a variety of direct measurement tools, from micro/nano-indentation to bending and uniaxial tension/compression tests of individual, machined trabeculae. These direct measurement studies estimate tissue stiffness to be from 1 GPa obtained from tensile testing to 13-15 GPa via ultrasonic technique, with bending and compression test results reporting values in between this range. (Kuhn et al. 1989; Ryan et al. 1989; Rho et al. 1993) However, these measurements are prone to error due to their small size.

2.3.2 The Back-Calculation Method for Determination of Tissue-Level Stiffness

An indirect way of determining tissue-level stiffness is to use a back-calculation method. (van Rietbergen B 1995) In this method, trabecular bone samples (spanning at least 3-5 trabecular lengths for continuum assumptions) are scanned with micro-CT and reconstructed into a 3D image. (Harrigan et al. 1988) The 3D reconstructed image is directly converted into a large-scale finite element model, and the model is solved using an initial guess for the tissue modulus and boundary conditions simulating uniaxial compression. This will give a computational estimation of the apparent elastic modulus. Uniaxial compression testing of trabecular bone samples are also conducted to obtain

values for the apparent elastic modulus. Under assumptions of linear elasticity, the true tissue modulus can be solved for as the ratio between the apparent modulus obtained in mechanical testing to the apparent modulus estimated from finite element modeling,

$$E_{tissue} = \frac{E(\text{exp})_{apparent}}{E(\text{FEM})_{apparent}} E(\text{FEM})_{tissue}$$

where $E(FEM)_{tissue}$ is equal to the initial guess for tissue modulus input into the finite element model. One study using this technique reported an r^2 value of 0.89 between the experimentally measured and calculated tissue modulus. (Hou et al. 1998)

2.3.3 Fatigue Behavior of Bone

Fatigue testing of bone is generally carried out at supraphysiological strains because failure can require over tens of millions of loading cycles at physiological strain levels and rates. (Schaffler et al. 1990) The endurance limit of cortical bone has been estimated at a normalized stress of 0.4%, (Moore et al. 2003) and the changes in stiffness and strength that occur during fatigue testing above this limit has been attributed to microdamage accumulation. (Moore et al. 2003) Creep has been shown to have a marginal impact on fatigue behavior at low stress levels. (Carter et al. 1976; Moore et al. 2004) In compressive fatigue testing, appreciable decreases in modulus occur in the later half of fatigue life; in tensile fatigue testing, however, there is an early, rapid decrease in modulus followed by a plateau before the rapid loss of modulus to failure. (Pattin et al. 1996) Trabecular bone also has a shorter fatigue life in tension than in compression. (Caler et al. 1989) However, fatigue properties *in vivo* are likely different from those determined *in vitro* due to the viscoelasticity of bone and the strain rate-dependence of fatigue life. (Donahue et al. 2006)

2.3.4 Fracture Toughness of Bone

Bone is a highly organized heterogeneous structure, composed of minerals and proteins organized into osteons and hemiosteons. This organization contributes greatly to the fracture toughness of bone. In a study in cortical bone by Nalla et al, it was shown that uncracked ligament bridging is an extrinsic toughening mechanism found in in-plane longitudinal cracks to bridge cracks upon opening. Collagen fibrils also contribute to crack-bridging in anti-plane longitudinal directions. The osteonal organization plays an important role in fracture toughening as well; osteonal cement lines can provide a weak path for crack propagation, which promotes deflected out-of-plane crack growth rather than growth through osteons. This mechanism contributes greatly to fracture toughness, as the stress intensity is reduced approximately 50% compared to an undeflected crack. (Nalla et al. 2003)

Microdamage formation itself contributes to the toughness of bone through crack-tip shielding. (Vashishth et al. 2000; Vashishth et al. 2000) Fatigue studies of microdamaged compact bone have demonstrated that very few *in vivo* cracks propagate during *in vitro* fatigue loading. (O'Brien et al. 2003) Cracks formed with *in vitro* mechanical testing often propagate to the same length as *in vivo* cracks. Crack propagation models estimate the average microcrack length would be 91.2 μm due to microstructural barriers, and that remodeling most likely targets the longest cracks for removal. (Taylor 1998; Sobelman et al. 2004)

The role of microdamage in the toughness of trabecular bone is less studied, but it is probable that toughening mechanisms similar to cortical bone at the microstructural level are in play. Bovine trabecular bone has been shown to have fatigue and creep

characteristics similar to cortical bone. (Zilch et al. 1980) However, it is likely that fracture toughness of human trabecular bone is variable due to large variations in density and architecture. Its organization as a cellular solid also distinguishes its toughness behavior from cortical bone: while crack propagation can easily turn unstable in cortical bone, crack propagation is quantum-controlled in trabecular bone as individual trabeculae fail. (Cook et al. 2009) In such a structure, it is advantageous for damage to localize within already damaged trabeculae, as the damage remains contained and the structure can be repaired or replaced. Transverse struts may act as sacrificial elements, protecting the integrity of load-bearing longitudinal elements as they dissipate energy. (Badiei et al. 2007) More data into crack growth mechanisms in trabecular bone is needed, as correlations with cortical bone mechanisms can only go so far.

2.4 Bone Microdamage

In a seminal study conducted by Harold Frost in 1960, *in vivo* microcracks in human ribs were differentiated from cracks formed during bone sample extraction by an en bloc basic fuchsin staining technique, demonstrating that microcracks form in the body due to physiological loading. (Frost 1960) It is now understood that microdamage formation and repair is an integral part of bone homeostasis in which both structural and material properties are modulated to maintain bone strength. (Seeman et al. 2006; Cheung et al. 2008) When a microcrack occurs, signaling mechanisms are activated which target that area for repair. Although the signaling process is not fully elucidated, evidence suggests that a disruption to the canalicular network connecting nearby osteocytes is responsible for osteocytic apoptosis, which may initiate the targeted remodeling process. (Verborgt et al. 2000; Verborgt et al. 2002; Noble 2005; Cardoso et al. 2009) Damaged

areas are resorbed and replaced with new osteoid, which then mineralizes over time to restore matrix to its original state.

The role of microdamage in skeletal fragility is fiercely debated: while some studies have shown decreased strength and stiffness with microdamage accumulation, (Carter et al. 1977; Burr et al. 1997; Yeh et al. 2001) others view damage accumulation as a toughening mechanism which allows for the release of strain energy. (Vashishth et al. 1997) Linear microdamage is associated with a quadratic loss of modulus which propagates more easily than diffuse damage, which can dissipate energy while limiting propagation. (Burr et al. 1998; Diab et al. 2006) In studies of fatigue life of bone with age, it was found that bone from younger individuals had a longer fatigue life due to the formation of diffuse damage, whereas bone from older donors formed fewer but longer linear microcracks. (Diab et al. 2006) Others have shown that the osteonal arrangement of cortical bone serves to arrest crack development and prevent damage propagation to overt fracture. (Hazenberg et al. 2006) A critical length of damage may be necessary to initiate targeted remodeling. (Sobelman et al. 2004) Thus, while the initiation of damage in itself may not be instrumental in apparent fracture, it is clear that microdamage morphology is important in assessing fracture risk due to damage accumulation.

2.4.1 Bone microdamage studies with bisphosphonates and fracture risk

Since bisphosphonate therapy is commonly prescribed in osteoporosis, it is important to examine the consequences of long-term suppression of bone turnover. Bisphosphonates can reduce bone turnover by as much as 80-90%, which increases bone density. (Turner 2002) However, they also suppress remodeling and cause increased bone mineralization, leading to an accumulation of microdamage that can degrade

mechanical properties and increase the brittleness of bone. It is important to understand the implications of microdamage accumulation in bisphosphonate-treated bone and determine if such accumulation leads to a weakening of bone matrix and subsequent increased fracture risk.

Many studies have attempted to define the role microdamage accumulation plays in bisphosphonate treatment. Suppression of bone resorption leads to damage accumulation in the elderly (Lee et al. 2003), and Flora demonstrated that dogs receiving 0.5 mg/kg/day of etidronate or clodronate fractured ribs spontaneously within 12 months. (Flora et al. 1981) Furthermore, rib, spinous process, or pelvic fractures were observed in dogs treated between 9 and 12 months with high doses of bisphosphonates. However, it is unclear whether these fractures were caused by an accumulation of microdamage or other factors. (Burr et al. 1997) In another study by Forwood, fracture incidence was evaluated in dogs treated for 2 years with risedronate. Researchers found no microdamage accumulation or observed no spontaneous rib fractures, despite reduced bone turnover of 80-90%. (Forwood et al. 1995) Furthermore, another study found that a certain amount of pre-existing microdamage actually increases fatigue resistance in cortical bone. (Sobelman et al. 2004) The same study also showed that damage induced during fatigue loading was greater in cortical bone samples from older individuals, indicating an age-related increase in susceptibility to microcracking. Bouxsein has suggested that, while microdamage accumulation is clearly associated with reduced mechanical properties, the ability of bone to undergo microdamaging under load is in fact a toughening mechanism that dissipates energy and helps prevent propagation of large microcracks through the matrix. (Bouxsein 2003) The multitude of researchers in this

field has yet to come to a consensus on the role of microdamage in bisphosphonate-treated bone and fracture risk.

2.4.2 Fluorescent Labeling of Microdamage

In 2000, Lee et al published a microdamage detection technique which allowed for site-specific fluorescence of damage. Microdamage forms cracks in the hydroxyapatite matrix which exposes unbound charged ions, 55% of which are calcium ions. (Lee et al. 2003) Lee was able to use fluorescent agents to form a strong chelate with unbound calcium ions lining the crack walls, allowing for site-specific detection of microdamage. In the study, Lee bulk stained human rib sections in 1% solutions of alizarin complexone, calcein, calcein blue, oxytetracycline, xylenol orange, and basic fuchsin. Microcrack density and length were quantified, and no differences between the stains were noted. Dyes were then applied sequentially to bovine trabecular bone samples undergoing compressive cyclic fatigue testing to enable labeling of crack growth. However, the transition between dyes was imprecise, and there was evidence of stain substitution in some areas. (Lee et al. 2000)

O'Brien et al improved the sequential labeling technique by using ion chromatography to measure the affinity of each fluorochrome for free calcium. Dye concentrations were optimized and applied to fatigue tested compact bone in orders of decreasing affinity. Stain substitution was therefore minimized, and they were able to demonstrate microdamage accumulation at different intervals in the fatigue test. (O'Brien et al. 2002) Since publication of this study, others have used the sequential staining technique to study propagating microcracks in ovarectomized sheep, (Kennedy et al. 2008) the effect of loading mode on crack propagation, (Wang et al. 2006) the fracture

behavior of bone at high strain rates in equine femurs, (Kulin et al. 2008) and the three-dimensional distribution of microdamage in trabecular bone. (Bigley et al. 2008)

2.4.3 Alterations in Bone Composition in Age-related Fragility and Microdamage

Many have speculated that compromising the bone matrix and mineral interaction leads to an age-related decrease in bone strength. (Boskey 2003; Paschalis et al. 2004; Wang et al. 2004) Ager hypothesized that collagen cross-linking chemistry changes with age, which may contribute to deterioration in bone quality. (Ager et al. 2005) Also, Boskey found that collagen crosslinking is predictive of future fracture risk. (Boskey 2003) Accumulation of advanced glycation end-products (AGEs) with age may contribute to increased fragility with aging, specifically through reduction in post-yield energy dissipation capacity. (Nyman et al. 2006) Therefore, many studies have linked increasing age to compromised bone matrix/mineral material, leading to a decrease in mechanical properties and toughness of bone (Wang et al. 2004).

A study examining the chemical composition of bone near areas of microdamage revealed a decreased carbonate/protein ratio and carbonate/phosphate ratio, and increased acid phosphate content. (Ruppel et al. 2006) It is speculated that increased tissue mineralization hastens the formation of microdamage, (Burr et al. 2003) but this study found no significant differences in phosphate/protein ratio or crystallinity between microdamaged and undamaged bone. Collagen crosslinking structure was also different in microdamaged areas, suggesting ruptured crosslinks. However, it is unclear whether these changes cause damage to form, or whether these changes are the result of damage formation since areas that were analyzed had already demonstrated cracking.

2.5 Micro-CT and its Use in Studying Trabecular Bone

Microcomputed tomography (micro-CT) is a powerful technology allowing three dimensional analyses of tissues at high resolution in a nondestructive manner. In trabecular bone studies, automated calculation of properties such as mineral content; trabecular thickness, spacing, and number; degree of anisotropy; and relative geometry of trabeculae (rod-like versus plate-like) allow quick and easy descriptions of trabecular bone organization.

Micro-CT works by measuring the X-ray attenuation (absorption) of the tissue, which is dependent on its density. Small variations in density can be resolved by micro-CT depending on the resolution of the detector. Images are taken slice by slice in three orthogonal directions, and a three-dimensional reconstruction array is directly created, rather than reconstructing a 3D image from series of two-dimensional slices. (Feldkamp et al. 1989; Tuan 2006)

Micro-CT systems have been used extensively to study alterations in trabecular bone structure due to age, gender, anatomical location, and pathology such as osteoporosis. In one study, human bone biopsies taken at five different skeletal sites were analyzed using micro-CT and 3D analysis methods. (Hildebrand et al. 1999) Trabecular bone in the femoral head was defined by high bone volume fractions, thick trabeculae, and plate-like structure. In the lumbar spine, analysis of the second and fourth vertebrae showed that bone volume fraction was lower than the femoral head, with thinner and more rod-like trabecular architecture. Analysis of the calcaneus revealed a structure similar to the lumbar spine, but with increased bone volume fraction. In the iliac crest, trabecular bone architecture was more varied, suggesting a mixed structure

type between the lumbar spine samples and the femoral head samples. This study demonstrates that trabecular architecture is dependent on anatomical site.

Recently, Mueller et al obtained morphometric indices from formalin-fixed radii of 50 men (mean age 79.7 ± 9.1 years) and 50 women (mean age 81.5 ± 8.9 years) at six different locations, beginning with the subchondral trabecular bone and ending near the middle of the diaphysis. (Mueller et al. 2009) In general, they found that most morphometric parameters differed significantly in gender and were independent of the analyzed region of interest. Total bone volume, trabecular bone volume density, and trabecular number were greater in men compared with women. The most significant differences in trabecular bone volume density were noted in the more distal regions, and gender differences evened out with sharp decreases in men as values were calculated along the radial shaft. Women also demonstrated thinner trabeculae in the metaphyseal regions, but thicker trabeculae in the diaphyseal regions. Another study compared trabecular bone architecture in the proximal femur between osteoporotic and non-osteoporotic populations. (Borah et al. 2001) Dramatic decreases in bone volume, connectivity density, and trabecular thickness are seen in osteoporosis, with related increases in trabecular spacing and more rod-like architecture. All of these studies demonstrate the power of micro-CT to characterize trabecular organization nondestructively, and suggest that architecture varies by age, gender, and anatomical location.

2.6 Finite Element Modeling in Bone Mechanics Studies

Finite element modeling (FEM) is a numerical technique used to solve a series of differential equations describing the physical behavior of a sample under a set of input

conditions. The advent of high resolution micro-CT scans has improved FEM studies of trabecular bone mechanics because the actual behavior under input conditions can be studied rather than behavior of an idealized trabeculated structure. Individual voxels (three-dimensional pixels) generated in the CT images can be converted into equally sized hexahedral elements in the finite element model. This sub-divides the sample into a series of smaller regions consisting of elements and nodes. Mathematical equations describing the displacement of nodes under a fixed load, for example, can be used with constitutive equations to predict how the sample will behave.

FEM has been used in the field of bone mechanics to describe the behavior of bone under physiological loading conditions, failure, and in pathologic states like osteoporosis. (Lotz et al. 1991; Lotz et al. 1991; Borah et al. 2001; Bevill et al. 2009) Generally, bone behavior is modeled under conditions of linear elasticity, homogeneity, isotropy, and small strains due to computational time and space constraints. Since bone behaves like a linear elastic material these assumptions are valid within certain limits. (Pugh et al. 1973; Pistoia et al. 2002) This concept has been shown in earlier studies, where using linear elastic FE analyses in combination with experimental data provided good results for the prediction of the bone failure load measured in experiments. (Lotz et al. 1991; Pistoia et al. 2002) Nagaraja specifically addressed the question of whether using inhomogeneous FE analysis rather than homogenous assumptions would improve the correlation strength and provide more precise stress/strain estimations of damage events. (Nagaraja et al. 2007) A modest improvement (<8%) in correlation strength of stress/strains to damage sites was found using inhomogeneous analysis. Stress/strain magnitude estimations were different by less than 9% between the two models. Thus, an

improvement in model estimations is achieved using inhomogeneous material properties, but the differences are modest. Furthermore, a study carried out in pelvic trabecular bone compared an idealized homogenous FE model to a more "realistic" model containing inhomogeneous material properties. (Dalstra et al. 1995) They also found that for comparative studies, homogenously distributed material properties can be assumed. Finally, trabecular bone within the femoral neck and intertrochanteric regions has demonstrated significant anisotropic behavior; however, Brown et al demonstrated that incorporating anisotropic properties in two-dimensional FE models results in no significant changes in stress distributions. (Brown et al. 1984; Lotz et al. 1991) Based on these previous studies, use of FEM under conditions of homogeneity, isotropy, and linear elasticity to study the microstructural stresses/strains of trabecular bone at the onset of structural yielding is validated within the linear elastic region for comparative studies.

In conclusion, much progress has been made in the microdamage field in the past 30 years. With the improvements in micro-CT and finite element modeling, it has become possible to study trabecular bone mechanics to greater depths than ever before. This thesis uses these improvements in technology and builds upon the work of others to study the initiation and propagation of microdamage in trabecular bone.

CHAPTER 3

AGING AND GENDER EFFECTS ON MICROSTRUCTURAL STRESS AND STRAIN ASSOCIATED WITH DAMAGE INITIATION

3.1 Introduction

Peak bone mass is reached at approximately age 30, after which a slow decline in bone mass begins throughout the skeleton at rates that vary among individuals and anatomical sites. For trabecular bone in particular, age-related changes include alterations in remodeling, extracellular matrix heterogeneity and composition (e.g. collagen and noncollagenous proteins, mineral, and water content), quantity (bone volume fraction), and microarchitecture (e.g. trabecular thickness, orientation, degree of anisotropy, and structure model index). (Hildebrand et al. 1999; Paschalis et al. 2004; Recker et al. 2004; Busse et al. 2009) Of these factors, reductions in bone quantity with corresponding alterations in microarchitecture have been the most extensively studied. Decreased bone volume fraction with age is typically associated with microstructural deterioration in the form of decreased trabecular thickness and connectivity with increased trabecular spacing and anisotropy. (Parfitt et al. 1983; Kimmel et al. 1990)

While architectural changes with aging in the trabecular bone are well documented, sex differences are less concrete. Histomorphometric studies have found few bone volume fraction or compressive strength differences attributable to sex in vertebral trabecular bone in age matched groups. (Bergot et al. 1988; Thomsen et al. 2000; Keaveny et al. 2002) One study reported an increased tendency for perforation of horizontal trabecular struts and increased trabecular spacing between horizontal

trabeculae in females compared with males, but found no other histomophometric sex differences. (Mosekilde 1989) It seems clear that architectural differences in trabecular bone between sexes are subtle, but less clear are sex differences in the response to damaging loads at the microstructural level. A recent study by Yeni et al reported a possible sex difference in the relationship between shear stress amplification and variability of stresses in the trabecular bone response to mechanical load. (Yeni et al. 2008) However, more research in this area is warranted.

Alterations in bone mass and microstructure are not the only phenomena that contribute to increased fragility. Decreased bone quality is also reflected in an accumulation of unrepaired microdamage, which may be the result of a breakdown in targeted remodeling of microdamage regions. (Burr et al. 1998; Burr et al. 2008) The relationship of microdamage with skeletal fragility has been previously investigated, and non-linear increases in crack density with age have been reported. (Schaffler et al. 1995; Burr et al. 1997; Mori et al. 1997; Fazzalari et al. 1998; Fazzalari et al. 2002) Gender differences in damage accumulation are less clear. One study found a similar prevalence of diffuse damage between males and females, but greater areas of diffuse damage in male bone, suggesting that while damage initiation factors may be similar between sexes, the mechanisms of damage progression and its removal may be gender-related. (Vashisth et al 2000) However, studies are inconclusive at this time.

In the present study, age and sex-related differences in micromechanical properties associated with microdamage initiation are investigated using a previously published technique which combines histology and 3D micro-CT reconstructions of trabecular bone with finite element modeling. (Nagaraja et al. 2007) Microstructural

stresses and strains associated with microdamage initiation of severe, diffuse, and linear morphologies were quantified in trabecular bone from the distal femur of younger women, older women, and older men. Additionally, changes in microarchitecture and mineralization were evaluated in association with trabecular bone microdamage initiation of different morphologies. We hypothesize that the stress threshold for microdamage initiation is lower in trabecular bone from older females but similar between genders, indicating a loss in bone quality with aging.

3.2 Methods

3.2.1 Specimen preparation

Fresh-frozen (-80°C) trabecular bone cores (18 mm in length, 5 mm in diameter) were harvested from the distal femur of three younger females (32-37 years old, n=9), three older females (71-80 years old, n=9), and three older males (68-78 years old, n=9) such that the principal material direction was approximately aligned with the loading axis. Based on available medical records, donors selected for this study did not have any prior history of metabolic bone diseases, osteoporotic fractures, or metastatic cancers. Stainless steel endcaps (5 mm depth) were glued to ends of each bone core specimen using cyanoacrylate glue (Prism 401, Loctite, Newington, CT, USA) to minimize the effects of end artifacts on mechanical testing data and prevent movement within the end-caps. (Keaveny et al. 1994) The specimens were wrapped in saline soaked gauze and stored at -20° C for one week until mechanical testing. (Linde et al. 1993)

3.2.2 Micro-CT imaging

All specimens were micro-CT imaged (μCT 40, Scanco Medical, Basserdorf, Switzerland) at a voxel resolution of 21 μm. A threshold to distinguish trabecular bone

from background was chosen through histogram analysis of grayscale images and remained consistent throughout all evaluations. Automated distance transformation algorithms were used to calculate morphological parameters including bone volume fraction, trabecular thickness, spacing, number, structural model index (SMI), connectivity and trabecular orientation (Hildebrand et al. 1999). Trabecular orientation was measured as the angle from the principal axis of the trabecula to the loading axis. Trabecular bone mineralization (in mg/cc HA) was computed from attenuation values of grayscale micro-CT images based on hydroxyapatite (HA) calibration standards. Specifically, for calibration of the linear attenuation coefficient (1/cm) to hydroxyapatite (HA) mineral density (mgHA/cm^3), a cylindrical HA phantom (ScanCo Medical, Basserdorf, Switzerland; 38mm diameter) was utilized. This phantom contained known density rods (0, 200, 400, and 800 mgHA/cm^3) embedded in resin. Scans were performed at the X-ray source energy used in this study (45 kVp). A 0.5mm Al filter was used for all scans. Reconstructions also incorporated a beam hardening correction curve.

3.2.3 Mechanical testing

Using a servo-hydraulic mechanical testing system (Mini Bionix 858, MTS Corp.), specimens were preconditioned for 3 cycles to 0.1% strain followed by a uniaxial compression ramp at a rate of 0.5% strain/s to 0.9% for female donors and 1.2% for male donors and held for 3 hours. (Figure 3.1) The yield strain endpoints were determined in preliminary testing, and it was decided that samples should be tested to a point consistent with the yield point on the stress-strain curve (using the 0.2% offset method) rather than the same yield strain which may not reflect the true yield point. Apparent strain was calculated using an effective gage length, defined as the exposed length plus half the

length embedded in the endcaps (Keaveny et al. 1997). Specimens were immersed in 0.9% physiologic saline plus protease inhibitors (Protease Inhibitor Cocktail Set V, Calbiochem) throughout mechanical testing to prevent tissue degradation.

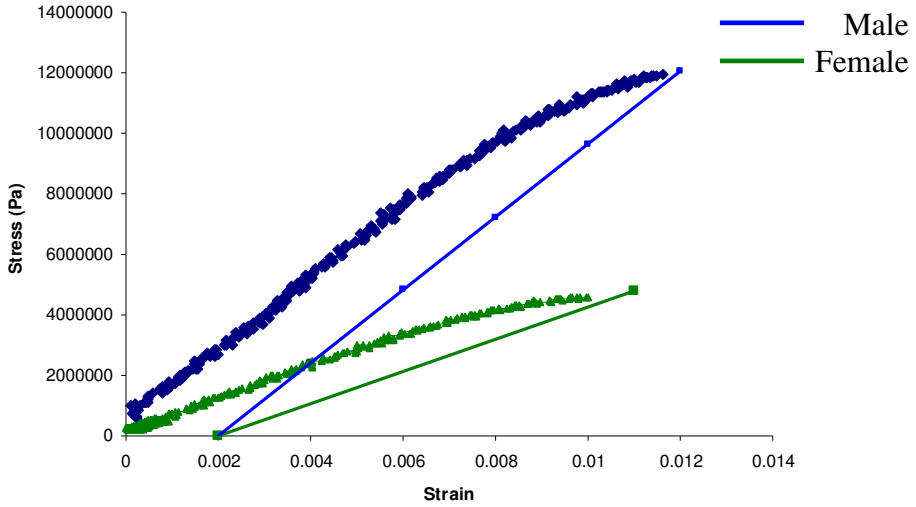

Figure 3.1 Strain yield differences between male and female donors. Using the 0.2% offset method, different strain yields were found in preliminary testing of trabecular bone samples from male and female donors in the distal femur. Sample sizes were small (n=3 donors/group), and additional testing with more donors for gender differences in strain yield points did not replicate these results.

3.2.4 Labeling, identifying, and classifying microdamage

Microdamage was detected using a sequential fluorescent labeling technique (O'Brien et al. 2002; Lee et al. 2003). Prior to mechanical testing, specimens were stained with 0.02% alizarin complexone for 8 hours at 4º C and atmospheric pressure to label pre-existing microdamage. Pre-existing microdamage included damage created from specimen extraction, exposed calcium in resorption cavities created during bone remodeling, and microdamage sustained *in vivo* prior to death. To improve stain penetration, marrow was removed from specimens prior to staining (WP-72W, WaterPik,

USA) and the top endcap was attached only after staining with alizarin complexone. After mechanical testing, the top endcap was carefully removed from samples using a diamond saw (Isomet 1000, Buehler Ltd., USA) to improve stain penetration. Specimens were then stained with 0.005% calcein for 8 hours at 4º C and atmospheric pressure to label microdamage incurred from mechanical testing.

After staining, specimens were dehydrated in a series of graded alcohols and embedded in methyl methacrylate (MMA). Prior to embedding, specimens were secured in custom alignment fixtures to facilitate registration of histological sections to corresponding micro-CT sections for the same specimen. MMA blocks were sectioned into 150-200 μm thick longitudinal slices on a diamond saw and mounted with Eukitt's mounting medium (EM Sciences, USA) onto glass slides.

Microdamage was assessed using 100X magnification (optical resolution: 1.11 μm) in the central four histology sections from each sample. The microdamage analysis region omitted trabeculae immediately adjacent to specimen edges to exclude trabeculae damaged by the coring process or end-cap removal. Pre-existing microdamage area was quantified with grayscale images taken under red epifluorescence. Test-induced microdamage area was quantified with grayscale images taken under green epifluorescence (Image-Pro Plus, Media Cybernetics, USA).

Microdamage was identified based on the criteria that cracks are intermediate in size (larger than canaliculi but smaller than vascular channels), have sharp borders, and a focus plane demonstrating depth of field (Burr et al. 1990; Huja et al. 1999). A classification system published by Moore and Gibson was modified to group test-induced damage into three morphological categories: severe, linear, and diffuse damage (Arthur

Moore et al. 2002; O'Neal et al. 2010). Severe damage was classified as either microdamage consisting of one primary crack with minor secondary cracks or through-thickness cracks, linear damage included both single and parallel cracks, and diffuse damage consisted of cross-hatch damage that was either equal in length and intensity (to distinguish it from severe damage) or damage with a large area of distribution (Figure 3.2).

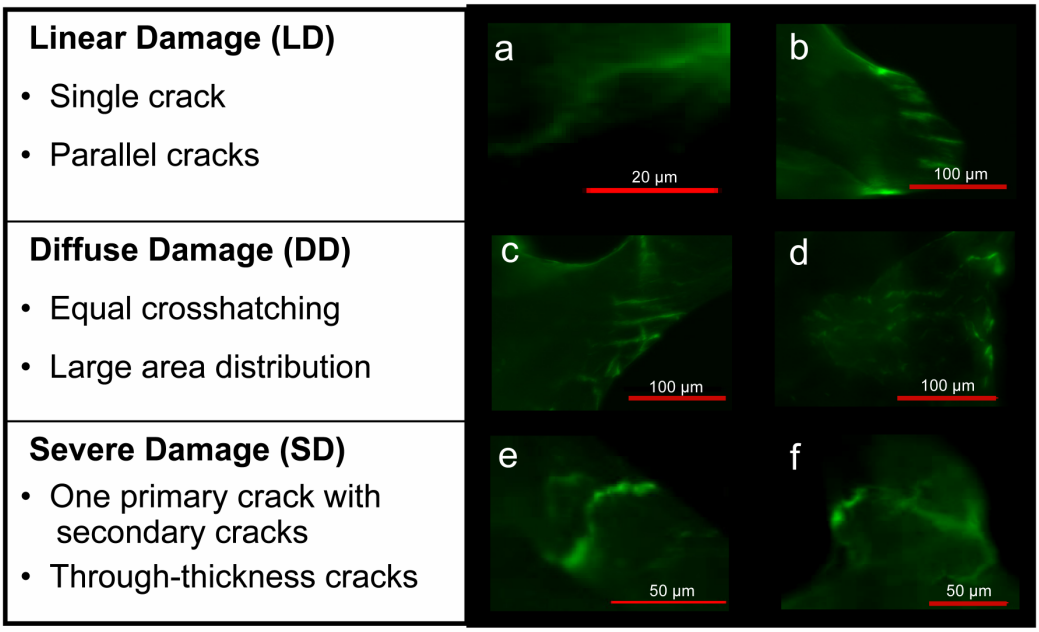

Figure 3.2. **Description of Microdamage Morphological Categories.** Damage was separated into three categories based on morphology. Bullet points indicate metrics used to categorize individual trabeculae.

Trabeculae exhibiting calcein-stained damage only were selected for finite element analysis (n=100 total trabeculae per age group). In the young female group, 44 severe, 20 linear, 17 diffuse, and 19 undamaged trabeculae were analyzed. In the old female group, 39 severe, 13 diffuse, 22 linear, and 26 undamaged trabeculae were

analyzed. In the old male group, 72 severe, 71 diffuse, 104 linear, and 26 undamaged trabeculae were analyzed.

3.2.5 Finite element analysis

Micro-CT images were used to create 3-D high-resolution finite element (FE) models for estimating the local stress and strain distributions (FEA software, Scanco Medical, Basserdorf, Switzerland). After thresholding the micro-CT images, individual voxels within the images were directly converted into 4-6 million hexahedral finite elements by assigning nodal connectivity and bone tissue properties. Approximately six voxels (21 μm/voxel) spanned the mean trabecular thickness, which provided accurate solution convergence (Guldberg et al. 1998). A conjugate gradient solver with an element-by-element matrix vector multiplication scheme allowed for the estimation of tissue-level stresses and strains (Van Rietbergen et al. 1996). A homogeneous linear isotropic analysis was utilized, and a Poisson's ratio of 0.3 was assumed.

The tissue modulus was back-calculated to match the apparent modulus obtained during testing of the specimens (Van Rietbergen et al. 1995). The back-calculated tissue moduli for the pre-menopausal group were 9.6 GPa (32 year old), 9.2 GPa (37 year old) and 10.7 GPa (37 year old). The back-calculated tissue moduli for the post-menopausal group were 10.5 GPa (71 year old), 10.3 GPa (76 year old) and 9.5 GPa (80 year old). The back-calculated tissue moduli in the older male group were 10.4 GPa (78 year old), 13.2 GPa (77 year old), and 11.5 GPa (68 year old). Boundary conditions simulating a 0.9% uniaxial compressive strain in female bone samples and 1.2% strain in male bone samples were applied to models to match the loading conditions in mechanical testing. Von Mises equivalent stresses/strains and maximum compressive principal

stresses/strains were extracted from the FE analysis. Microdamaged and undamaged trabeculae identified under green epifluorescence were then visually registered to the same trabeculae within the finite element models (demonstrated for the female group in Figure 3.3 for damaged and Figure 3.4 for undamaged), and average stress within each extracted trabecula was calculated.

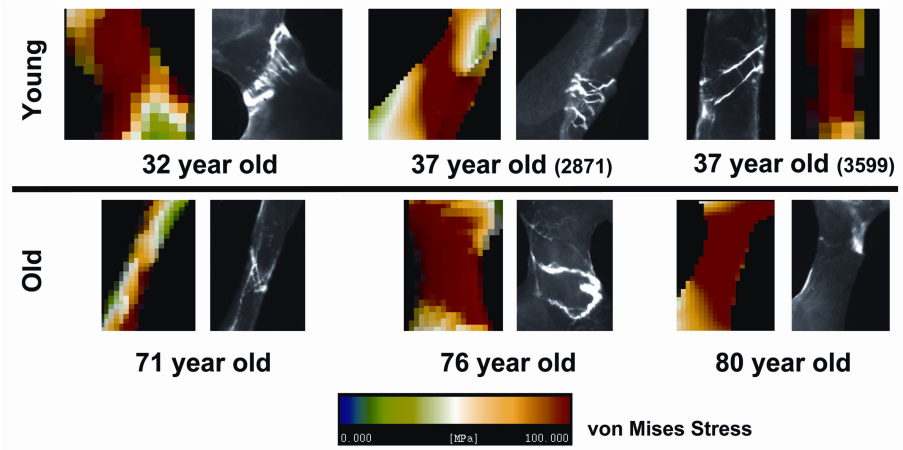

Figure 3.3. Representative microdamaged trabeculae extracted from histology sections and homogeneous finite element models (von Mises effective stress shown) for young and old donors.

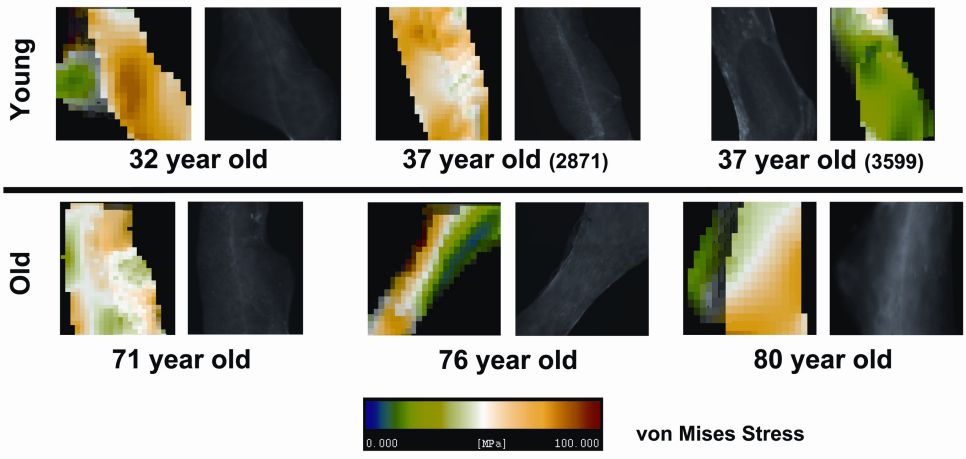

Figure 3.4. Representative undamaged trabeculae extracted from histology sections and homogeneous finite element models (von Mises effective stress shown) for young and old donors.

3.2.6 Statistics

One-way ANOVA was used to determine interdonor global architectural differences in each group. Interdonor differences were not significant for most architectural parameters (BV/TV, degree of anisotropy, SMI, trabecular number, and mineralization). Among older female donors, trabecular spacing was significantly different ($p=0.04$). Among younger female donors, trabecular thickness ($p=0.04$) and connectivity ($p=0.05$) were significantly different. Among older male donors, BV/TV ($p=0.03$), trabecular thickness ($p=0.002$), and trabecular spacing ($p=0.02$) were significantly different. Trabecular number, degree of anisotropy, SMI, mineralization, and connectivity were similar.

T tests were performed to determine statistically significant differences between age groups for the global architectural parameters reported in Table 3.1 after verifying normality. For comparisons of microstructural mechanical and architectural factors by damage category and age or sex, Kruskal-Wallis nonparametric tests with Mann-Whitney post-hoc pairwise comparisons were run for each combination of damage category and age or sex group to determine significant differences in the interaction. Since this approach may increase the probability of committing a Type I error, a Bonferroni correction was applied to the alpha level for pairwise comparisons within mechanical factors (VM and principal stress and strain) and architectural factors (mineralization, SMI, thickness, and orientation). This reduces the significance level of the tests to 0.0125. All values are reported as mean ± standard error.

3.3 Results

3.3.1 Global Architectural Comparisons by Age and Sex

Analysis of the global architectural characteristics of the trabecular specimens by micro-CT evaluation showed that older men and women were similar in their bone volume fraction, trabecular thickness, degree of anisotropy, SMI value, trabecular number, trabecular spacing, and connectivity density. Mineralization was higher in men compared with women (Table 3.1, $p<0.001$).

Global trabecular microarchitecture between younger and older women was similar for most architectural parameters (Table 3.1). There was a trend for increased trabecular number ($p=0.07$) and decreased trabecular spacing ($p=0.10$) in younger women. Trabecular bone from younger women contained more redundant struts compared to bone from older women ($p=0.01$), and average mineralization for the younger specimens was significantly lower ($p<0.001$) compared to older specimens.

Table 3.1. Global Architecture and Mineralization Comparisons by Age and Sex

Parameter	Young Female	Old Female	Old Male
Bone Volume Fraction	0.212 (0.012)	0.198 (0.021)	0.180 (0.017)
Trabecular Thickness (μm)	153.9 (12.0)	153.3 (9.0)	161.5 (9.9)
Degree of Anisotropy	1.87 (0.14)	2.00 (0.13)	1.79 (0.14)
Structural Model Index	1.03 (0.11)	0.93 (0.14)	1.03 (0.11)
Trabecular Number (mm^{-1})	1.57 (0.04)	1.45 (0.07)	1.40 (0.10)
Trabecular Spacing (mm)	0.58 (0.02)	0.64 (0.03)	0.69 (0.05)
Connectivity Density (mm^{-3})	7.21 (0.54)$^{\$}$	5.17 (0.62)$^{\$}$	5.57 (1.06)
Mineralization (mg HA/cc)	1022.0 (7.5)*	1062.8 (6.7)*+	1144.4 (6.0)+

*,+,$^{\$}$ indicates where pairwise comparisons between groups achieved significance ($p<0.01$)

3.3.2 Microstructural Stress/Strain Differences by Sex

In preliminary testing, the strain yield for women was determined to be 0.9% and 1.2% for men. In order to directly compare microstructural stresses/strain values

obtained from finite element modeling between the groups subjected to different strain endpoints, results were normalized to the maximum apparent stress/strain applied during the mechanical test resulting in a stress/strain amplification value. In other words, the resulting normalized stress/strain values reflect the degree of amplification of the trabecular mechanical value relative to the applied stress or strain.

Microstructural von Mises and principal stresses showed similar results (Figure 3.5 a and b). A significant difference in the stress amplification between severe and undamaged trabeculae was found in the female group ($p<0.01$). When microstructural von Mises and principal strain amplification was analyzed, a gender-related difference was observed for severely damaged trabeculae. Severely damaged trabeculae from men were associated with a decreased microstructural strain/apparent strain ratio than women ($p<0.01$). Differences within each gender group demonstrated significantly greater normalized strains in severe compared with undamaged trabeculae (Figure 3.6 a and b).

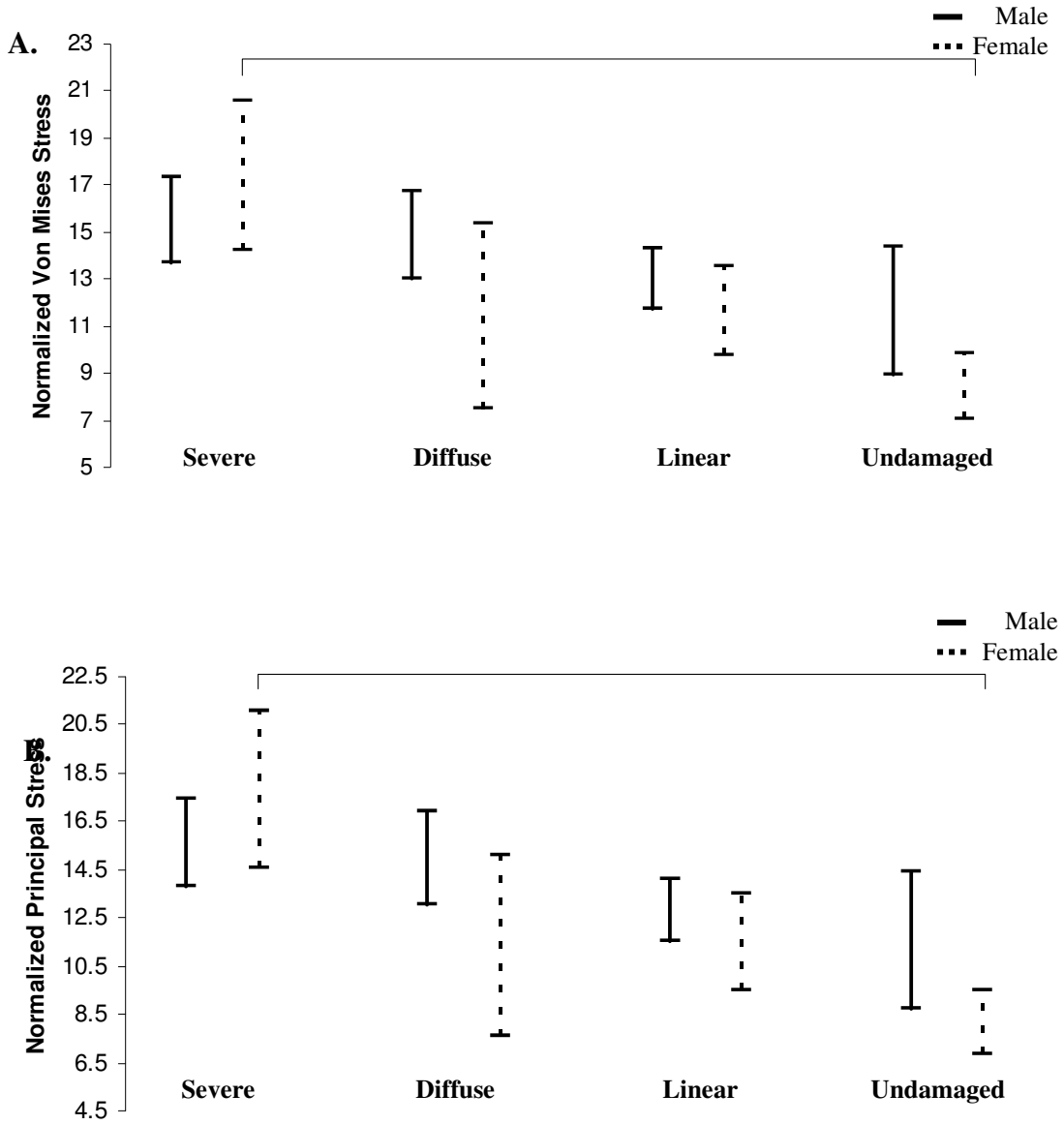

Figure 3.5. The 95% CI for normalized damage initiation stress levels by gender. A significant difference in the **3.5a**. von Mises and **3.5b**. principal stress amplification level of severely damaged trabeculae relative to undamaged in older females is observed. Bars indicate significant differences, $p<0.01$

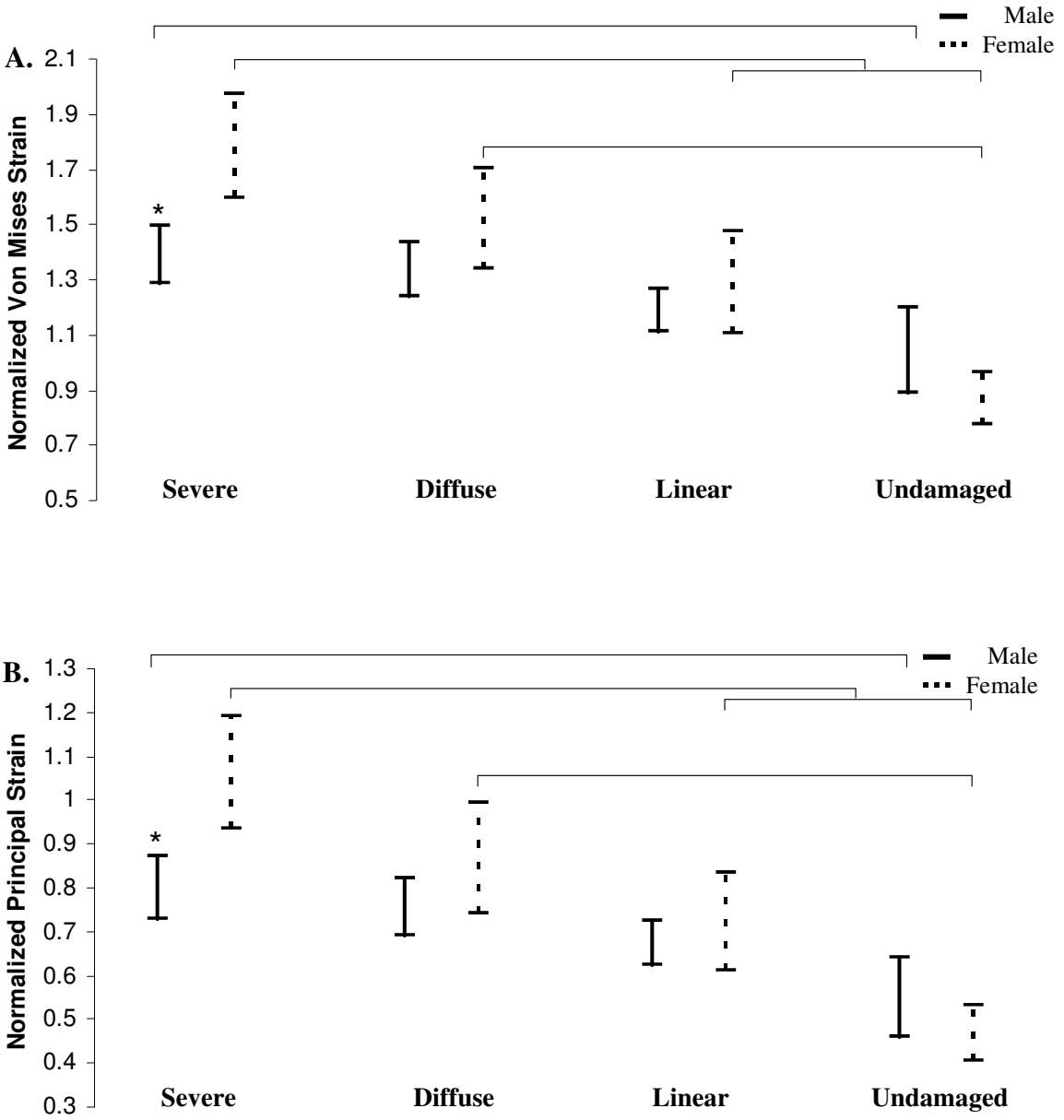

Figure 3.6. The 95% CI for normalized damage initiation strain levels by gender. For both **3.6a.** von Mises and **3.6b.** principal strain, severely damaged trabeculae in older males was significantly decreased compared with older females. Severely damaged trabeculae were also more strained than undamaged in both sexes. Bars indicate significant differences, $p<0.01$

3.3.3 Microstructural Stress/Stain Differences by Age

Differences in microstructural stresses and strains were found among damaged trabeculae between younger and older women. Severely damaged trabeculae possessed significantly higher von Mises and principal stresses than linear and undamaged trabeculae (Figure 3.7 a and b, $p<0.001$) in both the young and old age groups. In older subjects, undamaged trabeculae were under significantly lower von Mises and principal stress than all other damage types ($p<0.001$). A significant decrease in the von Mises stress of undamaged trabeculae in older donors compared to undamaged younger donors was observed. ($p<0.01$) and approached significance in the principal stress data ($p=0.014$).

Analysis of von Mises and principal strains revealed similar relationships to the stress results. In both the young and old age groups, severely damaged trabeculae possessed von Mises and principal strains that were significantly greater than linear and undamaged trabeculae (Figure 3.8 a and b, $p<0.003$). Diffusely damaged trabeculae in younger women had greater von Mises and principal strains than linearly damaged and undamaged trabeculae ($p<0.01$). In the older female age group, undamaged trabeculae were under less strain (von Mises or principal) compared with all other damage types ($p<0.003$). Among undamaged trabeculae, the older female group was under less strain than the younger female group for both strain measures ($p=0.014$ for principal strain, $p=0.013$ for von Mises strain).

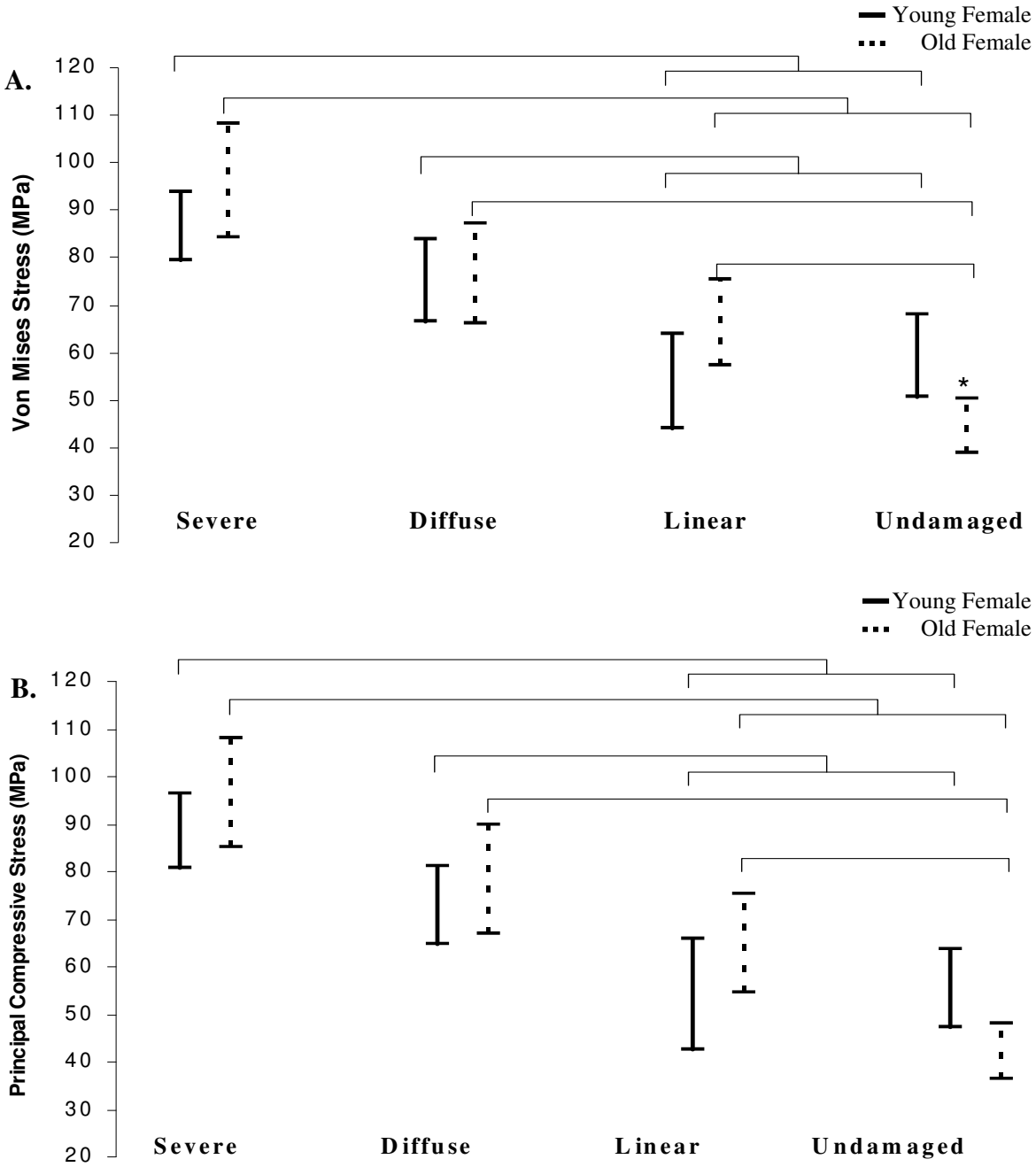

Figure 3.7. The 95% confidence intervals for 3.6a. von Mises and 3.7b. principal compressive stress initiation ranges calculated by damage category. A significantly greater stress range is demonstrated in young, undamaged trabeculae compared with old, undamaged trabeculae. Significant increases are also seen in the stress state of severely damaged trabeculae compared to linear and undamaged trabeculae in both age groups. Bars indicate significant differences ($p<0.01$).

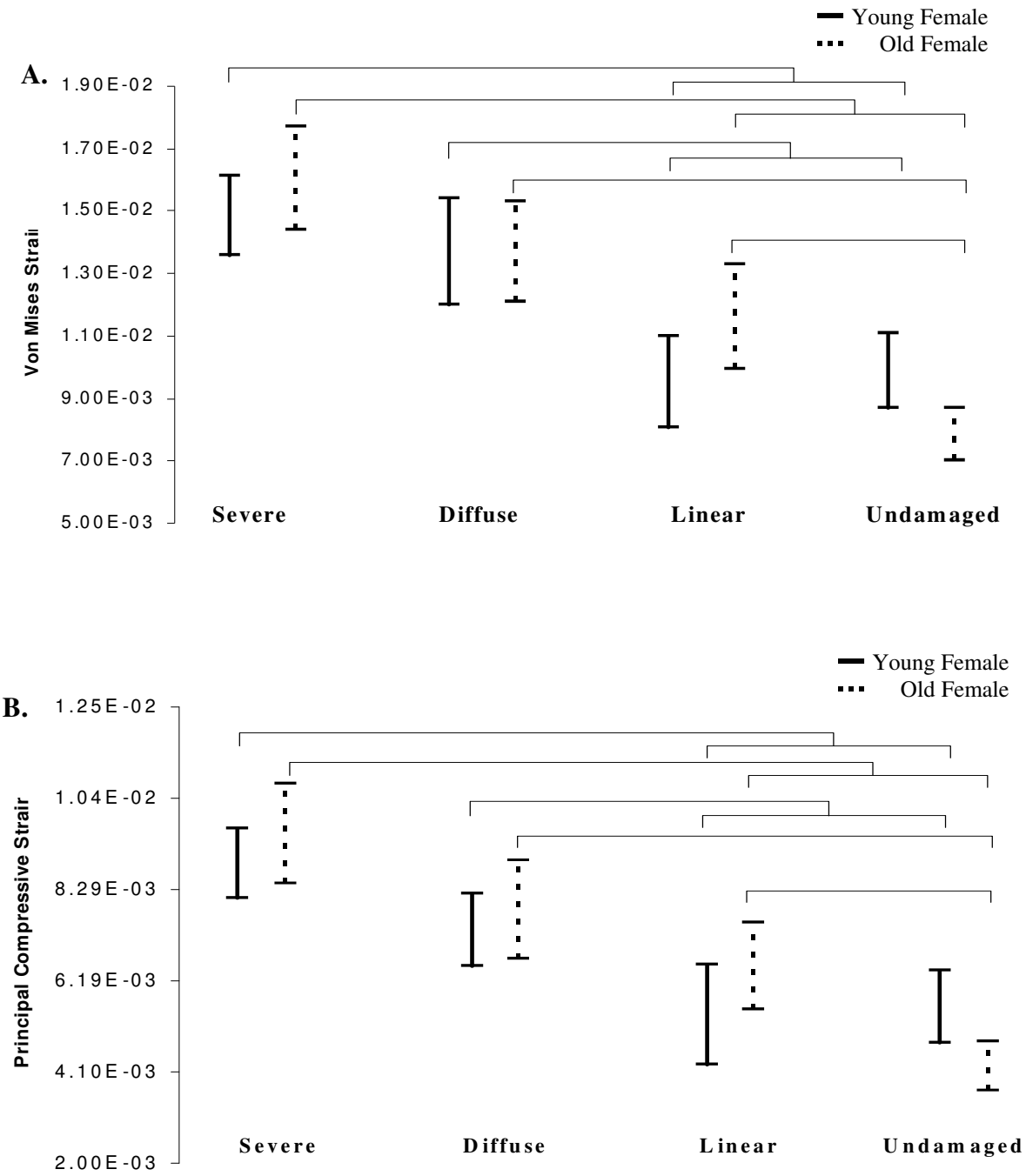

Figure 3.8. The 95% confidence intervals for 3.8a. von Mises and 3.8b. principal compressive strain initiation ranges calculated by damage category. Significant increases were seen in the strain state of severely damaged trabeculae compared to linear and undamaged trabeculae in both age groups. Bars indicate significant differences ($p \leq 0.01$).

3.3.4 Microarchitectural Differences by Sex

Architectural characteristics of damaged and undamaged trabeculae were analyzed and compared between the two gender groups. Mineralization values were increased for all damage categories in the male group compared with females ($p<0.01$), but no differences were found between damage categories (Figure 3.9a). Diffusely damaged trabeculae were significantly thicker than linearly damaged and undamaged trabeculae in the male group (Figure 3.9b, $p<0.01$). In the female group, severely damaged trabeculae were oriented closer to the loading axis compared with undamaged trabeculae (Figure 3.9c, $p<0.01$), but no such relationship was observed for male bone samples. No relationship between damage type and structural model index was found within or between gender groups (Figure 3.9d).

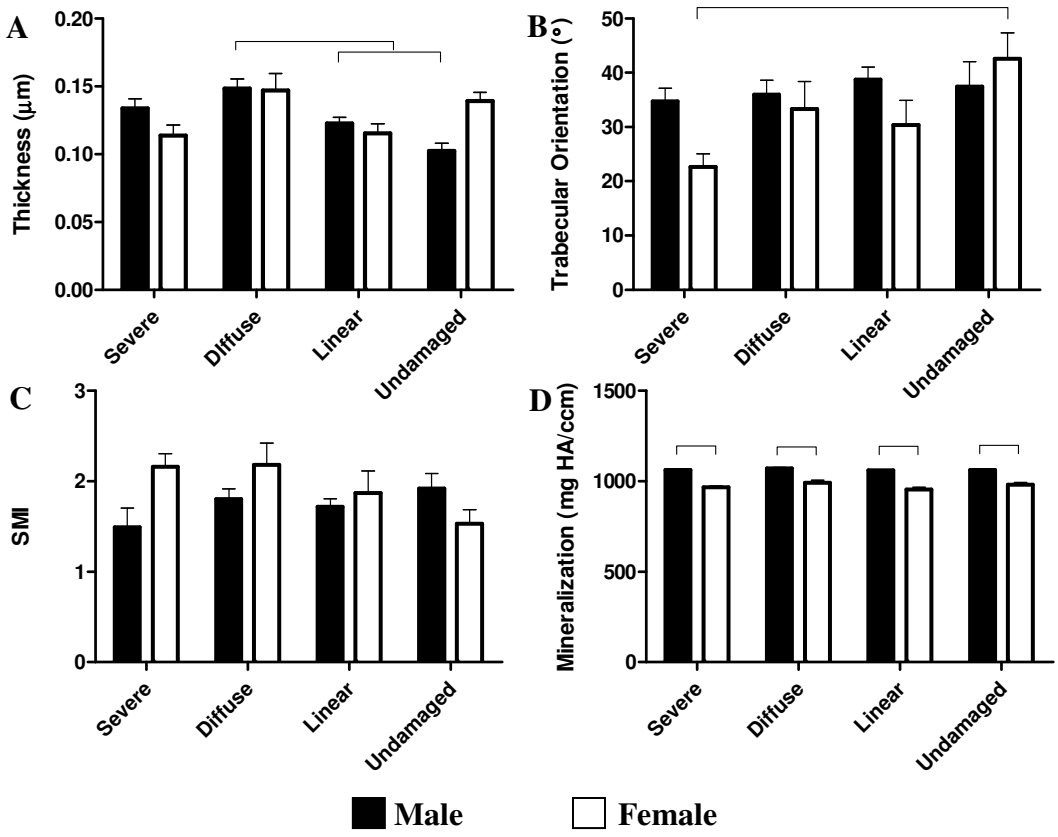

Figure 3.9. Trabecular bone microarchitecture and mineralization by gender. **3.9a.** Diffusely damaged trabeculae in males were significantly thicker than linear and undamaged trabeculae. **3.9b**. Severely damaged trabeculae in the female group were oriented closer to the loading axis than undamaged trabeculae. **3.9c**. No significant differences in SMI were found. **3.9d.** Male trabeculae were significantly more mineralized in all damage categories compare with female trabeculae. Bars indicate significant differences, $p<0.01$.

3.3.5 Microarchitectural Differences by Age

Individual trabeculae which underwent micromechanical analysis were also characterized by their structural model index (SMI), trabecular orientation, trabecular thickness, and mineralization to determine whether damaged trabeculae possessed different microarchitecture than undamaged trabeculae (Figure 3.10). Analysis of the SMI showed that severely damaged trabeculae are more rod-like than undamaged trabeculae in both pre- and post-menopausal groups ($p<0.003$, Figure 3.10a). Trabecular orientation was assessed to determine whether damage preferentially occurred in trabeculae oriented at particular angles from the loading axis (Figure 3.10b). In older samples severely damaged trabeculae were more commonly oriented along the longitudinal axis of the specimen in line with the loading axis ($p<0.01$). In younger samples linearly damaged trabeculae were at a significantly greater angle compared to the loading axis than both severe ($p<0.001$) and diffusely damaged ($p=0.001$) samples. When trabecular thickness was examined, severely damaged trabeculae in the older age group were significantly thinner than undamaged trabeculae ($p<0.01$). In the pre-menopausal group, severely damaged trabeculae were thinner than linearly damaged trabeculae ($p<0.01$, Figure 3.10c). Local mineral density was evaluated (Figure 3.10d), and severe, diffuse, and undamaged trabeculae were significantly more mineralized in the older age group compared to the younger age group ($p<0.001$).

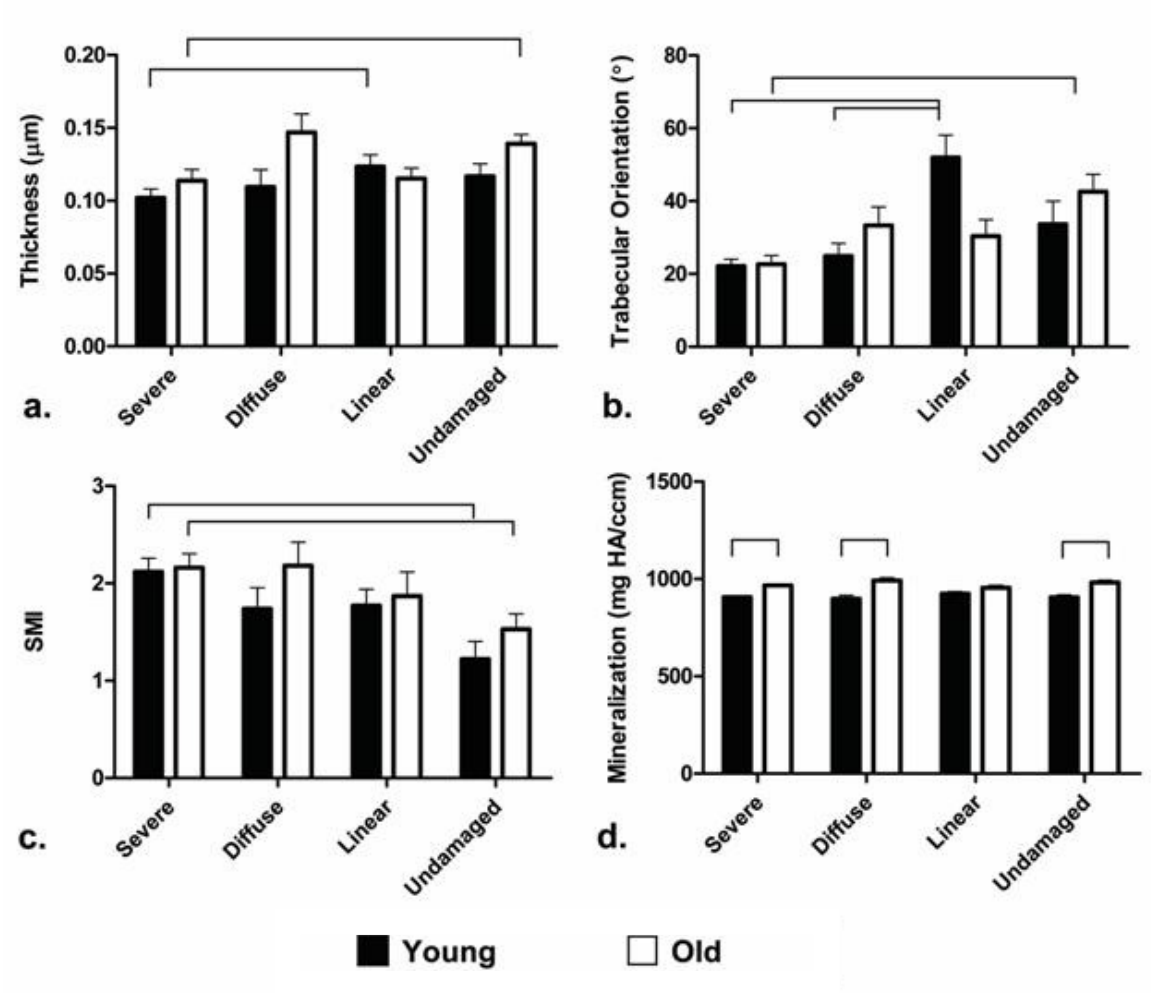

Figure 3.10. Trabecular bone microarchitecture and mineralization for young (32-37 year old) and old (71-80 year old) age groups. **3.10a**. Trabecular thickness is plotted, indicating that severely damaged trabeculae are thinner than undamaged in the older age group, and thinner than linearly damaged trabeculae in the younger age group ($p<0.01$). **3.10b**. Trabecular orientation relative to the loading axis is plotted, indicating that in the older age group, trabeculae aligned more acutely with the loading axis are more likely to sustain severe damaged compared to undamaged trabeculae. **3.10c**. SMI is plotted, showing more rod-like trabecular architecture in severely damaged trabeculae compared to undamaged trabeculae in both groups ($p<0.01$). **3.10d.** In severely damaged, diffusely damaged, and undamaged trabeculae, the trabecular mineralization was significantly increased in the post-menopausal group ($p<0.01$).

3.3.6 Microdamage Quantification Differences by Sex

Pre-existing damage incidents were counted from male and female donors. Levels of pre-existing damage were not different between the sexes (females: 1.5 ± 0.1 incidents/mm^2, males: 1.1 ± 0.1 incidents/mm^2). Among pre-existing damage types, linear microdamage was most prevalent (0.63 ± 0.05 incidents/mm^2 in males, 0.71 ± 0.08 incidents/mm^2 in females), significantly greater than the severe morphology in both males (0.19 ± 0.03 incidents/mm^2, $p<0.001$) and females (0.14 ± 0.03 incidents/mm^2, $p<0.001$) and greater than diffuse damage levels in males as well (0.33 ± 0.04 incidents/mm^2, $p<0.002$). Levels of test-induced damage (0.80 ± 0.1 incidents/mm^2 in males vs 1.52 ± 0.1 incidents/mm^2 in females, $p<0.001$) and damage demonstrating both fluorophores (0.72 ± 0.1 incidents/mm^2 in males vs 1.50 ± 0.2 incidents/mm^2 in females, $p<0.001$) were significantly greater in females compared with males.

3.3.7 Microdamage Quantification Differences by Age

The number of pre-existing severe and diffuse damage incidents was significantly greater in the older group (0.14 ± 0.03 and 0.64 ± 0.09 incidents/mm^2, respectively) than the younger group (0.03 ± 0.01 and 0.23 ± 0.04 incidents/mm^2, respectively; $p<0.003$). The number of pre-existing linear damage incidents was not different (0.71 ± 0.09 incidents/mm^2 in the older group vs. 0.64 ± 0.05 incidents/mm^2 in the younger group). Levels of severe, linear, and diffuse test-induced damage in the older group (0.48 ± 0.08, 1.67 ± 0.1, 0.82 ± 0.09 incidents/mm^2, respectively) was not significantly different from the younger group (0.59 ± 0.09, 2.03 ± 0.17, 1.03 ± 0.1 incidents/mm^2, respectively). Levels of damage demonstrating both fluorophores were very similar between age groups

(1.4 ± 0.16 incidents/mm^2 in the younger group vs 1.5 ± 0.23 incidents/mm^2 in the older age group).

3.4 Discussion

In this study, the stress and strain state of damaged and undamaged trabeculae from three groups, younger females, older females, and older males were compared to investigate whether age or gender-related differences existed in the micromechanical loading environment associated with microdamage initiation. Trabecular bone cores were stained with two calcium-chelating fluorescent dyes to separate *in vivo* damage from damage incurred from uniaxial compression loading to the yield strain (0.9% for women, 1.2% for men). Trabeculae exhibiting test-induced damage only were registered to solutions of principal and von Mises stresses and strains obtained from linear image-based finite element analysis. Results suggest that microdamage morphology is highly dependent on both the stress and strain magnitude, and that trabecular bone from younger women may be able to sustain higher stresses/strains without damaging compared with trabecular bone from older women. Furthermore, trabeculae developing severe damage may undergo significantly less relative deformation in older men compared with older women.

It is unclear whether a stress or strain-based criterion for damage initiation is most appropriate, and whether shear forces are important. In our study of aging effects on damage initiation, stress values were scaled using a back-calculated tissue modulus unique to each trabecular bone sample. We obtained a similar average tissue modulus between age groups (9.8 GPa for the older female group vs 10.2 GPa for the younger female group), so our corrections had a small impact on the age-related stress differences.

However, in the only age-related difference found among undamaged trabeculae, we observed the greatest differences using von Mises stress to characterize the micromechanical environment. Others have used von Mises stress to define microdamage formation and character, and the association between shear forces and cross-hatched damage morphology has been documented. (Fyhrie et al. 2000; Yeni et al. 2003; Yeni et al. 2008) Thus stress-based criteria with shear factors may be more sensitive to differences between groups than strain-based criteria, depending on the magnitude of the difference between tissue-level stiffness.

In our investigation of gender effects on microdamage initiation, differences in yield strains between males and females required microstructural stress and strain estimations to be normalized by the maximum strain and stress applied in order to compare between groups. In the stress data, no differences between genders were noted after accounting for differences in tissue-level stiffness (male: 11.5 GPa MPa vs female: 9.8 GPa). A statistically significant decrease in the strain amplification value for severely damaged trabeculae was found in male bone compared to female bone. This would suggest that trabecular struts in men underwent less deformation relative to the total structural deformation prior to fracture than female bone, and is supported by trabecular mineralization data which showed greater mineralization in all damage types in male donors. However, this difference may also be a result of the normalization by strain yield; since strains in female donors were normalized by a value less than 1, and strains in male donors were normalized by a value greater than 1, small strain differences were accentuated. To confirm these results, additional testing at the same strain yield in bone from donors with similar mechanical properties should be done.

We found that the older group had significantly increased levels of pre-existing damage compared with the younger group, but incidents of test-induced damage were actually higher in the younger group compared to the older group. These results indicate that pre-existing damage has an effect on subsequent damage formation, and has implications for our conclusions. Although the stress and strain values reported were obtained only for *de novo* damage, stress values were scaled according to the back-calculated tissue modulus. The fact that older bone had more pre-existing damage than younger bone results in an unequal deviation from the undamaged stiffness values between the age groups, meaning that the mechanical properties of our undamaged trabeculae in the old group may be underestimated, while the mechanical properties of the damaged trabeculae may be overestimated. Applying a correction would shift undamaged stress values upwards, and decrease damaged stress values, lessening the differences between the groups. Since the levels of pre-existing damage were similar between the older male and female groups, however, there would be no such effect on the stress values reported between older males and females. Additionally, strain values would also be unaffected as they are not dependent on the back-calculated tissue modulus.

Analyses into local trabecular architecture of older females revealed that damage severity correlated with trabeculae that were thinner, more rod-like, and oriented closer to the loading axis than their undamaged counterparts. Incorporating these results with local stress/strain data, we observed that damaged trabeculae have higher stresses in part because they are thinner, more slender, and oriented closer to the loading axis. Architectural differences appeared to have less an effect on damage formation in younger

females and older males. In addition, consistent with previous studies, we demonstrated that mineralization increases with age. (Paschalis et al. 1997; Boskey et al. 2005; McNamara et al. 2005)

Several important limitations must be considered when interpreting our data. We analyzed replicates from each donor due to the dependence of mechanical parameters on location within the distal femur. In order to obtain averages of tissue level behavior, we created a balanced design in which equal numbers of cores near the cortex and medullary cavity were analyzed. In statistical analyses, damage incidents were considered independent events because all models were linear and did not consider effects of evolving stresses of neighboring trabeculae on the loading environment. The donor effect is therefore random, and accounting for random factors associated with donors in ANOVA analysis did not affect outcomes. While this strategy allowed us to simultaneously examine trabeculae possessing a wide range of architectural characteristics, more samples from different donors should be analyzed in order to make stronger conclusions about the general population. Another limitation of our study is the use of a linear FE model, which may impact the magnitude of stresses and strains reported. Non-linear trabecular yielding at the microstructural level would be expected to affect severely damaged trabecular behavior and stress distribution. As this population represented a small percentage of total trabeculae (less than 1%), errors due to linear assumptions are not great enough to alter conclusions of the study. A further limitation is the use of different strain yields in gender groups. Additional testing with more donors did not replicate the strain yield differences in this study; therefore, results are not applicable to gender population differences.

In conclusion, this study has demonstrated that microstructural stress and strain magnitude is highly associated with the formation of microdamage of different morphologies in three different groups: young females, old females, and old males. Trabecular stresses in undamaged trabeculae of older women were lower compared to younger women, suggesting that the threshold for damage initiation may be reduced in this group. Also, strains associated with severely damaged trabeculae in men were significantly reduced compared to age-matched women. Studies in bone from a larger number of donors need to be conducted to further explore the conclusions from this study.

CHAPTER 4

INCREASED NUMBERS OF PROPAGATING SEVERE DAMAGE INCIDENTS CONTRIBUTES TO DECREASED FATIGUE LIFE IN OLDER WOMEN

4.1 Introduction

Fatigue microdamage of trabecular bone is formed after repeated loading in daily activities. (Burr et al. 1985) Damage formation is not necessarily pathologic; microdamage effectively dissipates strain energy within normal loading ranges and limits the development of more serious fractures at sites of high stress. (Vashishth et al. 1997) Due to remodeling mechanisms, microdamaged regions of trabeculae are targeted for repair, thus preserving the structural integrity of the trabecular lattice. (Burr et al. 1985) With aging, however, targeted remodeling processes diminish, allowing fatigue microdamage to accumulate. (Schaffler et al. 1995; Allen 2008) While isolated areas of linear crack accumulation have been shown to increase fatigue life, significant damage accumulation lowers stiffness and increases the probability of fracture. (Burr et al. 1998; Sobelman et al. 2004)

Morphological changes to trabeculae, including decreased thickness, increased spacing, loss of connectivity, increased anisotropy, and increased bone age and mineralization contribute to the deterioration of bone strength and stiffness and can promote microdamage formation and propagation. (Burr et al. 1997) Extensively damaged trabeculae are resorbed by targeted remodeling mechanisms, which increase the probability of failure – loss of a few trabeculae has a large impact on strength and stiffness. (Guo et al. 1994; Burr 2002) The effect of microdamage progression on

toughness changes with age has been studied extensively in cortical bone, (Schaffler et al. 1995; Vashishth et al. 1997; Norman et al. 1998; Vashishth et al. 2000; Zioupos 2001; Zioupos 2001) but less so in trabecular bone. (Seeman 2003; Cook et al. 2009)

In this study, trabecular bone cores from the femoral head of men and women aged 55-81 years were tested in a novel two step mechanical testing protocol in order to investigate the evolution of cracks of different morphologies under cyclic loads. We hypothesize that bone from older individuals will demonstrate decreased resistance to crack propagation, though we do not expect to see differences due to gender.

4.2 Methods

Femoral heads from 10 males and 10 females aged 55-81 years were obtained from the National Disease Research Interchange (NDRI). Donors had no history of bone disease, cancer, or use of medication altering bone morphology. Tissue was removed at autopsy within 12 hours of death and fresh frozen at -80°C. Donors were initially divided into four groups based on gender and age: young males (60.2 ± 3.7 years; mean ± s.d.), old males (77.2 ± 1.5 years), young females (63.0 ± 2.8 years), and old females (72.8 ± 4.8 years). After determining no gender-related differences in any measure, groups were combined to form two groups based on age (younger: 61.3 ± 3.1 years; older: 75.0 ± 3.9 years).

Two trabecular bone cores from each sample (5 mm diameter) were removed from the central portion of the femoral head using a trephine under constant irrigation with physiological saline such that the longitudinal axis was oriented approximately parallel with the material axis. Cores were sized to a final length of 18 mm with a diamond saw. Bone marrow was removed using a water pik (WP-72W, WaterPik, USA)

to improve stain penetration, and the ends of each core were glued with cyanoacrylate (Prism 401, Loctite, Newington, CT, USA) into stainless steel endcaps of 5 mm depth to minimize the effect of end-artifacts on mechanical testing. (Keaveny et al. 1994) Bone specimens were scanned with micro-CT at a voxel resolution of 16 um. (μCT 40, Scanco Medical, Basserdorf, Switzerland) A threshold was chosen to distinguish bone from background for 3D reconstructions and evaluations, and the same threshold was used for all samples. Evaluation of 3D reconstructed images yielded morphological descriptors (bone volume fraction, connectivity density, structural model index, trabecular number, trabecular thickness, trabecular spacing, and degree of anisotropy). Bone mineralization (in mg/cc HA) was computed from attenuation values of grayscale micro-CT images based on hydroxyapatite (HA) calibration standards.

4.2.1 Mechanical Testing

Each trabecular bone core (2 per donor, n=40) was mechanically tested using a two-step process (Figure 4.1). (Mini Bionix 858, MTS Corp.) Throughout the mechanical testing process, specimens were immersed in 0.9% physiological saline and 10 μmol/L protease inhibitor (E-64, Sigma Chemical) to prevent tissue degradation. In the first portion of mechanical testing (Figure 4.1a), cores were preconditioned for 3 cycles to 0.1% strain then loaded in static uniaxial compression at a strain rate 0.5% strain/second to a strain endpoint of 0.8% and held for three hours to create microdamage throughout the specimen.

In the fatigue portion of mechanical testing (Figure 4.1b), samples were first preconditioned for 10 compression cycles under strain control from 0.05% to 0.45% using a sinusoidal waveform at a frequency of 2 Hz. The initial modulus, E_0, was

calculated from the linear best-fit of the 10th loading cycle. Samples were then preloaded to 10 N and underwent compressive fatigue testing to a strain endpoint of 0.8% using a sinusoidal waveform at a normalized stress range ($\Delta\sigma/E_0$) of 0.005 and frequency of 2 Hz. Previous studies have shown that using a normalized stress is advantageous in comparing samples with wide variations in elastic modulus associated with bone volume differences. (Caler et al. 1989; Pattin et al. 1996; Moore et al. 2003) Tests were stopped after reaching a strain level of 0.8%, a point within the linear region of apparent mechanical behavior and below the yield point of 0.9% used in previous studies. (O'Neal 2010) Preliminary testing showed that stopping the test at this level of strain rather than at failure limits the number of severe damage incidents observed, allowing for the study of microdamage progression of linear and diffuse damage morphologies as well as severe morphologies. Also, previous studies have shown that stopping the tests at a predetermined maximum strain rather than at a set number of cycles correlated better with modulus reduction (an indication of damage accumulation), allowing for comparisons of fatigue mechanisms among samples with large strength and stiffness variations. (Moore et al. 2003) A ceiling was placed on the maximum number of cycles (150,000 cycles) after strain ratcheting was no longer observed. The number of cycles; plastic (1st cycle) and residual strain (last cycle); max strain at various time points; and the initial, preload, and final secant moduli were calculated for each specimen. Plastic strain accumulation was measured at the first fatigue loading cycle (after preconditioning).

4.1a. Step 1: Static Uniaxial Compressive Loading under Displacement Control

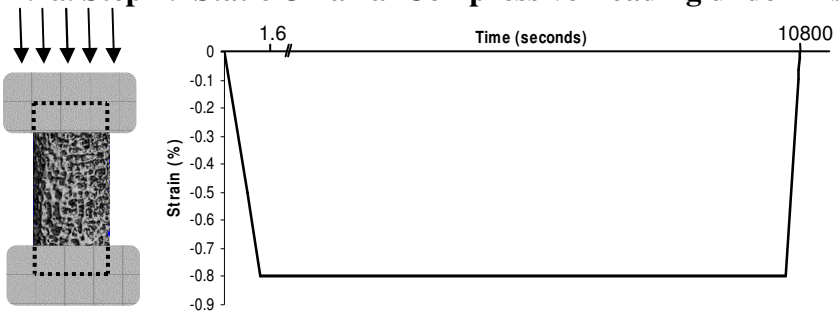

4.1b. Step 2: Cyclic Uniaxial Compressive Loading under Load

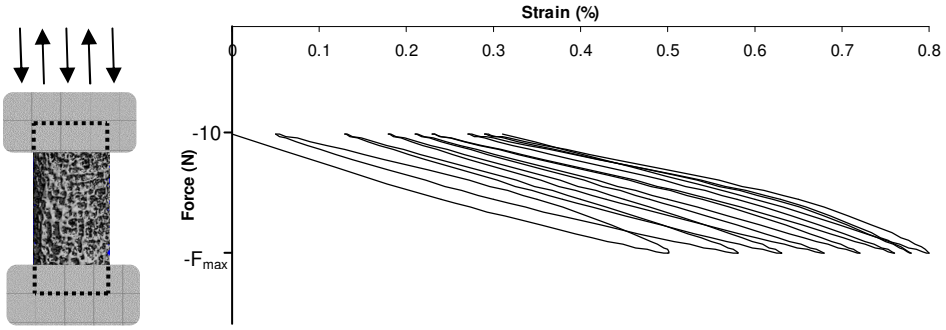

Figure 4.1 Stylized figure demonstrating two-step mechanical testing protocol. 4.1a. Part one of the mechanical testing protocol induced damage formation by compressing samples uniaxially to a strain end-point of 0.8%. **4.1b**. Part two of the mechanical testing protocol allowed for microdamage progression by cyclically compressing samples uniaxially between -10 N and a maximum force calculated at a normalized stress level ($\Delta\sigma/E_0$) of 0.005. The test ended when a strain of 0.8% was reached.

A two-step staining protocol with chelating fluorophores allowed for the study of changes in microdamage size and morphology between each portion of the mechanical test. (O'Brien et al. 2003) One core from each donor (n=20) was stained with 0.02% alizarin plus 10 μmol/L protease inhibitor at atmospheric pressure and 4°C for 8 hours after completion of the static loading portion of the mechanical test. Samples were stained again with 0.01% calcein after the cyclic loading portion of the mechanical test which labeled damage progression or *de novo* damage created in the fatigue portion of the mechanical test. (O'Brien et al. 2002) Microdamage analysis was chosen among

cores most similar in gross morphological parameters (Table 4.1). At the completion of mechanical testing and staining, cores were fixed in 70% ethanol for 24 hours then dehydrated using a graded alcohol infiltration procedure. Cores were embedded in methyl methacrylate and 6 slides of 100-150 μm thickness were cut along the longitudinal axis with a diamond saw.

4.2.2 Microdamage Analysis

Investigators were blinded to the demographic group of each sample for the microdamage analysis. Three slides from each core corresponding with the middle section of the cylindrical sample were evaluated, and the microdamage analysis region omitted trabeculae immediately adjacent to specimen edges to exclude trabeculae damaged by the coring process or end-cap removal. Microdamage was assessed at 100x and identified based on criteria that cracks are intermediate in size (larger than canaliculi but smaller than vascular channels), have sharp borders, and have a focus plane demonstrating depth of field. (Burr et al. 1990; Huja et al. 1999) Alizarin-labeled damage, encompassing damage formed during the static-loading portion of the mechanical test as well as *in vivo* damage and incidental damage from the core extraction, was counted under red epifluorescence. Calcein-labeled damage, including damage created *de novo* in the fatigue portion of the mechanical test as well as crack growth from initial alizarin-labeled damage, was counted under green epifluorescence. (O'Brien et al. 2002) Cracks exhibiting both alizarin and calcein fluorescence were evaluated from a composite image generated from two images of the damage incident under each filter. In all, over 1300 damage incidents were counted. Damage counts were normalized by bone slide surface area obtained with image analysis software.

(Axiovision, Zeiss Corportation, USA) Microdamage was classified into severe, diffuse, or linear morphological categories based on previously published criteria (Figure 4.6a, 4.7a, and 4.8a). (O'Neal et al. 2010) Propagated damage was classified based on whether alizarin and calcein-labeled damage areas were completely overlapping (contained), or whether the calcein-labeled areas extended beyond the initial alizarin-labeled damage area. Linear damage length and diffuse and severe damage area were measured using image analysis software. (Axiovision, Zeiss Corporation, USA)

4.2.3 Statistics

All statistical tests were conducted using Minitab statistical software. Global architectural differences, number of cycles, differences in modulus, and plastic and residual strain were evaluated for age group differences with two way ANOVA using age group as a fixed factor and specimen donor as a random factor. Differences in modulus within each age group at different points in mechanical testing were obtained with two-way ANOVA using the modulus as a fixed factor and specimen donor as a random factor. Tukey post-hoc pairwise comparisons were made between the three modulus time points.

Three-way ANOVA and Tukey post-hoc comparisons were used for evaluating differences in crack density, crack propagation density, and length/area changes using age group and damage type as fixed factors and specimen donor as a random factor. For all tests, $p<0.05$ was considered statistically significant.

4.3 Results

No differences due to gender were noted for any comparisons, so gender groups were combined and comparisons were made between younger and older groups (younger: 61.3 ± 3.1 years; older: 75.0 ± 3.9 years). Gross morphological properties are reported

for all mechanically tested samples (two cores/donor, n=40) and microdamage-assessed samples (one core/donor, n=20). An assessment of the global architectural properties of the trabecular bone samples revealed no significant differences between groups (Table 4.1).

Table 4.1 Architectural Characteristics of Trabecular Bone Samples by Age Group

Parameter	All Samples		Microdamage-Assessed Samples	
	Younger	Older	Younger	Older
Bone Volume Fraction	0.27 ± 0.02	0.23 ± 0.01	0.25 ± 0.02	0.23 ± 0.02
Connectivity Density	8.26 ± 0.64	7.09 ± 0.56	7.71 ± 0.63	6.85 ± 0.68
Structural Model Index	0.29 ± 0.20	0.63 ± 0.11	0.52 ± 0.17	0.63 ± 0.16
Trabecular Number	1.60 ± 0.07	1.46 ± 0.05	1.56 ± 0.07	1.43 ± 0.06
Trabecular Thickness	0.18 ± 0.01	0.18 ± 0.01	0.17 ± 0.01	0.18 ± 0.01
Trabecular Spacing	0.61 ± 0.03	0.67 ±0.03	0.62 ±0.03	0.68 ±0.03
Degree of Anisotropy	1.58 ± 0.05	1.62 ± 0.04	1.61 ± 0.08	1.65 ± 0.07
Mineralization	1063.4 ± 8.6	1062.8 ± 9.2	1078.9 ± 14.8	1083.9 ± 13.0

The number of cycles to the fatigue test endpoint approached significance between age groups (younger: 77372 ± 15984 cycles; older: 34944 ± 11964 cycles, p=0.06). A number of samples reached 150,000 cycles, which was the ceiling placed on all tests due to the observation that the modulus had stopped declining and max strain had stopped progressing by this point. In the younger group, 9 of 20 samples reached the limit, while only 3 of 20 samples reached the limit in the older group. An average value for the maximum strain per cycle was plotted as a function of number of cycles to illustrate how strains progressed during fatigue testing (Figure 4.2). Samples that went to 150,000 cycles are plotted separately from younger and older samples because their maximum strain/cycle changed very little throughout the test.

The elastic modulus of each sample was calculated at three intervals: at the initial static load to 0.8% strain, at the end of the 10^{th} pre-conditioning cycle before fatigue

testing, and at the final cycle of the fatigue loading protocol. The initial modulus was significantly greater than the pre-cyclic modulus and the final modulus in both the younger and older age group (Figure 4.3, $p<0.02$).

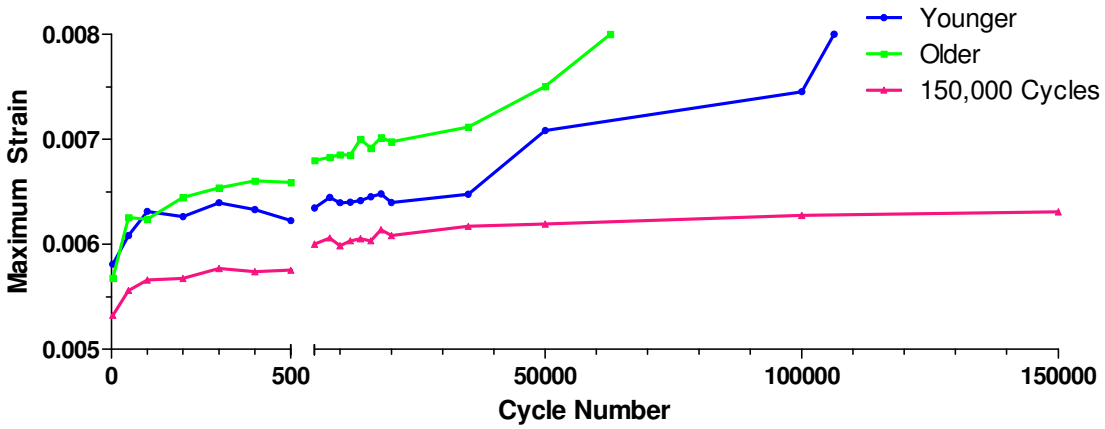

Figure 4.2. Changes in maximum strain per cycle in younger samples, older samples, and samples that went to 150,000 cycles. The greatest rate of change in maximum strain occurred within the first 100 cycles. Samples in the older group tracked at higher strain rates/cycle than samples in the younger group. Samples that went to 150,000 cycles had very little change in maximum strain throughout the test.

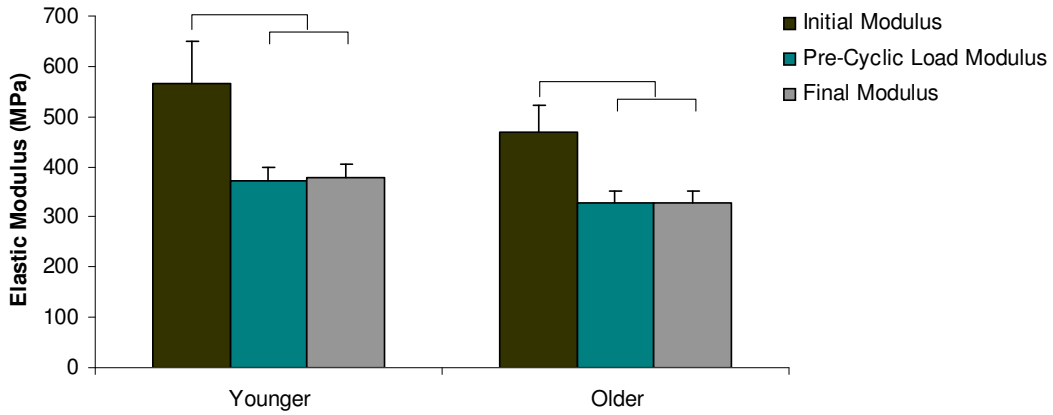

Figure 4.3. Elastic modulus changes during mechanical test by age group. Significant decreases in the elastic modulus after the initial static loading protocol were noted in both age groups. No differences in modulus due to the fatigue test were found. Bars represent significant differences, $p<0.05$ considered statistically significant.

Plastic strain was calculated in the first cycle as the difference between the initial and final strain and did not vary between the age groups (ε_p = 0.0004 for both younger and older groups). The residual strain upon unloading was obtained at the final cycle and did not differ between the age groups (ε_{res} = 0.03 for both younger and older groups).

Alizarin-labeled microdamage incidents (encompassing damage created *in vivo*, incidental damage created during core extraction, and damage created after the static load) were quantified and compared between younger and older age groups. Significantly increased incidents of linear damage relative to diffuse and severe damage were seen in both age groups (Figure 4.4, $p<0.005$). Also, significantly increased diffuse damage incidents compared to severe damage incidents were found in both age groups ($p<0.005$). There was significantly more linear damage in the older age group after the initial loading protocol compared to the younger age group ($p<0.001$).

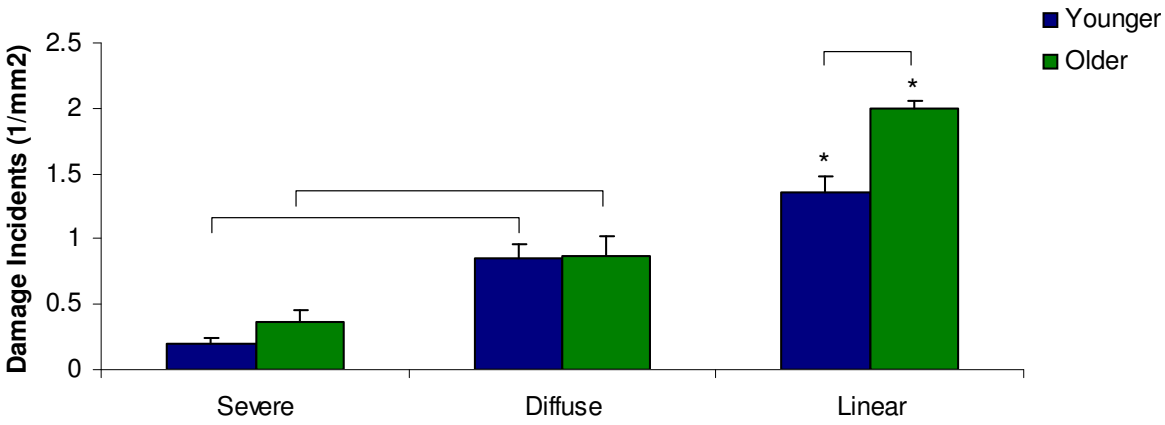

Figure 4.4. Microdamage density after initial static loading by age group. Linear damage incidents were most common in both age groups, significantly increased over diffuse and severe damage incidents. (*) Diffuse damage incidents were more common than severe damage incidents in both age groups. Finally, linear damage incidents were increased in the older group compared to the younger group. Bars represent significant differences, $p<0.05$ considered statistically significant.

Cyclic *de novo* damage was more rare, representing 6.7% of total calcein-labeled damage in the younger group and 7.1% in the older group. Of *de novo* damage incidents, significantly more linear damage than severe damage was observed in both age groups (Figure 4.5, younger: $p<0.04$; older: $p<0.001$), and in the older age group, linear damage incidents were significantly greater than diffuse damage incidents ($p<0.005$).

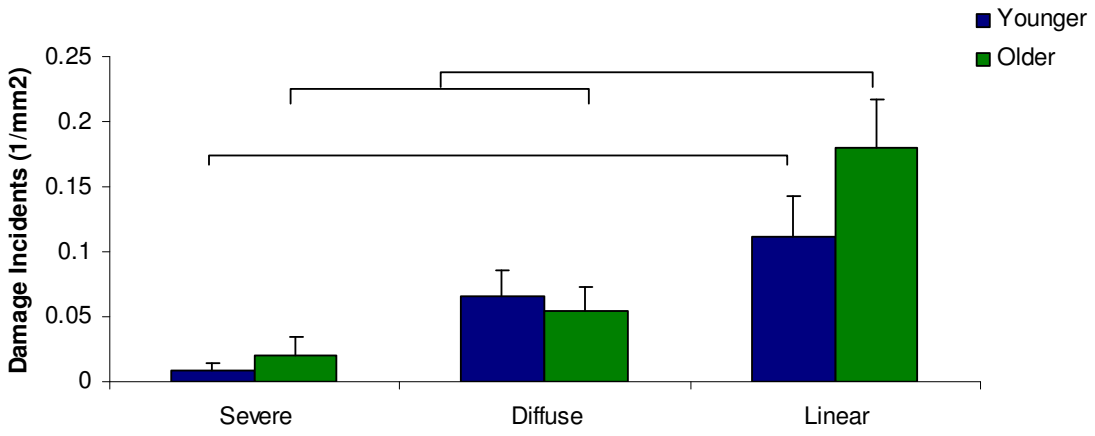

Figure 4.5 Microdamage density of *de novo* damage created with fatigue loading by microdamage morphology. More linear damage than severe damage was found in both age groups, and linear damage density was greater than diffuse damage density in the older group as well. $p<0.01$; bars indicate significant differences.

The percentage of damage propagating from static load-induced damage was not different between the age groups: 46% of the younger group and 43% of the older group's static load-induced damage (alizarin-labeled) was classified as propagated (exhibiting dual-fluorescence). Overwhelmingly, propagated damage adhered to the morphology it assumed at initial formation; less than 5% of total propagated damage changed morphological categories.

Propagated damage was classified according to its fluorescence pattern. Damage incidents demonstrating completely overlapping fluorescence of alizarin and calcein

labels were classified as contained damage, while calcein-labeled regions which increased the damage area or length of an initial alizarin-labeled damage incident were classified as extended damage (Figures 4.6a, 4.7a, and 4.8a). It was found that more linear propagated damage was of the contained than extended type in both age groups (Figure 4.6b, $p<0.001$). Linear damage which propagated had a smaller initial length than the contained damage, and increased to a final length similar to the contained damage length (Figure 4.6c).

No age-related differences in the propagation character (extended vs. contained) were found among diffuse, propagated damage incidents, although the damage area for the younger group was significantly greater than the older group in the initial and final extended damage area (Figure 4.7b and c, $p<0.05$). The percent of area expansion between the initial and final propagated area was greater in the younger group (34%) compared to the older group (23%) as well. In damage of a severe morphology, damage incidents in the older group were significantly more extended than contained (Figure 4.8b, $p<0.02$), while no differences were seen in the younger age group. When the severe damage areas were compared, the younger group had a significantly larger damage area in the initial and final extended damage group compared with the older group. (Figure 4.8c, $p<0.02$) The final extended damage area was also significantly greater than the damage area of contained propagation. ($p<0.03$) However, the percent of area expansion between the initial and final propagated area were similar between the groups (13% increase in younger vs 12% increase in older). Finally, evaluation of total propagated damage revealed no preferences in terms of contained or extended character in either age group.

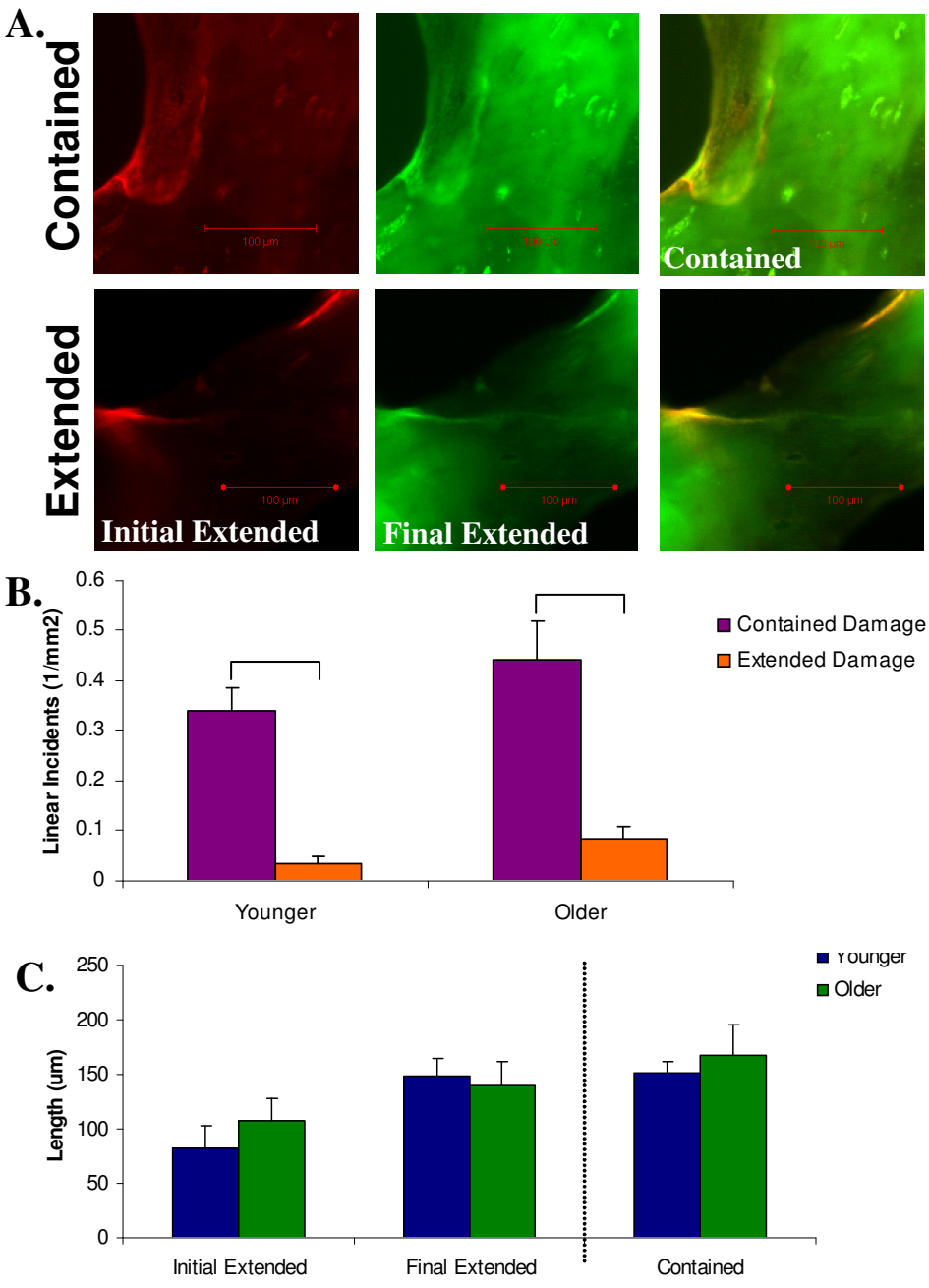

Figure 4.6. Linear propagated damage images, character, and length by age group. **4.6a.** Examples of the two groups of propagated linear damage, contained and extended, are shown under filters for each fluorescent stain as well as the composite image (alizarin=red, calcein=green). **4.6b.** Comparisons of the number of contained versus extended damage incidents demonstrated that damage of a linear morphology was more likely to remain confined to its initial damage length in both age groups. **4.6c.** Length measurements of linear damage incidents showed that the initial length of damage (initial extended) which extended during the fatigue test (final extended) did not exceed the length of contained linear damage incidents for both age groups. Bars represent significant differences, $p<0.05$ considered statistically significant.

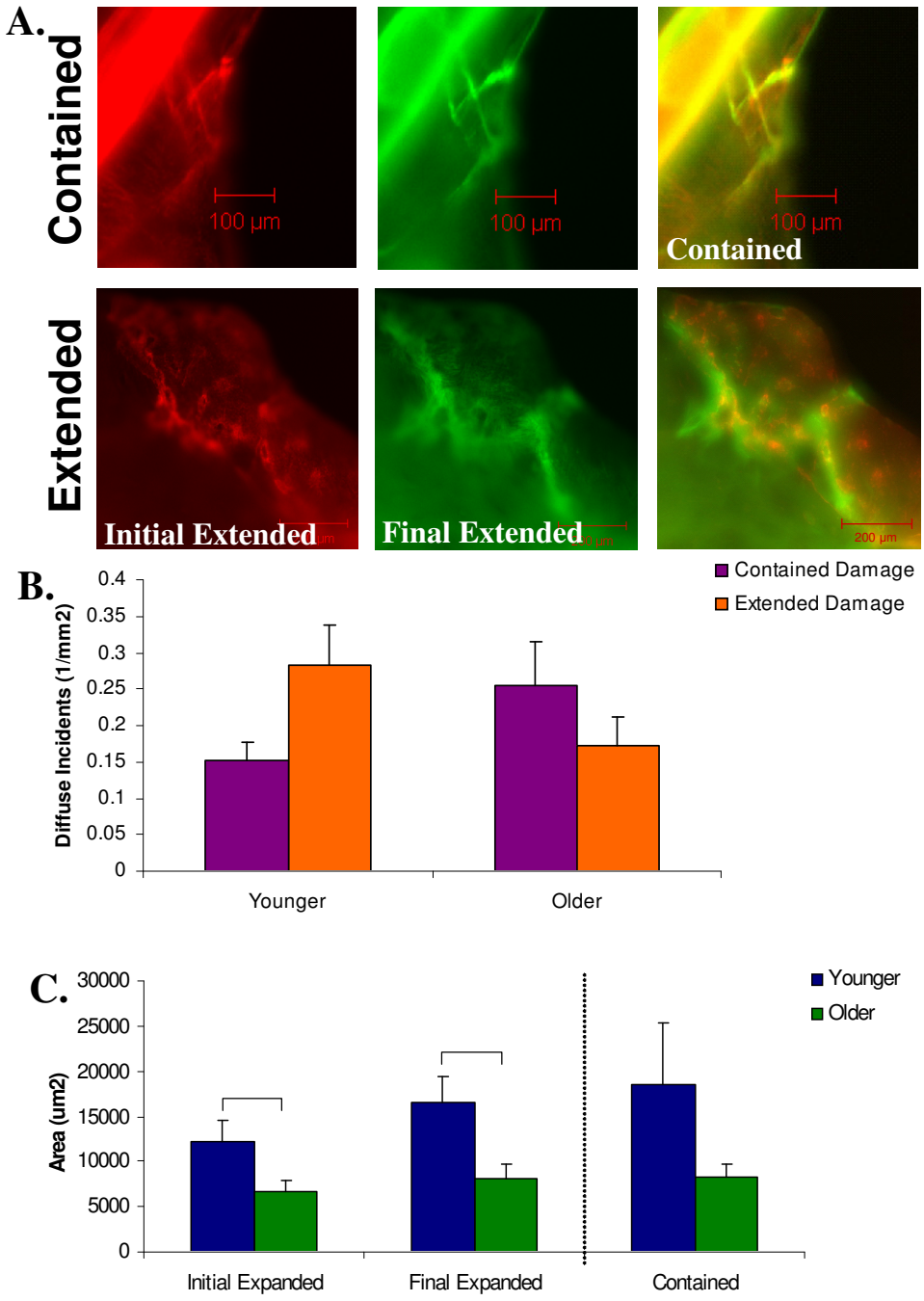

Figure 4.7. Diffuse propagated damage images, character, and length by age group. **4.7a.** Examples of the two groups of propagated diffuse damage, contained and extended, are shown under filters for each fluorescent stain as well as the composite image (alizarin=red, calcein=green). **4.7b.** No significant differences by propagation type or age group were seen in diffuse damage incidents. **4.7c**. Measurements of the initial extended diffuse damage area after static loading and final extended damage area after cyclic loading showed significant increases in the younger group compared to the older group. The final extended damage area did not exceed the damage area for contained damage in either age group. Bars represent significant differences; $p<0.05$ considered statistically significant.

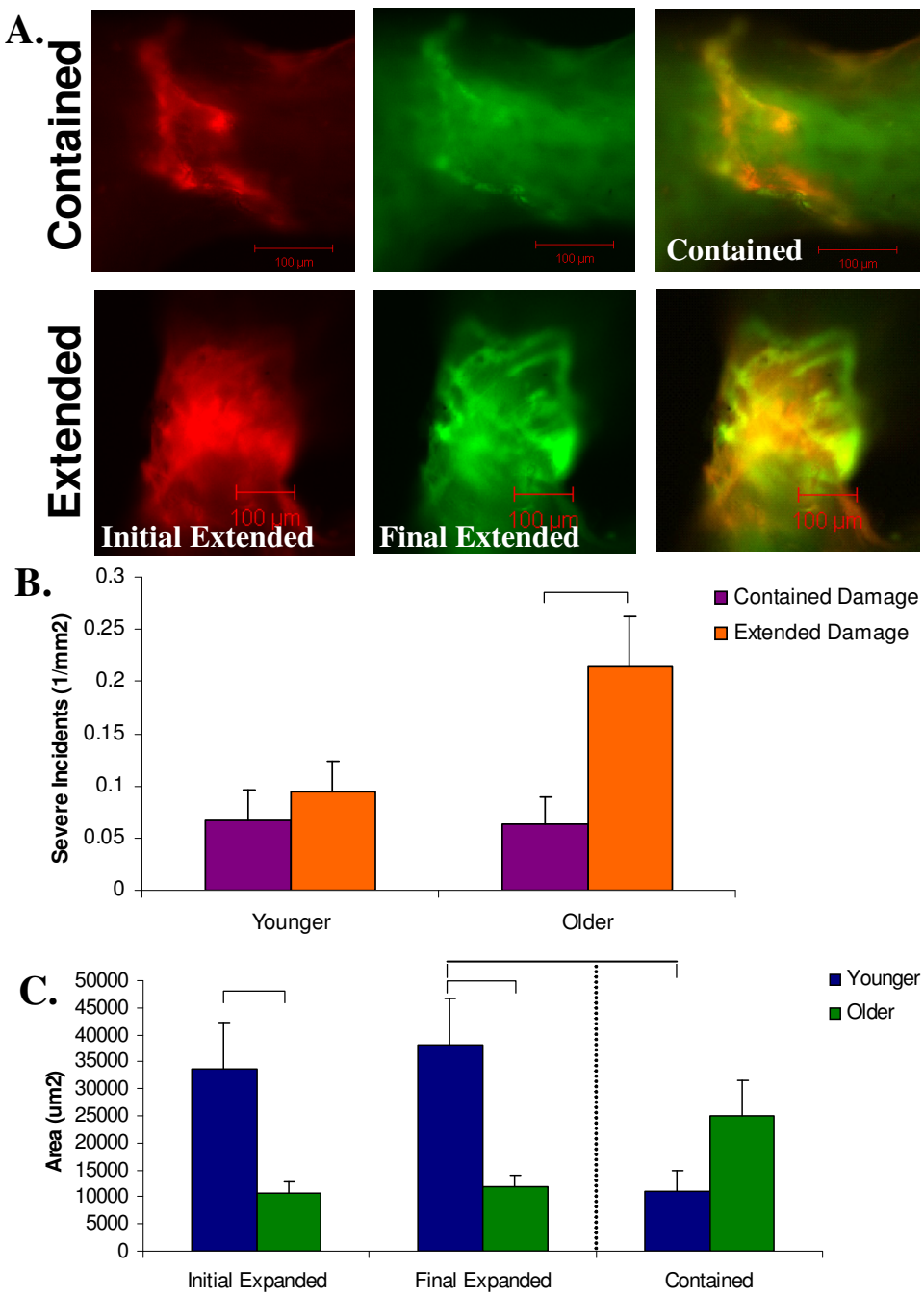

Figure 4.8. Severe propagated damage images, character, and length by age group. 4.8a. Examples of the two groups of propagated severe damage, contained and extended, are shown under filters for each fluorescent stain as well as the composite image (alizarin=red, calcein=green). **4.8b.** In the older age group, propagated severe damage was more likely to be extended than contained. **4.8c**. Damage areas in the initial extended group after static loading and final extended group after cyclic loading were greater in younger compared to older groups. In the younger group, the final extended damage area was significantly greater than the contained damage area. Bars represent significant differences; $p<0.05$ considered statistically significant.

4.4 Discussion

In this study, trabecular bone cores from the femoral head of 10 younger and 10 older individuals were subjected to a two-step mechanical testing protocol. Microdamage was first induced with static uniaxial compressive loading to 0.8% then propagated with cyclic uniaxial compressive loading under a modest normalized stress range. Testing was confined within the region of linear elastic apparent behavior and stopped at a below-yield strain of 0.8%. It was found that samples from older donors reached the fatigue test endpoint with a significantly fewer number of cycles than younger individuals. This is associated with greater numbers of extending severe damage incidents in the older group compared to the younger group.

In the fatigue portion of the mechanical test, we observed translation of the stress-strain loop along the strain axis. While some have suggested this translation is due to creep (Carter et al. 1983), further investigation has shown that it is due to microdamage accumulation and propagation. (Moore et al. 2003; Moore et al. 2003; Moore et al. 2004) In this study, examination of the changes in maximum strain with cycle showed sharp increases in the first 100 cycles of the fatigue test, then slower increasing strain until the test endpoint. Furthermore, the strain tracked highest in samples from older donors, and lowest in samples that went to 150,000 cycles. The greater change in strain from cycle 2 to cycle 100 found in samples from older donors (0.0008) compared with samples from younger donors (0.0006) and samples that went to 150,000 cycles (0.0004) demonstrates the differences in the initial rate of microdamage propagation between these groups and may be an important indicator of crack resistance.

At the normalized stress level used in this study, we did not observe significant differences in the linear crack density or crack length in either age group due to cyclic loading. Others have also reported that crack length remains fairly stable in *in vitro* loading protocols due to microstructural barriers that arrest crack propagation. (Wang et al. 2006) Since there are few differences in the linear damage data between the static and cyclic loading protocol as well as between the age groups, it is unlikely that these damage incidents have a large impact on trabecular bone's progression towards failure.

In diffusely damaged trabeculae, a larger damage area was found in younger individuals compared with older individuals. Furthermore, the percent area expansion was also greater in younger compared with older trabecular bone. This result is at odds with the observation that the strain endpoint was reached more quickly in samples from older donors than younger donors. Rather, it illustrates an efficient energy dissipation strategy which protects the overall structural integrity of the trabecular bone lattice by localizing damage expansion with a morphology that is less likely to propagate. (Diab et al. 2005; Badiei et al. 2007; Cook et al. 2009) Thus, it does not appear that this mechanism is the driving force behind the age-related differences in the number of cycles between the younger and older donors.

Examination of severe damage density showed that, while the number of severe damage incidents was similar between the two age groups, cracks in samples from older donors were more likely to be expanding in area with fatigue. Despite the large differences in severe damage area between the age groups, the percent of damage expansion was very similar between the groups. This suggests that the age-related differences in the time to the fatigue strain endpoint were driven by the number of severe

damage incidents that were expanding, rather than the damage area of severely damaged trabeculae. It is advantageous to concentrate damage progression in trabeculae which are already compromised because finite element modeling studies have demonstrated that the probability of overt fracture increases as the number of failed trabeculae increases. (Guo et al. 1994; Cook et al. 2009) Differences in bone mineral age and density, alterations in collagen quality, and other changes in the composition of the bone matrix may play a role in severe damage expansion. (Currey et al. 1996; Zioupos 2001; Wang et al. 2002; Seeman 2003)

It was surprising to see that the initial severe damage area of younger individuals was so much greater than older individuals. This observation is likely to be an artifact of the mechanical testing protocol. It is probable that the older bone was initially more damaged, and that sites vulnerable to damage initiation due to a concentration of strains/stresses already exhibited microcracks. (Schaffler et al. 1995; Vashishth et al. 1997) In the less damaged core from younger donors, vulnerable sites would be more likely to experience higher stresses/strains at damage initiation than *in vivo*, resulting in more extensive initial damage. This phenomenon has been noted before in the investigation of damage initiation stresses/strains in alendronate-treated bone, where decreased amounts of severe damage were formed in alendronate-treated bone which had increased levels of *in vivo* damage compared to controls. (O'Neal et al. 2010) In this study, damage formed *in vivo* was not explicitly labeled separately from mechanical test induced damage due to the inability to differentiate between three stains, although others have shown that this is possible. (O'Brien et al. 2003)

We did not note a change in the elastic modulus between the beginning and end of the cyclic loading protocol in any of the groups. Further investigation revealed that the samples that reached 150,000 cycles experienced an average *increase* in the elastic modulus of 11%, while all other samples experienced an average *decrease* in modulus of 2% ($p<0.02$). This phenomenon has been observed in many previously published studies of fatigue loading in trabecular bone. (Linde et al. 1987; Michel et al. 1993; Moore et al. 2003) It is possible that a viscoelastic steady state had not been reached in the first 10 preconditioning cycles of the fatigue test, leading to an underestimation of stiffness. (Linde 1994) The effect would be particularly pronounced in samples that went to 150,000 cycles due to their greater initial stiffness (419.9 ± 34.7 MPa in 150,000 cycle samples vs. 317.1 ± 99.5 MPa in all others) relative to other samples. (Linde 1994; Sobelman et al. 2004)

There are a number of limitations to consider in interpreting these results. All mechanical tests were carried out at room temperature rather than body temperature. This could have the effect of prolonging fatigue life, and has been shown to increase fatigue life by a factor of three in bovine cortical bone. (Carter et al. 1976) Also, strain levels used in this study, while remaining at levels below the uniaxial yield strain, are still higher than would be expected due to physiological loading. (Yang et al. 2011) For gender comparisons, no differences in number of cycles or the amount of microdamage were found, though achieved power ($1-\beta=0.2$ for both parameters) was too low to detect subtle differences. Although consistent with other studies failing to show gender differences in fatigue life, the study should be expanded to explore gender differences further. (Sobelman et al. 2004) Finally, damage morphology and stain location were

evaluated from thin slides, which may result in some erroneous classifications if additional cracks or evidence of damage propagation extended into the plane perpendicular to the evaluated planes. The large number of damage incidents evaluated in this study should limit the influence of such errors if they occurred.

In conclusion, a novel mechanical testing protocol was used to characterize the propagation of microdamage in trabecular bone of the proximal femur in younger and older individuals. A decreased number of cycles to the test endpoint in older individuals were attributed to the damage area expansion of a greater number of trabeculae exhibiting severe damage morphology. These results add to the growing body of work exploring fatigue damage mechanisms in trabecular bone and particularly those mechanisms which are relevant in age-related bone fragility.

CHAPTER 5

ONE YEAR OF ALENDRONATE TREATMENT LOWERS MICROSTRUCTURAL STRESSES ASSOCIATED WITH TRABECULAR MICRODAMAGE INITIATION

5.1 Introduction

Alendronate, a bisphosphonate used to treat low bone density associated with osteoporosis, has been shown to decrease fracture risk at both vertebral and non-vertebral sites. (Liberman et al. 1995; Seeman 1999; Iwamoto et al. 2008) It achieves this risk reduction principally by increasing bone mineral density at the structural level. Positive effects at the tissue level may also improve fracture risk early in treatment by improving trabecular microarchitecture and reducing the number of trabecular stress risers (unfilled resorption pits) at sites of remodeling. (Seeman 2007) Studies conducted in canine models have shown, however, that one year of alendronate treatment is associated with decreased toughness and increased microcrack density, though these two findings may be the result of different mechanisms since further investigation found them to be unrelated. (Allen et al. 2006) Furthermore, studies by Stepan *et. al*. found increased crack density in osteoporotic women using alendronate compared to treatment-naïve osteoporotic controls, whereas another study of osteoporotic women did not find significantly increased microdamage frequency compared to cadaver controls. (Stepan et al. 2007) A better understanding of the mechanistic basis of damage formation with alendronate treatment can provide new insight into the underlying mechanisms of bone fragility.

Bone derives its ability to resist fracture by forming microdamage when subjected to loading. Traditionally, microdamage in trabecular bone has been grouped into two different morphological categories: linear microcracks and diffuse damage. Histologically, linear microcracks are identified as individual, sharply defined cracks, while diffuse damage referst to a cluster of cracks. (Wenzel et al. 1996; Reilly et al. 2000) It has been shown that different damage morphologies affect the biomechanical properties of bone differently (Burr et al. 1998; Diab et al. 2005; Diab et al. 2006). Diffuse damage formation plays a significant role in prolonging the fatigue life of bone and resisting a catastrophic fracture. (Burr et al. 1998; Diab et al. 2005) In contrast, linear microcracks can reduce bone strength and stiffness and are traditionally associated with the terminal phase of fatigue fracture characterized by rapid crack propagation and catastrophic failure. (Burr et al. 1998; Diab et al. 2005) Severe damage (defined by Moore and Gibson as a primary crack with secondary cracks, or through-trabecular thickness cracks) also occurs at a later stage in the fracture process (Arthur Moore et al. 2002; Wang et al. 2006) Although microdamage accumulation has been documented with alendronate use, its significance to bone fragility is still unknown. (Stepan et al. 2007)

We have previously reported a specimen-specific finite element technique to assess trabecular level stresses associated with microdamage initiation in bovine trabecular bone. (Nagaraja et al. 2005; Nagaraja et al. 2007) With this technique, the relationship between local damage events and trabecular stress magnitude can be directly assessed and associated with trabecular architectural characteristics. The overall goal of the study was to investigate whether changes in bone quality occurring after one year of

alendronate treatment will result in an increased propensity to form microdamage. The specific objectives were to (a) quantify the von Mises stress state of trabeculae demonstrating different morphologies of damage and compare between alendronate-treated and control groups, and (b) to determine if changes in microarchitectural characteristics due to alendronate treatment are associated with damage morphology.

5.2 Materials and Methods

5.2.1 Animals

Detailed methods regarding alendronate administration for this study have been previously reported. (Allen et al. 2006) Briefly, one-year-old female beagle dogs were randomized into three groups and treated with oral doses of saline (1.0 mL/kg/day) or alendronate (ALN, 0.2 mg/kg/day or 1.0 mg/kg/day) for one year. The ALN 0.2 and ALN 1.0 doses approximate the clinical doses used for the treatment of postmenopausal osteoporosis and Paget's disease, respectively. The group treated with saline served as the control group. All procedures were approved by the Indiana University School of Medicine Animal Care and Use Committee.

5.2.2 Sample Extraction

Twelve right distal femurs from beagle dogs (n=4 in each treatment group) were obtained for analysis. One trabecular core from each specimen (diameter = 5 mm; length = 18 mm) was extracted by coring through the condyle of the distal femur in the approximate principal material direction using a trephine under constant irrigation with 0.9% physiological saline + 10 μmol/L protease inhibitor (E-64, Sigma Chemical) followed by sizing with a diamond saw. The protease inhibitor (PI) was used throughout

the experiment to minimize tissue degradation. The specimens were wrapped in saline-soaked gauze and stored at -20°C until testing.

5.2.3 Microdamage labeling, Micro-CT imaging, and Mechanical Testing

Bone marrow was removed from trabecular cores using a water pik (WP-72W, WaterPik, USA) to improve stain penetration, and one endcap was placed on the end of each sample. Trabecular cores were stained for 8 hours in 0.02% Alizarin ComplexOne + 10 μmol/L PI at 4°C then washed with distilled water for 1 hour to label pre-existing damage, encompassing either *in vivo* damage or damage occurring from the core extraction. The ends of the trabecular cores were glued into 5 mm deep stainless-steel endcaps to minimize end artifact effects in the mechanical test. (Keaveny et al. 1994) Samples were imaged with micro-computed tomography (μ-CT; μCT 40, Scanco Medical, Basserdorf, Switzerland) at a voxel resolution of 20 μm prior to mechanical testing. Trabecular cores were then mechanically tested, in which they were first preconditioned for 3 cycles to 0.1% strain then loaded in displacement-controlled uniaxial compression (Mini Bionix 858, MTS Corp.) at a rate of 0.5% strain/second to the yield strain (determined to be 1.2% in preliminary testing) and held for 3 hours. The apparent strain was calculated using a gauge length of the exposed length of the bone measured with digital calipers plus half the length of each bone end embedded in endcaps. (Keaveny et al. 1997) Throughout testing, bone cores were immersed in 0.9% physiological saline + 10 μmol/L PI.

After testing, one endcap was removed with the diamond saw to improve stain penetration, and cores were stained with 0.01% calcein to label test-induced microdamage for 8 hours at 4°C then washed with distilled water for 1 hour. (Vashishth

D 1994; O'Brien et al. 2002) After staining, cores were fixed in 70% ethanol for 24 hours then dehydrated using a graded alcohol infiltration procedure. Cores were embedded in methyl methacrylate in a prescribed orientation which allowed visual registration with the 3D reconstructed μ-CT image, and 6 slides of thickness 150 μm were obtained along the longitudinal axis with the diamond saw from each sample.

5.2.4 Microdamage Identification and Classification

Test-induced microdamage was identified based on the criteria that cracks are intermediate in size (20 – 150 μm; larger than canaliculi but smaller than vascular channels), have sharp borders, and a focus plane demonstrating depth of field. (Allen et al. 2006; Stepan et al. 2007) Areas of diffuse staining with no clearly defined cracks were not counted as microdamage. A classification system published by Moore and Gibson was modified to group damage into three broad morphological categories: severe, linear, and diffuse damage (Figure 5.1*)*. (Arthur Moore et al. 2002) Severe damage was classified as either microdamage consisting of one primary crack with minor secondary cracks or cracks propagating through the thickness of the trabecula. Linear damage included both single and parallel cracks, and diffuse damage consisted of cross-hatch damage that was either equal in length and intensity (to distinguish it from severe damage) or damage with a large area of distribution.

Damage was observed at 100x magnification using fluorescence microscopy and quantified by an investigator blinded to the treatment group, then re-evaluated by a second investigator also blinded to the treatment group. A 70% concordance rate in the number of damage events identified between each investigator was obtained, with the highest concordance rate being in the severe group (88%), and the lowest concordance

rate being in the linear damage group (60%). Any differences in the count were reconciled between the two investigators, so that the total damage count is confirmed by both investigators. An area of interest for damage analysis was generated on each slide by excluding tissue less than 500 μm from each sample edge. Damage incidents demonstrating three staining patterns were counted and normalized by surface area (crack density, #/mm2). A damage incident is defined as a discrete damage event, so that both linear and diffuse damage occurrences as classified by Figure 5.1 would each count as one damage event. The three patterns of staining were 1) those which fluoresced predominantly under red epifluorescence corresponding to the emission wavelength of alizarin, 2) those which fluoresced predominantly under green epifluorescence corresponding to the emission wavelength of calcein, and 3) those which fluoresced under both red and green epifluorescence equally in intensity and location.

5.2.5 Micro-CT Image Processing and Finite Element Analysis

3D micro-CT reconstructions of trabecular bone cores were thresholded to distinguish bone from background, and automated distance transformation algorithms were used to compute morphological parameters such as bone volume fraction, trabecular thickness and connectivity, structural model index (SMI), and degree of anisotropy (DA). Mineralization values were computed from attenuation values of grayscale μ-CT images based on hydroxyapatite (HA) calibration standards.

Micro-CT images were used to create 3-D high-resolution finite element (FE) models for estimating local stress distributions (FEA software, Scanco Medical, Basserdorf, Switzerland). A homogeneous, linear elastic, isotropic model was used, and an initial tissue modulus of 10 GPa and a Poisson ratio of 0.3 were assumed. Using

Scanco software, individual damaged and undamaged trabeculae identified first during histological microdamage categorization were extracted from the 3-D reconstructed μ-CT image manually (Table 5.1*)*. By manually delineating trabeculae from the reconstructed μ-CT image rather than the FEM estimation of stress distribution, the investigators were not influenced by the stress predictions when determining cut-off points. Values for von Mises stress along the extracted trabeculae were obtained by averaging the values of all elements from the FEM solution corresponding to the voxels of the extracted trabeculae. (Figure 5.1) Stress results were scaled to the back-calculated tissue modulus using a previously published procedure. (van Rietbergen B 1995) Briefly, the apparent modulus obtained from mechanical testing within the elastic region is compared to the predicted apparent modulus computed from finite element models which used an initial estimate of the trabecular tissue modulus (10 GPa). The ratio of the apparent modulus obtained from mechanical testing and predicted by finite element is multiplied by the initial estimate of the tissue modulus to obtain the effective tissue modulus based on mechanical testing results.

Table 5.1 Sample Sizes for Trabecular Stress Analysis after 1 year of Treatment

Treatment Group	Severe	Linear	Diffuse	Undamaged	Total
Control	62 (40.3%)	26 (16.9%)	31 (20.1%)	35 (22.7%)	154
0.2 mg/kg/day	28 (27.2%)	31 (30.1%)	25 (24.3%)	19 (18.4%)	103
1.0 mg/kg/day	49 (36.3%)	25 (18.5%)	30 (22.2%)	31 (23.0%)	135

Percentages indicate the proportion of each damage type counted relative to total trabeculae counted in each treatment group

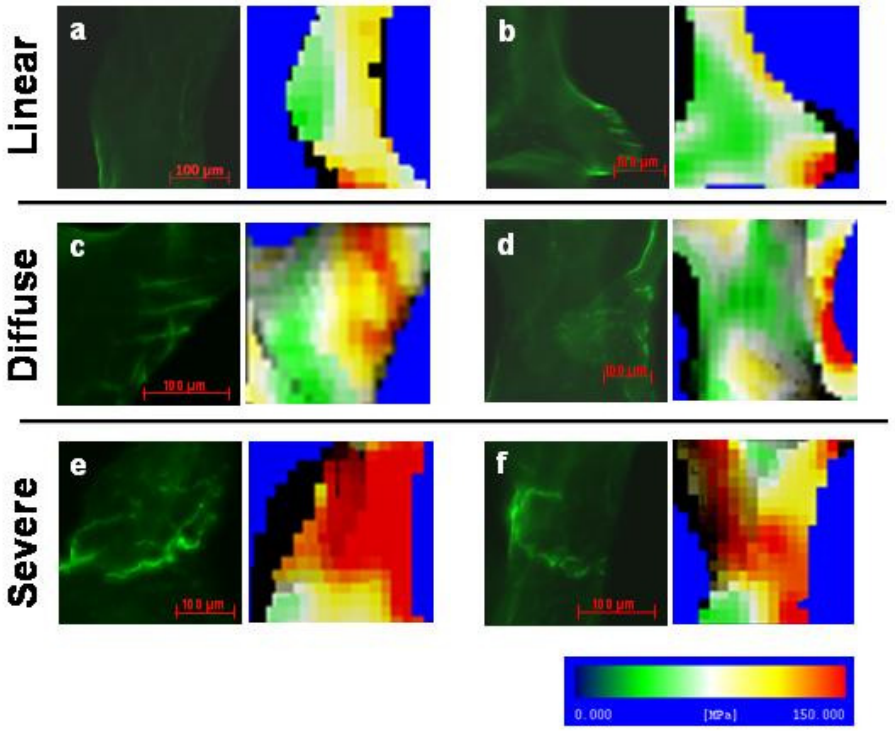

Figure 5.1. Microdamage description and classification, with FEA von Mises stress predictions. Linear damage includes a) single cracks and b) parallel cracks. Diffuse (crosshatch) damage includes c) cracks with equal crosshatching and d) cracks over a large area distribution. Severe damage includes e) one primary crack with minor secondary cracks and f) cracks through the trabecular thickness.

5.2.6 Statistics

All statistical tests were performed using MINITAB software (Minitab, Minitab Inc., USA). Differences in global architectural parameters between the two treatment groups and the control group were deduced using Kruskal-Wallis nonparametric tests. Differences in crack density were determined with ANOVA analysis followed by Tukey pairwise comparisons. $p<0.05$ was considered significant.

To determine differences in mechanical and architectural parameters of damaged and undamaged trabeculae by treatment group and microdamage category, Friedman's statistical test was conducted for the treatment groups and the four damage categories.

Kruskal-Wallis nonparametric tests were used to determine differences between damage categories within each treatment group, followed by post-hoc nonparametric pairwise comparisons. A Bonferroni correction was used, as five measures (von Mises stress, mineralization, trabecular thickness, SMI, and trabecular orientation) were made on each analyzed trabeculae. This reduced the p value for a significant difference to $p \leq 0.01$. All data are presented as mean ± standard error.

5.3 Results

Comparisons of alendronate's effect on the global properties of trabecular bone are shown in Table 4.1. Alendronate-treated trabecular bone exhibited trends towards increased bone volume fraction, mineralization, trabecular thickness, trabecular number, and connectivity density, though none of these differences were significantly different than controls. There were no significant differences between the apparent moduli obtained during mechanical testing of alendronate samples compared to controls, nor were there differences in the back-calculated tissue moduli of alendronate-treated samples compared to controls. No dose-dependent differences in apparent properties were noted.

Figure 5.2 shows the crack density separated out as those cracks that were either alizarin or calcein stained only, cracks exhibiting overlapping fluorescence, and total damage (all cracks independent of color). There was a significantly greater density of alizarin-labeled cracks in the treated groups compared with cracks exhibiting overlapping fluorescence ($p<0.05$). No significant differences in crack density were seen across groups for calcein-labeled cracks or in total damage.

Table 5.2 Apparent Level Architectural Properties by Treatment Group

Parameter	0.2 mg/kg/day	1.0 mg/kg/day	Control
Bone Volume Fraction (BV/TV)	0.20 (0.01)	0.19 (0.01)	0.13 (0.01)
Mineralization (mg HA/ccm)	1040.3 (6.1)	1040.3 (1.0)	1011.9 (6.2)
Trabecular Thickness (μm)	107.8 (5.4)	106.7 (2.6)	87.8 (2.3)
Connectivity Density (mm^{-3})	24.5 (1.2)	25.2 (1.2)	18.7 (1.4)
Structural Model Index (SMI)	1.12 (0.08)	1.33 (0.04)	1.43 (0.06)
Degree of Anisotropy	1.43 (0.02)	1.31 (0.02)	1.41 (0.04)
Trabecular Number (mm^{-1})	2.25 (0.04)	2.21 (0.05)	2.06 (0.05)
Apparent Modulus (MPa)	872.7 (71.0)	825.2 (57.6)	600.0 (73.5)
Tissue Modulus (GPa)	12.3 (1.9)	13.1 (2.2)	14.7 (1.1)

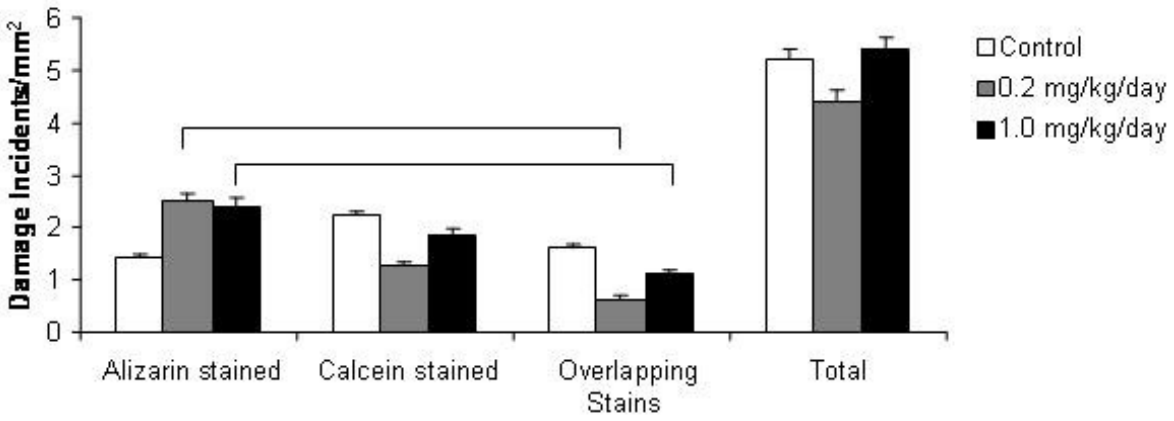

Figure 5.2 Total damage quantified based on fluorescence and plotted by treatment group. The total damage columns are created by totaling damage counted in the three previous columns for each treatment group, and no significant differences were found. Bars represent significant differences. $p<0.05$, mean ± SE. is plotted

In order to determine the effects of alendronate treatment on tissue level biomechanical properties, trabecular level von Mises stresses were compared to controls at microdamaged sites. As shown in Figure 5.3, severely damaged trabeculae in the control group were under the greatest von Mises stress, significantly greater than severely damaged trabeculae in both of the alendronate treatment groups ($p<0.001$). A treatment

effect was also discerned in the linearly damaged group, where the von Mises stress state of the linearly damaged control group was significantly greater than both alendronate treatment groups ($p<0.01$).

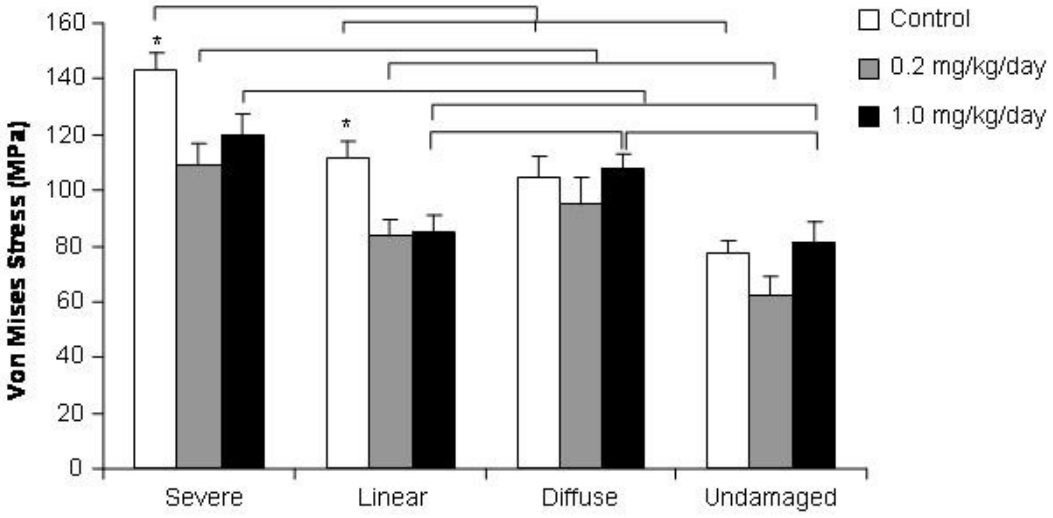

Figure 5.3 Von Mises stress plotted by treatment group and damage morphology. The stress state of trabeculae exhibiting severe and linear damage was decreased in both treatment groups compared with controls. In the control group, severe damage was associated with the greatest stress compared with all other damage groups. In both treatment groups, the stress state of severely damaged trabeculae was significantly increased compared with linear and undamaged trabeculae. Bars between damage morphologies within the same treatment group indicate significant differences. $p<0.01$ indicates significance, mean + SE is plotted.

The stress state of trabeculae exhibiting different damage morphologies were also compared within each treatment group. Severely damaged trabeculae in the control group were under significantly greater stress than all other damage morphologies in the same group ($p<0.01$). In both alendronate treatment groups, severely damage trabeculae were under greater stress than linear and undamaged trabeculae in the same group ($p<0.01$). Finally, diffusely damaged trabeculae in the ALN1.0 treatment group were

under significantly greater stress than linear and undamaged trabeculae in that group ($p<0.01$).

Alterations in local mineral density were analyzed by treatment group and damage morphology. No differences due to dosage were observed, so the two treatment groups were combined. Diffusely damaged trabeculae were significantly more mineralized in bone treated with alendronate compared to controls ($p<0.01$). Similarly, undamaged trabeculae were significantly more mineralized in treated compared with untreated controls ($p<0.001$). Within the treated group, severely damaged trabeculae were less mineralized than undamaged trabeculae ($p<0.01$, Figure 5.4a).

To determine whether trabecular architectural characteristics were associated with damage morphology, trabecular thickness, structural model index, and trabecular alignment were computed for each extracted trabecula undergoing stress analysis. No differences in any of these architectural parameters were found between the two alendronate treatment doses; thus, the data were pooled and compared to controls. Severely damaged trabeculae were thinner than trabeculae sustaining other damage types in alendronate-treated samples ($p<0.01$, Figure 5.4b); this was not true for the control group. Analysis of the SMI values for damaged trabeculae revealed that severely damaged trabeculae subjected to alendronate treatment were more rod-like than their diffusely damaged counterparts ($p<0.01$, Figure 5.4c). Finally, the trabecular orientation, computed as the angle between the material axis and the loading axis, was significantly more acute in severely damaged trabeculae compared to undamaged trabeculae of the treated group ($p<0.01$). Severely, linearly, and diffusely damaged trabeculae were also

more aligned with the loading axis compared with undamaged trabeculae from the control group ($p<0.01$, Figure 5.4d).

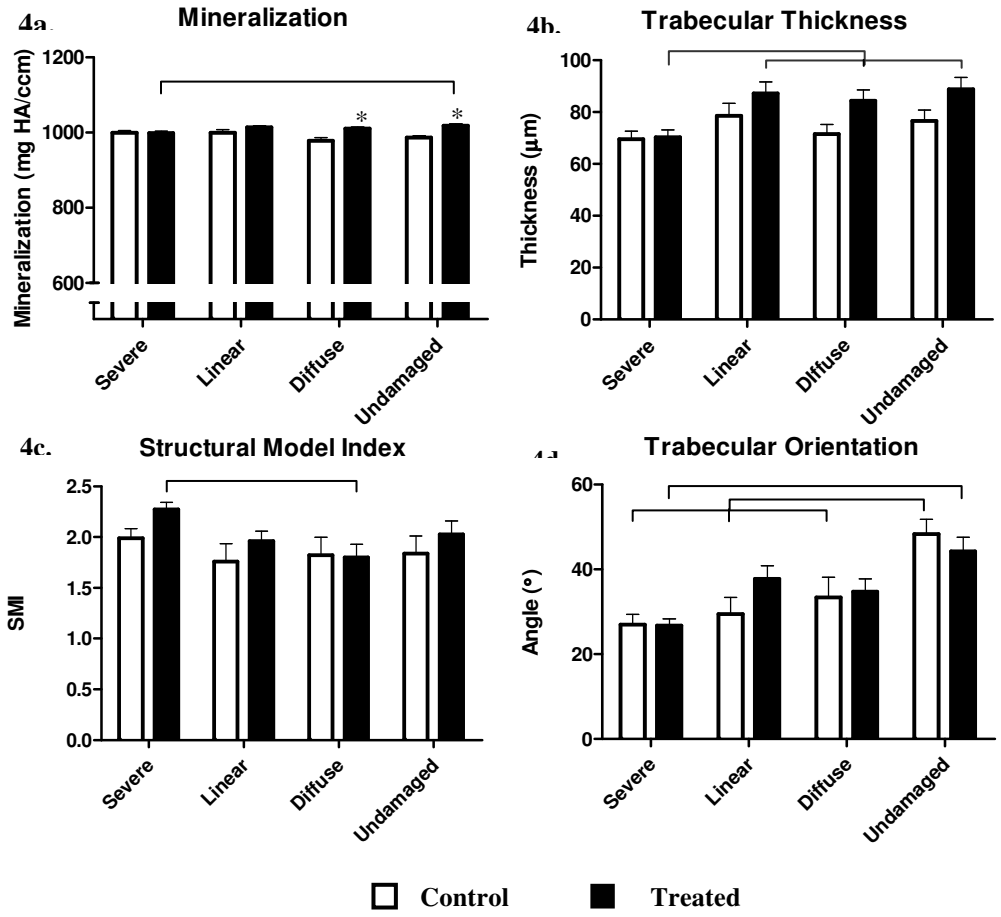

Figure 5.4 Trabecular mineralization and architectural characteristics plotted by treatment group and damage morphology. There were no differences due to treatment dose, so the two samples were combined. **5.4a**. Trabecular mineralization is plotted with respect to damage morphology and treatment; severely damaged trabeculae were less mineralized than undamaged trabeculae in the treated group. Within diffuse and undamaged trabeculae, treatment was associated with increased mineralization relative to control.(*) **5.4b.** Trabecular thickness is plotted with respect to treatment and damage morphology; severely damaged trabeculae were significantly thinner than other trabeculae in the treated group. **5.4c.** Structural model index is plotted with respect to damage morphology and treatment; severely damaged trabeculae are more rod-like than diffusely damaged trabeculae. **5.4d.** The angle between the principal material axis and the loading axis is plotted; undamaged trabeculae were generally aligned perpendicular to the loading axis in both treatment and control groups. Bars indicate significant differences between damage morphologies within the same group. $p<0.01$ indicates significance, mean + SE plotted

5.4 Discussion

In this study, a novel method of determining tissue-level mechanical and architectural parameters associated with microdamage morphology was used to assess the effect of alendronate on trabecular bone microstructure. Others have inferred that trabecular von Mises stresses increase with damage severity, but this is the first study that quantifies microstructural stresses by damage morphology. (Arthur Moore et al. 2002; Yeni et al. 2003) This study concludes that alendronate administration alters the tissue level biomechanical properties of trabecular bone, resulting in a decreased von Mises stress necessary for initiation of severe and linear microdamage.

Many previously published studies have utilized the fluorescent staining protocol developed by O'Brien *et al*. to separate *in vivo* damage from test-induced damage. (O'Brien et al. 2002; Wang et al. 2005; Zarrinkalam et al. 2005) In our execution of this protocol, we were able to separate cracks formed *in vivo* from those induced during uniaxial compression loading by examining their fluorescence under green and red epifluorescence. Though total *in vivo* damage was not significantly greater in alendronate treated bone, linear crack density was increased in this population, which is in agreement with previously published work. (Allen et al. 2006) However, it was difficult to determine whether cracks which fluoresced under both red and green epifluorescence equally are the product of crack propagation, double staining due to the sharing of calcium binding sites between the two fluorophores, or filter interference. Due to these difficulties, we chose to exclude cracks which exhibited this overlapping fluorescence from the stress analysis due to the uncertainty of their origins.

Previous studies have correlated microdamage formation to trabecular shear stress, suggesting that shear forces play a significant role in trabecular bone failure. (Fyhrie et al. 2000; Yeni et al. 2003; Yeni et al. 2008) The contribution of shear forces to failure can be evaluated with the von Mises stress parameter, which is commonly used to predict yielding in complex loading conditions when the shear stress reaches a critical value on the octahedral plane. Fyhrie *et al* demonstrated that von Mises stress concentrations correlated with sites of cracking in mechanically tested and *in vivo* damaged trabecular bone. (Fyhrie et al. 2000) Our findings suggest that trabecular bone treated with alendronate may be more susceptible to severe and linear microdamage formation because of a decreased von Mises stress magnitude required to induce damage compared to controls. Linear damage can reduce the biomechanical properties of bone and is traditionally associated with the terminal phase of bone fracture characterized by rapid crack propagation and catastrophic failure (Burr et al. 1998; Diab et al. 2005); thus, alendronate administration may predispose trabecular bone to the formation of more ominous microdamage patterns in the form of severe and linear microdamage. (Burr et al. 1997; Burr et al. 1998; Diab et al. 2005) These observations may account for increased microcrack density in trabecular bone treated with alendronate for one year as more damage would form if the initiation threshold is lowered in this population. (Allen et al. 2006)

Alendronate treatment has been shown to increase the thickness and mineralization of trabeculae, and this study corroborates that finding. (Recker et al. 2005) We found that thinner trabeculae with decreased mineral density and rod-like morphology are more likely to sustain severe damage in the treated samples compared to

non-treated controls. The data suggest that the vulnerability of trabeculae to damage based on thinness is relative to the average trabecular thickness of the sample, for at the thickness of alendronate-treated severely damaged trabeculae, untreated trabeculae at the same thickness were undamaged. There are two possible mechanisms to explain this finding: either there is a decrease in bone quality factors (tissue-matrix characteristics) in alendronate-treated trabeculae that promote damage formation, or architectural changes stemming from alendronate treatment expose the vulnerability of thinner trabeculae to damage. Since trabecular stresses in severely damaged trabeculae were actually decreased compared to control samples, indicating that architectural changes do not place greater stresses on thinner trabeculae, this suggests that some other factor(s) related to bone quality facilitates severe damage formation in alendronate-treated bone.

It is well documented that due to the suppression of bone remodeling, alendronate increases tissue mineralization. (Allen et al. 2006; Allen 2007) When mineralization density was compared based on trabecular damage morphology, we found that mineralization was only increased in alendronate-treated samples which were diffusely damaged or undamaged. Severely and linearly damaged trabeculae in alendronate-treated samples were not differently mineralized compared to control trabeculae with the same damage morphology. We have previously shown that microdamage initiation occurs around areas of decreased mineralization, and speculate that regions of low mineral/matrix ratio may result in greater local tissue compliance leading to damage initiation. (Nagaraja 2009) This effect may be seen only at the 1 year stage of treatment as matrix mineral will continue to age and stiffen as bone turnover declines.

Some aspects of the present study limit its broad applicability. This study was conducted in bone from twelve animals, or four per treatment group. This limits the power of the study to resolve stress differences due to treatment dose ($1-\beta=0.49$) or global architectural changes like bone volume fraction with alendronate treatment ($1-\beta=0.34$). Our stress analysis was conducted by analyzing almost 400 trabeculae, so we are more confident in the power of the study to resolve differences in the stress state due to damage morphology ($1-\beta$ approaches 1). Also, bone used for the microdamage analysis came from non-osteoporotic animals; thus, it is difficult to apply conclusions to osteoporotic humans using bisphosphonate therapies. However, our study focused on changes in intrinsic level properties of trabecular bone elicited by alendronate use, and the bone physiology of humans and dogs is sufficiently similar to allow such investigations. (Aerssens et al. 1998; Shaw 2005) Conclusions from this study are also limited by the assumption of linearity, homogeneity, and isotropy at the microstructural level, which somewhat limits the accuracy of the mechanical values obtained. However, Nagaraja et.al. has shown that including inhomogeneous tissue moduli in finite element models offers only a modest improvement in the correlations between microdamage initiation and local stresses. Furthermore, strong correlations between stress magnitudes and damage severity argue in favor of the finite element models' accuracy in predicting tissue-level biomechanical properties. (Nagaraja et al. 2007) Additionally, the conservative nature of the statistical tests used adds confidence to the conclusion that distinct differences in the state of stress of trabeculae bearing different microdamage to patterns exist.

In conclusion, alendronate alters local mechanical and architectural properties of trabecular bone which may increase its susceptibility to damage after just one year of treatment. This study furthers our understanding of local tissue failure mechanisms, particularly in relation to the factors influencing damage morphology formation. The clinical implications of these findings are unclear since alendronate reduces fracture risk within one year of treatment. (Black et al. 2000)

CHAPTER 6

THREE YEARS OF ALENDRONATE TREATMENT DOES NOT CONTINUE TO DECREASE MICROSTRUCTURAL STRESSES AND STRAINS ASSOCIATED WITH TRABECULAR MICRODAMAGE INITIATION

6.1 Introduction

Bisphosphonates such as alendronate increase bone mass by reducing bone turnover, and clinical studies have demonstrated their efficacy at reducing osteoporotic fracture risk in areas with high levels of trabecular bone like the wrist, vertebral body, and proximal hip. (Black et al. 1996; Black et al. 2000; Rodan et al. 2002) However, gains in bone strength and stiffness at the apparent level come at the expense of negative changes in the mineral and organic phases leading to a deterioration of the tissue-level material properties. For instance, alendronate is associated with the gains in mineralization which contribute to improved bone strength and stiffness, but also leads to increases in non-enzymatic collagen crosslinking which can compromise bone toughness. (Allen 2007) These changes may also cause an increased formation of microdamage, and reductions in bone turnover can allow such damage to accumulate. (Allen et al. 2006) Indeed, increased microdamage density has been documented after one year of treatment in animal studies. (Mashiba et al. 2000; Allen et al. 2006) Microdamage accumulation itself can impact tissue-level material properties and may be a sign of decreased tissue quality. (Schaffler et al. 1989; Ruppel et al. 2006)

Microdamage accumulation is not linear with increasing years of alendronate treatment. Studies conducted in bisphosphonate-treated beagle dogs have shown that

microdamage density is increased relative to controls after one year of treatment, but has not continued to increase after three years of treatment. (Allen et al. 2007) There are many possible explanations for these findings: either continued gains in bone volume fraction and mineralization between 1 and 3 years' treatment may improve the bone's ability to resist damage formation, or a new equilibrium level for bone turnover may be sufficient to prevent further damage accumulation. (Allen et al. 2007) Also, increased mineral homogeneity and reduced formation of new basic multicellular units (BMU) with prolonged treatment reduce stress concentrations which can serve as nucleation sites for damage formation. (Roschger et al. 2001; Boivin et al. 2002; Seeman 2007)

In a recent study, increased microcrack density with alendronate treatment correlated with decreased tissue-level stresses associated with initiation of damage. (O'Neal et al. 2010) It is unclear, however, whether such changes are sustained throughout the course of treatment. In the present study, stresses and strains associated with microdamage formation were obtained using image-based finite element modeling of the distal femur from beagle dogs treated with three years of alendronate. By investigating the response of alendronate-treated trabecular bone to damaging loads, microstructural changes that occur with prolonged treatment can be studied to determine factors which may contribute to the formation of microdamage. The goal of this study was to determine whether tissue level stresses and strains associated with damage initiation changed throughout the course of alendronate treatment. We hypothesize, based on observations of stabilized microdamage density between one and three years treatment, that damage initiation stresses and strains at three years' treatment will not be different from those at one year of treatment.

6.2 Methods

6.2.1 Animals

Detailed methods about the care and treatment regimen of animals whose tissues were used in this study have been published previously. (Allen et al. 2006) Briefly, 1 year old skeletally mature beagle dogs were randomized into three groups and given either a saline solution control (n=4, 1 mL/kg/day) or alendronate every day at either a post-menopausal osteoporosis treatment dose (n=4, 0.2 mg/kg/day), Paget's disease treatment dose (n=4, 1.0 mg/kg/day) for three years. All procedures were approved by the Indiana University School of Medicine Animal Care and Use Committee.

6.2.2 Trabecular Bone Core Extraction and Micro-CT Imaging

The right distal femur from beagle dogs was secured using a vice such that the extraction angle was oriented parallel to the principal material axis. Using a drill press with attached diamond-tipped core drill, 5 mm diameter bone cores were extracted under constant irrigation with saline. (#102055, Starlite Industries, USA) Cores were sized to a length of 18 mm with a diamond precision saw, and bone marrow was removed using a water pik. (WP-72W, WaterPik, USA) Stainless steel endcaps (5 mm depth) were glued with cyanoacrylate to each bone core end to prevent crushing and limit the effect of end artifacts on mechanical testing. Cores were imaged with micro-computed tomography (μ-CT; μCT 40, Scanco Medical, Basserdorf, Switzerland) at a voxel resolution of 16 μm. Images were thresholded and evaluated to obtain parameters of bone volume fraction; trabecular thickness, number, and spacing; connectivity; structural model index; and degree of anisotropy. Mineralization values were obtained from the attenuation of grayscale μ-CT images based on hydroxyapatite (HA) calibration standards.

6.2.3 Fluorescent Staining and Mechanical Testing

Trabecular bone cores were stained at atmospheric pressure and 4°C for 8 hours in 0.02% Alizarin ComplexOne + 10 μmol/L protease inhibitor (E-64, Sigma Chemical) then washed with distilled water for 1 hour to fluorescently label pre-existing damage, encompassing *in vivo* damage and damage occurring from the core extraction. (O'Brien et al. 2002)

Cores were preconditioned for 3 cycles to 0.1% strain then loaded at a rate of 0.5% strain/second in displacement-controlled uniaxial compression to the yield strain, determined to be 1.2% in preliminary testing, and held for 3 hours. The apparent strain was calculated using a gauge length of the exposed length of the bone measured with digital calipers plus half the length of each bone end embedded in endcaps. (Keaveny et al. 1997) During the test, cores were immersed in 0.9% physiological saline + 10 μmol/L protease inhibitor.

After testing, the top endcap was removed and cores were stained with 0.01% calcein at atmospheric pressure and 4°C for 8 hours then washed with distilled water for 1 hour to label test-induced damage. (O'Brien et al. 2002) Samples were held in 70% ethanol for 24 hours then underwent a graded alcohol infiltration protocol to completely dehydrate the samples. Cores were embedded in methylmethacrylate, cut using a diamond precision saw to a thickness of 120 μm, and mounted onto slides in an orientation allowing for visual registration with the 3D micro-CT reconstructed image.

6.2.4 Histological Evaluation

Microdamage was evaluated with fluorescent microscopy at 100x magnification based on the criteria that cracks are intermediate in size (20 – 150 μm; larger than

canaliculi but smaller than vascular channels), have sharp borders, and have a focus plane demonstrating depth of field. (Allen et al. 2006; Stepan et al. 2007) A classification system published by Moore and Gibson was modified to group damage into three broad morphological categories: severe, linear, and diffuse damage. (Arthur Moore et al. 2002; O'Neal et al. 2010) Severe damage was classified as microdamage consisting of either one primary crack with minor secondary cracks or cracks propagating through the thickness of the trabecula. Linear damage included both single and parallel cracks, and diffuse damage consisted of both cross-hatch damage equal in length and intensity (to distinguish it from severe damage) and damage with a large area of distribution. Areas of diffuse staining with no clearly defined cracks were not counted as microdamage. Investigators were blinded to the sample treatment group when conducting microdamage histological evaluations.

6.2.5 Finite Element Analysis and Histological Registration

The 3D reconstructed micro-CT image of each trabecular bone core was used to create high resolution finite element models of von Mises and principal compressive stress and strain distributions. Direct voxel conversion methods were used for mesh generation, and linear elastic, homogeneous, and isotropic material behavior was assumed. (van Rietbergen B 1996) Boundary conditions were set to simulate uniaxial compressive loading to the yield strain. The tissue modulus for FEA was initially assigned to 10 GPa with a Poisson's ratio of 0.3.

Test-induced microdamaged and undamaged trabeculae identified and categorized histologically were visually registered to its 3D micro-CT reconstructed image, allowing for digital extraction of the trabeculae of interest from the lattice. A trabecular value for

the mechanical parameter associated with damage type was obtained by averaging the value of each element corresponding to the voxel within the extracted trabeculae. Only green fluorescing (test-induced) damage and undamaged trabeculae underwent this analysis (n=416 for control, n=391 for low dose, n=346 for high dose). Stress values were scaled according to the experimental Young's modulus calculated from the stress-strain curve during the mechanical test using a back-calculation method. (van Rietbergen B 1995)

6.2.6 Statistics

All statistical tests were performed using MINITAB software (Minitab, Minitab Inc., USA). Parametric analyses were used for all comparisons after data met the requirement for normality. Differences in global architectural parameters between 3 year treatment groups (Table 5.1) were determined with one-way ANOVA and Tukey post-hoc tests. Two-way ANOVA with Tukey post-hoc analysis was used to determine differences in global architectural parameters due to treatment group and treatment duration. Differences in crack density were determined with two-way ANOVA followed by Tukey post-hoc analysis for treatment group and damage type comparisons. $p<0.05$ was considered statistically significant.

To determine differences in mechanical and architectural parameters of damaged and undamaged trabeculae by treatment group and microdamage category, two-way ANOVA with Tukey post-hoc analysis was conducted. Three-way ANOVA with Tukey post-hoc comparisons were conducted to assess statistical significance of the mechanical or architectural parameters with respect to damage state, treatment effect, and treatment duration. A Bonferroni correction was applied for the 4 multiple comparisons made for

trabecular mechanical properties (von Mises and principal compressive stress and strain). The correction was also applied for the 4 multiple comparisons made in the trabecular architectural parameter analysis (trabecular thickness, structural model index, orientation, and mineralization). This reduced the p value for a significant difference to $p \leq 0.013$. All data are presented as mean ± standard error.

6.3 Results

Comparisons of global architectural properties across treatment groups show few differences between groups (Table 6.1). Among the samples treated for 3 years with alendronate, the bone volume fraction was not different among the control and treatment groups. Trabecular number, thickness, and spacing were also similar between groups. No differences were found in connectivity density, structural model index, or degree of anisotropy. A specimen-specific tissue modulus was back-calculated from values of the experimental and FEM apparent moduli; tissue moduli for the control group were similar to the low dose group and high dose group. Average mineralization values were also similar between 3 years treated and control groups. Between 1 and 3 years' treatment, mineralization increased in control (1 year: 1011.9 ± 6.2 mg HA/ccm, 3 year: 1081.5 ± 15.0 mg HA/ccm, $p<0.005$) and low dose treatment groups (1 year: 1040.3 ± 6.1 mg HA/ccm, 3 year: 1091.1 ± 12.6 mg HA/ccm, $p<0.03$).

Table 6.1 Global Architectural Characteristics by Treatment Group

Parameter	Control	0.2 mg/kg/day	1.0 mg/kg/day
Bone Volume Fraction (BV/TV)	0.22 ± 0.07	0.19 ± 0.03	0.20 ± 0.04
Connectivity Density (mm^{-3})	20.8 ± 1.0	23.8 ± 2.6	22.5 ± 2.3
Structural Model Index (SMI)	1.1 ± 0.7	1.2 ± 0.2	0.95 ± 0.58
Trabecular Number (mm^{-1})	2.2 ± 0.1	2.2 ± 0.1	2.2 ± 0.1
Trabecular Thickness (μm)	115.8 ± 17.5	104.8 ± 17.8	98.6 ± 8.6
Degree of Anisotropy (DA)	1.49 ± 0.20	1.47 ± 0.04	1.51 ± 0.12
Mineralization (mg HA/ccm)	1081.5 ± 15.0	1091.1 ± 12.6	1077.3 ± 30.0
Tissue Modulus (GPa)	11.5 ± 2.7	13.6 ± 2.8	12.2 ± 2.8

Severely damaged trabeculae were under greater von Mises stress than all other damage types within each treatment and control group (Figure 6.1, $p<0.001$). In the low dose treatment group, diffusely damaged trabeculae were also under greater stress than linear and undamaged ($p<0.001$). In the control group, diffusely damaged trabeculae were under greater stresses than undamaged trabeculae ($p<0.001$).

Stress differences between treatment groups were also observed: in the low dose treatment group, the average von Mises stress associated with diffuse damage was significantly increased compared with control (Figure 6.1, $p=0.002$), and increased stresses in severely damaged trabeculae approached significance relative to controls as well. ($p=0.02$). This reverses trends found in severely damaged trabeculae treated for 1 year with alendronate, where von Mises stress values were significantly decreased compared with controls. (O'Neal et.al. 2010) In this study, stress levels in the low dose group were also significantly greater than the high dose group in severely damaged trabeculae ($p=0.006$). Similar results were seen in the analysis of principal compressive stress data except in the between group differences of the severely damaged trabeculae,

where stress comparisons approached, but did not achieve, significance (p=0.02 between low and high dose treatment; p=0.04 between low dose treatment and control).

In comparing von Mises stress values between 1 and 3 year treatment groups, an increase in the stress value associated with severe damage in the low dose treatment group was the only significant change observed (p<0.001). No differences in the principal compressive stresses associated with damage between 1 and 3 year treatment groups were seen.

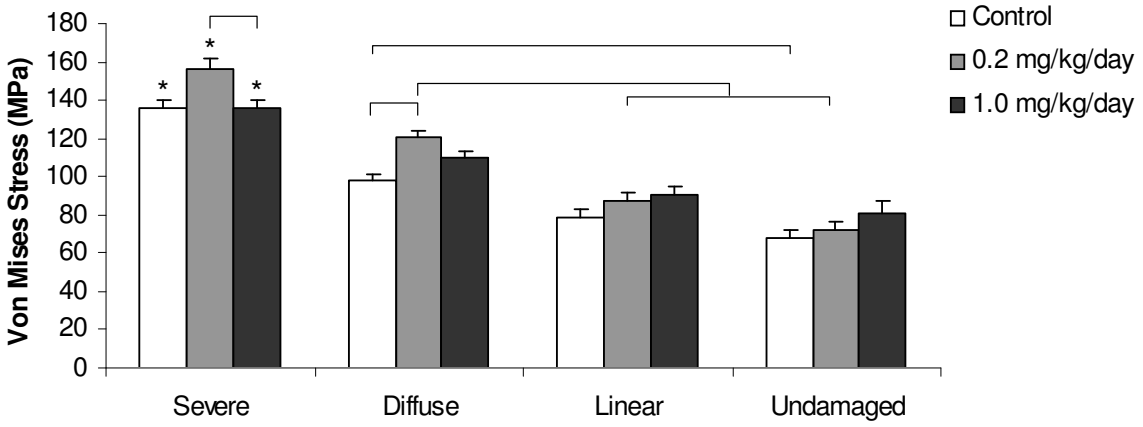

Figure 6.1 Von Mises stress values by damage type and treatment group. Significantly increased stresses in severely damaged trabeculae relative to all other damage types were observed in each treatment group (*). Stresses were also increased in severely damaged trabeculae in the low dose treatment group compared with those in the high dose treatment group. Again in the low dose treatment group, stresses were increased in diffusely damaged trabeculae relative to controls. Bars represent significant differences, p<0.012; mean + SEM plotted

Strain states (both von Mises and principal compressive) were analyzed, and by both measures, severely damaged trabeculae were under significantly greater strain than all other damage types in the control and low dose treatment group at 3 years (Figure 6.2, p<0.001). Severely damaged trabeculae were under greater strain than linear and

undamaged trabeculae in the high dose group ($p<0.001$). Also, diffusely damaged trabeculae were under greater principal compressive strain than undamaged trabeculae in all treatment groups ($p<0.01$). Finally in alendronate treated groups, diffusely damaged trabeculae were at higher strains than linearly damaged trabeculae ($p<0.001$). No differences were found in the von Mises strain states of trabeculae between treatment groups. Principal strain results, however, showed significantly increased strains in severely damaged trabeculae treated with low dose alendronate compared with the high dose treated group ($p<0.01$). No differences in either strain measure were seen between 1 and 3 years' treatment.

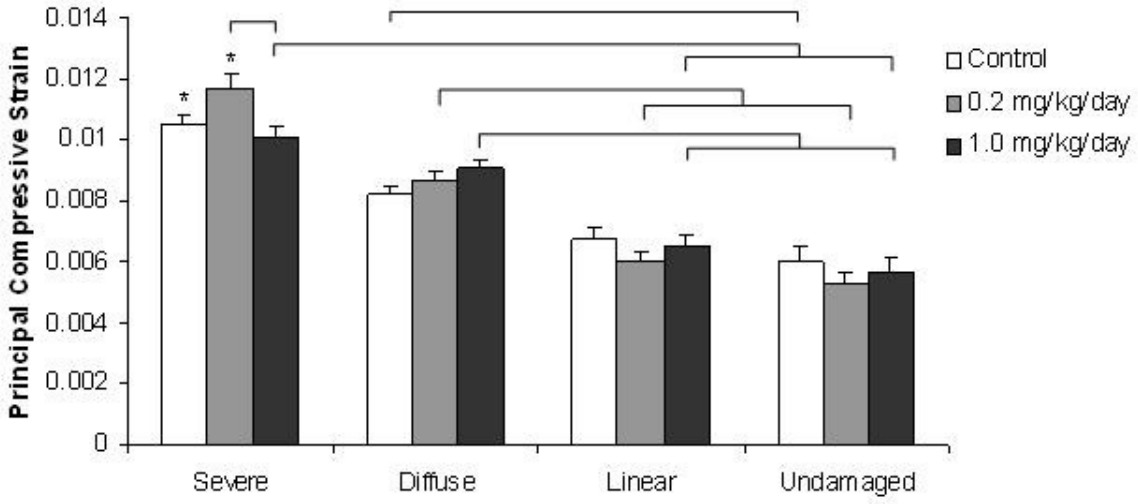

Figure 6.2 Principal compressive strain values by damage morphology and treatment group. Significantly increased trabecular strains in severely damaged trabeculae were seen compared with all other damage types in the control and low dose treatment group (*) and in linearly damaged and undamaged trabeculae in the high dose treatment group. Strains associated with severe damage were decreased in the high dose compared with low dose treatment group. Diffusely damaged trabeculae were also under greater strain compared with linear and undamaged trabeculae in both treated groups, and undamaged trabeculae in the control group. $p<0.012$; bars indicate significant differences. Mean + SEM plotted.

Architectural characteristics of trabeculae undergoing mechanical parameter comparisons were determined from detailed morphometric analysis of the trabecula extracted from the 3D micro-CT reconstructed image. Structural model index values showed that diffusely damaged trabeculae exhibited plate-like architecture compared with the more rod-like severe and undamaged trabeculae in treatment and control groups ($p<0.01$). In the treated groups, severely damaged trabeculae were more rod-like than diffusely damaged trabeculae ($p<0.01$). When trabecular thickness was analyzed, it was apparent that thinner trabeculae were more likely to sustain severe damage than remain undamaged, regardless of treatment or control group ($p<0.01$). Trabecular mineralization was greater in the severely damaged, low dose treatment group compared with controls and the high dose treatment group; in controls, severely damaged trabeculae were less mineralized than undamaged. No association with trabecular orientation was noted in any treatment or control group.

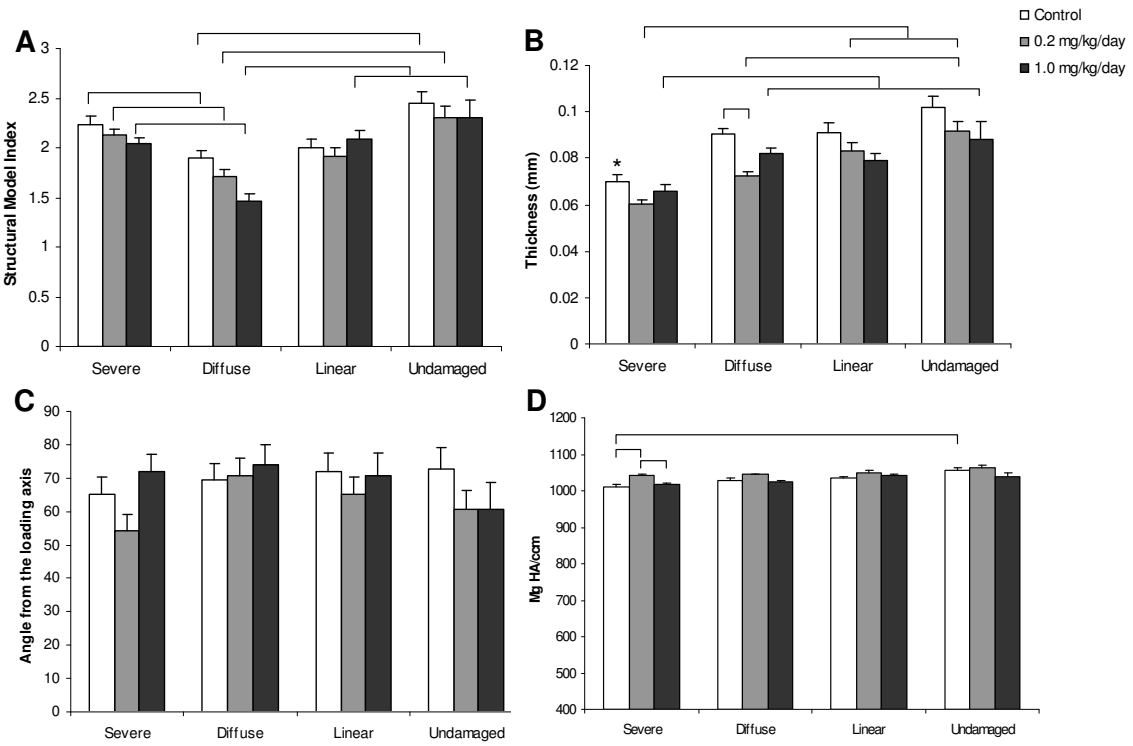

Figure 6.3 Architectural characteristics of trabeculae by damage type and treatment group. **6.3a**. Characterization of the structural model index of damaged trabeculae showed rod-like architecture of severe and undamaged trabeculae relative to diffusely damaged trabeculae in all treatment groups. **6.3b**. Severely damaged trabeculae were thinner than undamaged trabeculae in all treatment groups. **6.3c**. Evaluation of the trabecular orientation relative to the loading axis did not show differences in the formation of damage of different morphologies. **6.3d**. Severely damaged trabeculae in the low dose treatment group were significantly more mineralized than severely damaged trabeculae in the low dose and control groups. $p<0.012$, bars represent significant differences; mean ± SEM plotted.

Histological analysis of pre-existing (alizarin-labeled) damage showed primarily linear damage, with an increased linear damage density in the high dose treatment group (1.03 ± 0.14 incidents/mm^2) compared with low dose (0.45 ± 0.05 incidents/mm^2) and control group (0.47 ± 0.08 incidents/mm^2, $p<0.01$). Test-induced (calcein-labeled) damage density was significantly increased compared with pre-existing damage density in each treatment and control group. (Figure 6.4, $p<0.05$) Damage exhibiting both the alizarin and calcein stain was totaled separately, and no differences were found between

treatment or control groups. Damage totals (the sum of pre-existing, test-induced, and dual-stained damage) were not significantly different between treatment or control groups. Also, damage totals were not significantly different between 1 and 3 years' treatment.

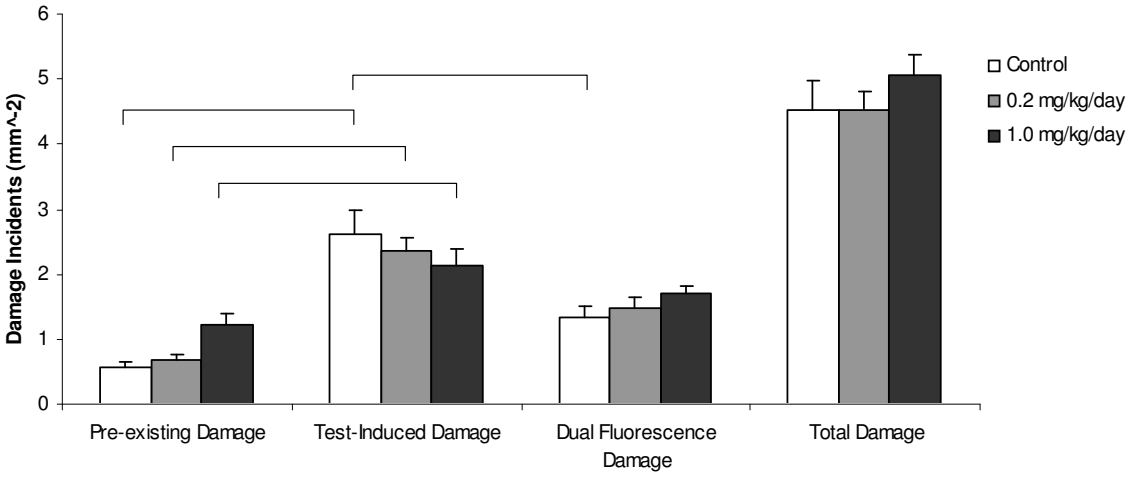

Figure 6.4 Damage quantification totals by treatment group. There was significantly increased test-induced damage compared with pre-existing damage in each treatment group. Also, there was a larger amount of test-induced damage than damage demonstrating dual fluorescence in the control group. $p<0.05$, bars indicate significant differences. Mean ± SEM is plotted.

6.4 Discussion

In this study, the effect of prolonged daily alendronate treatment on trabecular stresses and strains associated with microdamage initiation were investigated using image-based finite element modeling. It was found, compared with controls, that in the low dose alendronate treatment group the principal compressive and von Mises stresses were increased significantly in diffusely damaged trabeculae ($p<0.01$), and approached significance in severely damaged trabeculae ($p=0.02$) compared with controls. This finding reverses a trend observed in a similar study conducted after 1 year of treatment at

the same doses, where von Mises stresses of severely and linearly damaged trabeculae were significantly decreased in alendronate-treated groups compared with controls. (O'Neal et al. 2010) These results suggest that while alendronate may initially reduce the ability of trabecular bone to resist damage formation, by 3 years of treatment the tissue level properties have stabilized.

Image-based finite element modeling is a powerful tool which can be used to integrate the contributions of trabecular geometry, material property, and spatial position to capture the loading environment of a single trabecula. It is advantageous in small, complex systems because of the difficulty in obtaining individual trabecular stresses and strains from direct measurement. Stresses obtained from FEM were linearly scaled to reflect specimen-specific differences in stiffness calculated from the linear elastic region of the apparent level stress-strain curve. (van Rietbergen B 1995) This method ensures that average tissue-level stresses between groups are similar despite differences in bone volume fraction and mineralization which influence the mechanical strength and maximum applied load.

Previous studies have used the von Mises yield criterion to describe the micromechanical environment of trabecular bone. (Fyhrie et al. 2000; Yeni et al. 2008) The von Mises yield criterion is useful in this context because it accounts for the contribution of normal and shear stresses/strains to characterize the loading environment of trabeculae. Particularly for damage exhibiting severe or cross-hatched morphology, it is clear that shear forces play an important role in damage evolution. (Fyhrie et al. 2000) Principal compressive stresses/strains have also been used to characterize microstructural damage mechanics, and as previous studies correlating these measures to microdamage

incidents have failed to produce a dominant criterion, results from all of these measures are reported. (Nagaraja et al. 2005)

Overall, trabecular level stresses and strains remained relatively constant between 1 and 3 years in all treatment and control groups. An increase in the von Mises stress value associated with severe damage in the low dose treatment group was the only treatment durational difference noted. Thus, the extension of alendronate treatment to 3 years does not continue to decrease damage initiation stresses relative to controls, as seen after 1 year of treatment. Rather, the susceptibility of trabecular bone to microdamage formation appears to stabilize, and data on microdamage quantification reported in this study and others corroborate this conclusion. (Allen et al. 2007) We hesitate to conclude that bone quality is improved overall with prolonged alendronate treatment because other studies have documented decreased toughness in alendronate treated bone, but did not attribute such findings to microdamage formation. (Allen et al. 2007; Allen et al. 2008) Rather, findings from this study help elucidate the complexities of the mechanical changes leading to reduced microdamage formation at the tissue level.

In this study, we observed a significantly increased mineral density in severely damaged trabeculae from the low dose treatment group compared with severely damaged trabeculae in the high dose treatment group and controls (Figure 6.3). Furthermore, the mineral density was significantly increased in the severely damaged trabeculae at 3 years' low dose alendronate compared to values after 1 year of treatment at the same dose ($p<0.001$). (O'Neal et al. 2010) Though our finite element models were homogenous and did not account for local stiffness differences in stress calculations, values for microstructural stresses were scaled according to the stiffness at the apparent level,

resulting in an 11% increase in the back-calculated tissue modulus between 1 and 3 years in the low dose treatment group. We speculate that changes in the mineralization profile at the microstructural level may contribute to increased resistance to damage initiation. Since bone turnover is suppressed with alendronate, secondary mineralization is more complete in bone multicellular units (BMU) and may provide additional strength against damaging forces. (Boivin et al. 2002) However, additional analyses with inhomogeneous models are warranted to confirm this hypothesis.

Evaluation of the architectural characteristics within damage morphological groups revealed few differences between treatment and control groups and few changes from one to three years. Decreased trabecular thickness and rod-like geometry were associated with severe damage formation in this study, and the observation has been made by others in different populations. (Shi et al. ; Arlot et al. 2008) This suggests that the influence of trabecular geometry on damage susceptibility remains fairly consistent.

A number of limitations must be considered when placing the results of this study in the context of fracture risk with prolonged alendronate treatment. The use of intact (non-ovariectomized), relatively young beagle dogs limits the translation of this study's findings to osteoporotic human populations, and the small number of samples in each group may not capture the full variability of trabecular bone architecture in the population. Additionally, while the assumptions of linear elasticity, isotropy, and homogeneity at the microstructural level provide a good estimate of tissue level mechanical properties, they are not completely accurate in describing tissue-level trabecular behavior, particularly when used to understand evolving properties in the face of microdamage progression. For this reason, it should be understood that stress/strain

calculations refer only to predictions from the undamaged state, and do not account for changes which may occur once the damage initiation process has begun. However, this study illuminates the microstructural mechanics associated with microdamage formation and sheds some light on the effect of alendronate administration on those mechanisms.

In this study, tissue-level stresses and strains from alendronate-treated trabecular bone were computed with FEM, registered with histological observations of microdamage incidents, and compared to control groups and stress/strain levels obtained after 1 year of treatment. We conclude that changes in damage initiation stresses/strains occur early in treatment (within the first year) and do not continue to deteriorate with alendronate treatment up to 3 years. We speculate that improvements in the mineralization profile of trabeculae may account for these findings.

CHAPTER 7

CONCLUSIONS AND FUTURE RECOMMENDATIONS

7.1 Conclusions

Bone fractures in the elderly are more likely to lead to life-threatening health complications than those in younger populations, not only decreasing their quality of life, but also straining the health care industry with the burden of providing long term care and support for these patients. The elderly population is expected to represent 20% of the US population in 2030, (AOA 2006) highlighting the great need for research that can lead to the prevention of non-traumatic bone injury.

Bone fragility fractures are most prevalent in areas with a high proportion of trabecular bone like the hip, wrist, and vertebrae. A significant factor in the development of such fractures is osteopenia, or low bone mass, but it is not the only factor. (McCreadie et al. 2000) Other factors influencing trabecular bone fragility are numerous: structural changes in bone volume fraction, connectivity, trabecular number, thickness, spacing, and anisotropy; compositional changes in mineralization, collagen crosslinking, and accumulation of AGEs; and changes in mechanical adaptation, including microdamage formation and repair. (Schaffler et al. 1989; Burr et al. 1997; Hildebrand et al. 1999; Yeh et al. 2001; Paschalis et al. 2004; Busse et al. 2009) Microdamage density in particular can be an independent predictor of bone strength. (Burr et al. 1997) In the preceding chapters, factors influencing microdamage initiation and progression were explored as a function of age, sex, and the use of therapeutics designed to limit the osteoporotic loss of bone mass. The goal of this work was to demonstrate that changes in

trabecular bone quality due to these influences are reflected in the mechanics of microdamage initiation and propagation.

In chapter 3, a powerful technique combining finite element modeling with 3D reconstructed micro-CT images of trabecular bone was used to obtain estimations of stresses and strains on individual damaged trabeculae from three groups: younger women, older women, and older men. Results suggest that microdamage morphology is highly dependent on both the stress and strain magnitude, and that trabecular bone from pre-menopausal women may be able to sustain higher stresses/strains without damaging compared with trabecular bone from post-menopausal individuals. However, the response to damaging loads appears similar between men and women aged 68-81 years, though severely damaged trabeculae in men underwent less deformation than severely damaged trabeculae in women. In chapter 4, we describe a two-step mechanical loading process used to induce and propagate microdamage, and explored aging and gender differences in their resistance to microdamage progression. We found that samples from older donors reached the fatigue test endpoint with a fewer number of cycles than younger individuals, and attributed this result to an increased number of severe damage incidents which were expanding in area. However, no gender differences were found. Finally in chapters 5 and 6, microstructural stresses and strains associated with microdamage initiation were investigated in trabecular bone from dogs treated for 1 or 3 years with alendronate. After one year of alendronate administration, tissue level biomechanical properties of trabecular bone are altered, resulting in a decreased von Mises stress necessary for initiation of severe and linear microdamage. By three years of treatment, however, damage initiation stresses and strains had stabilized.

7.2 Future Recommendations: Microdamage Initiation Stress Differences by Age and Gender

In this study, the stresses and strains of individual trabeculae were obtained from finite element solutions visually registered with histological identification of microdamage of different morphologies. Results were compared between younger and older females, and between older males and older females. We found that trabecular stresses in undamaged trabeculae of older women were lower compared to younger women, suggesting that the threshold for damage initiation may decrease with increasing age. Also, normalized strains associated with severely damaged trabeculae in men were significantly reduced compared to age-matched women.

Although the stress and strain estimations were matched to trabecular damage created experimentally under known loading conditions, models used trabecular bone structures in their undamaged state for the calculations. Changes in the stress/strain values with damage formation and propagation were not captured with this technique. Damage formation has been shown to dissipate energy, thereby relieving stresses on nearby trabeculae and increasing the fracture toughness of the bone. (Vashishth et al. 1997) In order to gain a full understanding of the role of trabecular damage in the energy-absorbing function of trabecular bone, non-linear finite element modeling should be utilized. Until very recently, the use of complex models on structures with a very large number of elements has been too computationally expensive to execute. With advances in computing power, however, it is now possible to conduct non-linear finite element analyses on trabecular bone structures that meet the requirements for continuum

assumptions. (Kosmopoulos et al. 2008) Further refinement of techniques used in this study can give new insight into damage mechanics of trabeculae.

The correlation of von Mises and principal compressive stresses and strains with damage morphology produced good results consistent with our understanding of interactions between the magnitude of loading and damage formation. However, these criteria were developed for yield prediction in materials with similar tensile and compressive strengths. Studies in bone have demonstrated asymmetry in apparent behavior; specifically, greater strength in compression than tension. (Niebur et al. 2001) Furthermore, at the microstructural level, differences in the morphology and behavior of damage based on whether loading is predominantly in tension or compression have been described. (Diab et al. 2005) Therefore, use of asymmetric yield criteria may improve damage predictions and more accurately represent yielding behavior. (Niebur et al. 2000; Bayraktar et al. 2004)

Throughout this thesis, damage has been classified into categories based on morphology, severe, diffuse, and linear, which were derived from a previously published classification system. (Arthur Moore et al. 2002) However, much debate centers on the driving mechanisms behind the assumed morphology. Results in this thesis suggest that crack morphology is driven greatly by the magnitude of stresses and strains placed on the trabeculae, but others have shown a dependence of crack morphology on a tensile versus compressive loading environment. (Diab et al. 2005) The methods described in chapter 3, 5, and 6 can be used to spatially correlate damage regions with tensile or compressive loading derived from the directions of principal compressive stresses and/or strains obtained with finite element modeling. Furthermore, correlations between observed

damage regions of specific morphologies and goodness-of-fit predictions by different yield criteria can provide additional data about the mode of loading.

Statistical models used throughout this thesis were built using parametric and non-parametric methods which evaluated mean/median differences between groups to determine statistical significance. However, particularly for research involving prediction and risk assessment in human disease, Bayesian statistical methods may be of more utility. Bayesian methods incorporate pre-existing knowledge about the relationship between two variables with new evidence to provide more precise conclusions. They are especially useful in hierarchical models, as used throughout this thesis, and provide a way to pool data from different data sets in order to evaluate relationships between parameters more fully. Future studies can apply Bayesian models to new data sets to evaluate significant differences in the context of pre-existing data regarding the relationship between two parameters. This approach help elucidate global patterns of architectural and mechanical parameters' effects on damage initiation as a function of differences in age and gender.

Currently, experiments dependent upon user-driven identification and classification of microdamage are limited by the enormous amount of time required for in-depth analysis. As a result, sample sizes reported in microdamage comparison studies are relatively small. Development of an automated identification system based on damage fluorescent staining intensity was developed in this lab; however, results were complicated by non-specific staining and the inability to obtain information regarding damage morphology. (Nagaraja 2006) Future studies focused on automating microdamage analyses would greatly expand the potential for future experiments to

capture population variability. Some studies are currently underway towards achieving that goal. (Bigley et al. 2008)

Alternatively, the use of radiopaque dyes to identify microcracks in bone structures would allow for the use of micro-CT systems to image the character and distribution of damage. Such a dye would be extremely valuable to microdamage research, not only in identifying damage, but also in generating finite element models which incorporate damage sites in their analyses. Some research towards this end has already been conducted, particularly with the use of barium sulfate. (Leng et al. 2008; Landrigan et al. 2011) While barium sulfate has shown some promise as a radiopaque dye in bone, its primary mechanism of action is space-filling rather than targeted. Future studies could focus on developing dyes with greater specificity, exploiting the availability of calcium-binding sites in damage similar to the mechanism of action of the calcium-chelating fluorescent dyes used in this study. (O'Brien et al. 2002)

7.3 Future Recommendations: Resistance to Microdamage Progression by Age and Gender

In this study, differences in microdamage progression were investigated between younger females, older females, younger males, and older males. A decreased number of cycles to the strain endpoint were found in older samples, reflecting decreased tissue resistance to microdamage progression. Histological observations of microdamage at the trabecular level offered clues towards an explanation for this finding. Specifically among severely damaged trabeculae, the damage area was greater in bone from younger individuals, while the number of trabeculae whose damage area was increasing was greater in older individuals. This suggests that in trabecular bone, the damage area of a

single trabecula is not as important to the fatigue life of the entire sample as is the number of damage incidents, as the damage remains localized and can be removed. (Cook et al. 2009)

While results from this study are compelling, further investigations into the factors causing age-related differences in crack growth resistance should be undertaken. Specifically, combining histological damage quantification with non-linear finite element modeling to determine microstructural stresses and strains associated with crack progression can add much to the understanding of trabecular bone mechanics. Very few modeling studies of fatigue using trabecular bone structures have been completed, but recent work by Kosmopoulos et al verified hypotheses determined using idealized cellular solids about the role of trabecular failure in overt fracture. (Kosmopoulos et al. 2008) Expanding the use of these techniques can add to the understanding of how forces are redistributed with additional loading cycles within a trabecular bone lattice.

One limitation of this study was the inability to capture microdamage progression patterns during the fatigue portion of mechanical testing. Though the measurements of crack density and area expansion before and after the test were illuminating, it is unknown which damage areas contributed towards the initial sharp increases in strain and which areas contributed to the slowly increasing strain towards failure. Though use of additional fluorescent dyes could be used to obtain a snapshot of fatigue mechanisms during the test, (O'Brien et al. 2002) we were unable to differentiate between three or more applied stains. Recently, high speed photography was used to image damage areas under compression loading as damage was forming. (Thurner 2006; Thurner 2007) Using a similar method, future studies could capture microdamage progression in cyclic

loading to address unanswered questions regarding damage localization and compartmentalization.

In this study, we associated the decreased number of cycles found in older donors with an increased number of trabeculae whose damage area was increasing. In younger samples, however, extensive damage area of trabeculae did not appear to hasten overt trabecular failure. It has been suggested that this behavior is analogous to a crumple zone in cars, where sacrificial elements allow energy to be dissipated in order to preserve the integrity of other nearby structures. (Badiei et al. 2007; Cook et al. 2009) Finite element models of idealized cellular solids have shown that while isolated areas of failed structures may indeed have this effect, damaged structures inevitably congregate and lead to the failure of the entire structure. (Guo et al. 1994) It is unclear whether a loading situation would arise *in vivo* which would call this mechanism into play, but future studies could be undertaken to address this apparent paradox in the fatigue behavior of trabecular bone.

7.4 Future Recommendations: The Effect of Alendronate Treatment on Microdamage Initiation

In this study, the microstructural stresses and strains associated with microdamage formation were obtained using image-based finite element modeling of the distal femur from beagle dogs treated for one or three years with alendronate. It was found that with alendronate treatment at low doses, stresses were increased significantly in diffusely damaged trabeculae and approached significance in severely damaged trabeculae compared with controls. These results reverse findings after one year of low-dose alendronate treatment, where von Mises stresses of severely and linearly damaged

trabeculae were significantly decreased compared with controls. These results suggest that while alendronate may initially reduce the ability of trabecular bone to resist damage formation, by 3 years of treatment the tissue level properties have stabilized.

The results in this study are compelling; however, they were conducted in trabecular bone of the distal femur, and conclusions may not translate to different parts of the skeleton. It is known that bisphosphonates accumulate in greater concentrations in bone undergoing constant remodeling, such as the jaw and sites with trabecular bone. (Rodan et al. 2002) Thus, it seems reasonable that the effects of alendronate treatment may be unevenly distributed throughout the skeleton. Studies similar to those detailed in chapters 5 and 6 can be done to determine the effect of alendronate on microstructural properties in different skeletal sites.

Additionally, in chapters 5 and 6, microdamage initiation thresholds were studied after the application of a single static load to yield. Though the mechanics of microdamage initiation are an important indication of bone quality, resistance to microdamage progression is also an important factor in evaluating the microstructural properties of bone. Very few studies have investigated how crack propagation mechanisms in bone treated with bisphosphonates may differ from untreated bone. Evidence that changes occurring at the ultrastructural level, particularly in the degree of glycation of the tissue, can increase tissue brittleness and reduce toughness. (Allen 2007; Tang et al. 2009) Conducting studies similar to those performed in chapter 4 coupled with analysis of compositional changes in the tissue matrix could add additional insight into the effects of alendronate treatment on microstructural properties of bone.

Recently, concerns about the effects of long-term remodeling suppression on

bone's mechanical properties have been corroborated by reports of an increased microdamage density with treatment. (Allen et al. 2006) Two iliac crest bone biopsy studies conducted in human tissue found conflicting results regarding increased crack density with alendronate use. (Chapurlat et al. 2007; Stepan et al. 2007) Since microdamage accumulation is linked to decreased bone strength and stiffness, (Burr et al. 1997; Hoshaw et al. 1997) more studies need to be done in human subjects to determine definitively whether a link between bisphosphonate use and microdamage accumulation exists, and whether there are clinical implications for such findings.

Case reports describing atypical fractures of the femoral diaphysis in women taking bisphosphonates have led to questions about the long-term safety of these therapeutics. (Osugi et al. 2011) Currently, little data exists which directly link bisphosphonate use with atypical fracture; however, the rarity of such fractures makes it difficult to design studies investigating possible associations. (Neviaser et al. 2008; Black et al. 2010) Nonetheless, lingering doubts have led physicians to consider drug holidays for patients taking bisphosphonates for an extended period of time (>5 years). (Shane 2010) A recent study investigating the implications of a drug holiday after 2 years of treatment on fracture risk found an increased incidence of hip fractures in women who discontinued the drug, but more data are needed to address this issue. (Curtis et al. 2008) Future studies should be undertaken that investigate the consequences of discontinuing bisphosphonates after 5 years of treatment, and determine how long drug holidays should last before fracture risk increases.

7.5 Concluding Remarks

In this thesis, we have explored factors influencing microdamage initiation and

propagation in two conditions relevant to clinical health: aging and bisphosphonate use. We have demonstrated that, through the combined use of fluorescent microscopy, micro-CT, and finite element modeling, microstructural bone quality can be represented by alterations in bone's ability to resist the formation and propagation of microdamage. With this technique, we have demonstrated that the changes in trabecular bone that occur with aging may result in a reduced ability to resist microdamage formation and propagation. Furthermore, we showed that 1 year of alendronate use may reduce the ability of trabecular bone to resist microdamage formation resulting in an increased microcrack density, but that by 3 years of treatment, the microstructural properties have recovered. Results from this thesis may be used in future investigations into the mechanisms of microdamage formation and progression that contribute to bone fragility.

REFERENCES

Abrahamsen, B., Eiken, P., et al. (2009). "Subtrochanteric and diaphyseal femur fractures in patients treated with alendronate: a register-based national cohort study." J Bone Miner Res **24**(6): 1095-102.

Aerssens, J., Boonen, S., et al. (1998). "Interspecies differences in bone composition, density, and quality: potential implications for in vivo bone research." Endocrinology **139**(2): 663-70.

Ager, J. W., Nalla, R. K., et al. (2005). "Deep-ultraviolet Raman spectroscopy study of the effect of aging on human cortical bone." J Biomed Opt **10**(3): 034012.

Allen, M. R. and Burr, D. B. (2007). "Three years of alendronate treatment results in similar levels of vertebral microdamage as after one year of treatment." J Bone Miner Res **22**(11): 1759-65.

Allen, M. R., Burr, D.B. (2007). "Mineralization, Microdamage, and Matrix: How Bisphosphonates Influence Material Properties of Bone." BoneKEy-Osteovision **4**(2): 49-60.

Allen, M. R., Burr, D.B. (2008). "Skeletal Microdamage: Less About Biomechanics and More About Remodeling." Clinic Rev Bone Miner Metab **6**: 24-30.

Allen, M. R., Iwata, K., et al. (2006). "Alterations in canine vertebral bone turnover, microdamage accumulation, and biomechanical properties following 1-year treatment with clinical treatment doses of risedronate or alendronate." Bone **39**(4): 872-9.

Allen, M. R., Reinwald, S., et al. (2008). "Alendronate reduces bone toughness of ribs without significantly increasing microdamage accumulation in dogs following 3 years of daily treatment." Calcif Tissue Int **82**(5): 354-60.

AOA (2006). "Department of Health and Human Services." Date Accessed August 1, 2006. **http://www.aoa.gov/prof/Statistics/statistics.asp**.

Arlot, M. E., Burt-Pichat, B., et al. (2008). "Microarchitecture Influences Microdamage Accumulation in Human Vertebral Trabecular Bone." Journal of Bone and Mineral Research **23**(10): 1613-1618.

Arthur Moore, T. L. and Gibson, L. J. (2002). "Microdamage accumulation in bovine trabecular bone in uniaxial compression." J Biomech Eng **124**(1): 63-71.

Badiei, A., Bottema, M. J., et al. (2007). "Influence of orthogonal overload on human vertebral trabecular bone mechanical properties." J Bone Miner Res **22**(11): 1690-9.

Bala, Y., Farlay, D., et al. (2010). "Time sequence of secondary mineralization and microhardness in cortical and cancellous bone from ewes." Bone **46**(4): 1204-12.

Bamias, A., Kastritis, E., et al. (2005). "Osteonecrosis of the jaw in cancer after treatment with bisphosphonates: incidence and risk factors." J Clin Oncol **23**(34): 8580-7.

Bayraktar, H. H., Gupta, A., et al. (2004). "The modified super-ellipsoid yield criterion for human trabecular bone." J Biomech Eng **126**(6): 677-84.

Bergot, C., Laval-Jeantet, A. M., et al. (1988). "Measurement of anisotropic vertebral trabecular bone loss during aging by quantitative image analysis." Calcif Tissue Int **43**(3): 143-9.

Bevill, G. and Keaveny, T. M. (2009). "Trabecular bone strength predictions using finite element analysis of micro-scale images at limited spatial resolution." Bone **44**(4): 579-584.

Bigley, R. F., Singh, M., et al. (2008). "Validity of serial milling-based imaging system for microdamage quantification." Bone **42**(1): 212-215.

Black, D. M., Cummings, S. R., et al. (1996). "Randomised trial of effect of alendronate on risk of fracture in women with existing vertebral fractures. Fracture Intervention Trial Research Group." Lancet **348**(9041): 1535-41.

Black, D. M., Kelly, M. P., et al. (2010). "Bisphosphonates and fractures of the subtrochanteric or diaphyseal femur." N Engl J Med **362**(19): 1761-71.

Black, D. M., Thompson, D. E., et al. (2000). "Fracture risk reduction with alendronate in women with osteoporosis: the Fracture Intervention Trial. FIT Research Group." J Clin Endocrinol Metab **85**(11): 4118-24.

Bocanegra-Perez, S., Vicente-Barrero, M., et al. (2009). "[Osteonecrosis of the jaw secondary to oral alendronate: Report of three cases]." Rev Med Chil **137**(2): 275-9.

Boivin, G. and Meunier, P. J. (2002). "Effects of bisphosphonates on matrix mineralization." J Musculoskelet Neuronal Interact **2**(6): 538-43.

Borah, B., Gary, J. G., et al. (2001). "Three-dimensional microimaging (MRmuI and muCT), finite element modeling, and rapid prototyping provide unique insights into bone architecture in osteoporosis." The Anatomical Record **265**(2): 101-110.

Boskey, A. and Mendelsohn, R. (2005). "Infrared analysis of bone in health and disease." J Biomed Opt **10**(3): 031102.

Boskey, A. L. (2003). "Bone mineral crystal size." Osteoporos Int **14**: 16-21.

Bouxsein, M. L. (2003). "Mechanisms of osteoporosis therapy: a bone strength perspective." Clin Cornerstone **Suppl 2**: S13-21.

Brown, T. D. and DiGioia, A. M., 3rd (1984). "A contact-coupled finite element analysis of the natural adult hip." J Biomech **17**(6): 437-48.

Burr, D. B. (2002). "Targeted and nontargeted remodeling." Bone **30**(1): 2-4.

Burr, D. B. and Allen, M. R. (2008). "Low bone turnover and microdamage? How and where to assess it?" J Bone Miner Res **23**(7): 1150-1; author reply 1152-3.

Burr, D. B., Forwood, M. R., et al. (1997). "Bone microdamage and skeletal fragility in osteoporotic and stress fractures." J Bone Miner Res **12**(1): 6-15.

Burr, D. B., Martin, R. B., et al. (1985). "Bone remodeling in response to in vivo fatigue microdamage." J Biomech **18**(3): 189-200.

Burr, D. B., Miller, L., et al. (2003). "Tissue mineralization is increased following 1-year treatment with high doses of bisphosphonates in dogs." Bone **33**(6): 960-9.

Burr, D. B. and Stafford, T. (1990). "Validity of the bulk staining technique to seperate artifactual from in vivo bone microdamage." Clin. Orthop. Relat. Res. **260**: 305-208.

Burr, D. B., Turner, C. H., et al. (1998). "Does microdamage accumulation affect the mechanical properties of bone?" J Biomech **31**(4): 337-45.

Busse, B., Hahn, M., et al. (2009). "Increased calcium content and inhomogeneity of mineralization render bone toughness in osteoporosis: mineralization, morphology and biomechanics of human single trabeculae." Bone **45**(6): 1034-43.

Caler, W. E. and Carter, D. R. (1989). "Bone creep-fatigue damage accumulation." J Biomech **22**(6-7): 625-35.

Cardoso, L., Herman, B. C., et al. (2009). "Osteocyte apoptosis controls activation of intracortical resorption in response to bone fatigue." J Bone Miner Res **24**(4): 597-605.

Carter, D. R. and Caler, W. E. (1983). "Cycle-dependent and time-dependent bone fracture with repeated loading." J Biomech Eng **105**(2): 166-70.

Carter, D. R. and Hayes, W. C. (1976). "Fatigue life of compact bone--I. Effects of stress amplitude, temperature and density." J Biomech **9**(1): 27-34.

Carter, D. R. and Hayes, W. C. (1977). "Compact bone fatigue damage: a microscopic examination." Clin Orthop Relat Res(127): 265-74.

Caverzasio, J. (2008). "Strontium ranelate promotes osteoblastic cell replication through at least two different mechanisms." Bone **42**(6): 1131-6.

Chapurlat, R. D., Arlot, M., et al. (2007). "Microcrack frequency and bone remodeling in postmenopausal osteoporotic women on long-term bisphosphonates: a bone biopsy study." J Bone Miner Res **22**(10): 1502-9.

Cheung, A. M. and Detsky, A. S. (2008). "Osteoporosis and fractures: missing the bridge?" JAMA **299**(12): 1468-70.

Choi, K. and Goldstein, S. A. (1992). "A comparison of the fatigue behavior of human trabecular and cortical bone tissue." J Biomech **25**(12): 1371-81.

Compston, J. (2002). "Mechanisms of bone loss and gain in untreated and treated osteoporosis." Endocrine **17**(1): 21-7.

Cook, R. B. and Zioupos, P. (2009). "The fracture toughness of cancellous bone." J Biomech **42**(13): 2054-60.

Cummings, S. R., Eckert, S., et al. (1999). "The effect of raloxifene on risk of breast cancer in postmenopausal women: results from the MORE randomized trial. Multiple Outcomes of Raloxifene Evaluation." JAMA **281**(23): 2189-97.

Cummings, S. R. B., D.M., Rubin, S.M. (1989). "Lifetime risks of hip, Colles', or vertebral fracture and coronary heart disease among white postmenopausal women." Arch Intern Med **149**: 2445.

Cummings, S. R. K., D.B.; Harris, F.; Genant, H.K.; Ensrud, K.; LaCaroix, A.Z.; Black, D.M. (2002). "Improvement in spine bone density and reduction in risk of vertebral fractures during treatment with anti-resorptive drugs." Am J Med **112**: 281-289.

Cummings, S. R. M., L.J. (2002). "Epidemiology and outcomes of osteoporotic fractures." Lancet **359**: 1761.

Currey, J. D. (1984). "Effects of differences in mineralization on the mechanical properties of bone." Philos Trans R Soc Lond B Biol Sci **304**(1121): 509-18.

Currey, J. D., Brear, K., et al. (1996). "The effects of ageing and changes in mineral content in degrading the toughness of human femora." J Biomech **29**(2): 257-60.

Curtis, J. R., Westfall, A. O., et al. (2008). "Risk of hip fracture after bisphosphonate discontinuation: implications for a drug holiday." Osteoporos Int **19**(11): 1613-20.

Dalstra, M., Huiskes, R., et al. (1995). "Development and validation of a three-dimensional finite element model of the pelvic bone." J Biomech Eng **117**(3): 272-8.

Delmas, P. D., Bjarnason, N. H., et al. (1997). "Effects of raloxifene on bone mineral density, serum cholesterol concentrations, and uterine endometrium in postmenopausal women." N Engl J Med **337**(23): 1641-7.

Diab, T., Condon, K. W., et al. (2006). "Age-related change in the damage morphology of human cortical bone and its role in bone fragility." Bone **38**(3): 427-31.

Diab, T. and Vashishth, D. (2005). "Effects of damage morphology on cortical bone fragility." Bone **37**(1): 96-102.

Dobnig, H., Stepan, J. J., et al. (2009). "Teriparatide Reduces Bone Microdamage Accumulation in Postmenopausal Women Previously Treated with Alendronate." J Bone Miner Res.

Dobnig, H. and Turner, R. T. (1995). "Evidence that intermittent treatment with parathyroid hormone increases bone formation in adult rats by activation of bone lining cells." Endocrinology **136**(8): 3632-8.

Donahue, S. W. and Galley, S. A. (2006). "Microdamage in bone: implications for fracture, repair, remodeling, and adaptation." Crit Rev Biomed Eng **34**(3): 215-71.

Ettinger, B., Black, D. M., et al. (1999). "Reduction of vertebral fracture risk in postmenopausal women with osteoporosis treated with raloxifene: results from a 3-year randomized clinical trial. Multiple Outcomes of Raloxifene Evaluation (MORE) Investigators." JAMA **282**(7): 637-45.

Fazzalari, N. L., Forwood, M. R., et al. (1998). "Assessment of cancellous bone quality in severe osteoarthrosis: bone mineral density, mechanics, and microdamage." Bone **22**(4): 381-8.

Fazzalari, N. L., Kuliwaba, J. S., et al. (2002). "Cancellous bone microdamage in the proximal femur: influence of age and osteoarthritis on damage morphology and regional distribution." Bone **31**(6): 697-702.

Fisher, J. E., Rogers, M. J., et al. (1999). "Alendronate mechanism of action: geranylgeraniol, an intermediate in the mevalonate pathway, prevents inhibition of osteoclast formation, bone resorption, and kinase activation in vitro." Proc Natl Acad Sci U S A **96**(1): 133-8.

Fleisch, H. (1998). "Bisphosphonates: mechanisms of action." Endocr Rev **19**(1): 80-100.

Flora, L., Hassing, G. S., et al. (1981). "The long-term skeletal effects of EHDP in dogs." Metab Bone Dis Relat Res **3**(4-5): 289-300.

Forwood, M. R., Burr, D. B., et al. (1995). "Risedronate treatment does not increase microdamage in the canine femoral neck." Bone **16**(6): 643-50.

Frost, H. (1960). "Presence of microscopic cracks in vivo in bone." Bull Henry Ford Hosp **8**: 25-35.

Fuchs, R. K., Allen, M. R., et al. (2008). "Strontium ranelate does not stimulate bone formation in ovariectomized rats." Osteoporos Int **19**(9): 1331-41.

Fuchs, R. K., Allen, M. R., et al. (2008). "In situ examination of the time-course for secondary mineralization of Haversian bone using synchrotron Fourier transform infrared microspectroscopy." Matrix Biol **27**(1): 34-41.

Fyhrie, D. P., Hoshaw, S. J., et al. (2000). "Shear stress distribution in the trabeculae of human vertebral bone." Ann Biomed Eng **28**(10): 1194-9.

Goh, S. K., Yang, K. Y., et al. (2007). "Subtrochanteric insufficiency fractures in patients on alendronate therapy: a caution." J Bone Joint Surg Br **89**(3): 349-53.

Goulet, R. W., Goldstein, S. A., et al. (1994). "The relationship between the structural and orthogonal compressive properties of trabecular bone." J Biomech **27**(4): 375-89.

Grbic, J. T., Black, D. M., et al. (2010). "The incidence of osteonecrosis of the jaw in patients receiving 5 milligrams of zoledronic acid: data from the health outcomes and reduced incidence with zoledronic acid once yearly clinical trials program." J Am Dent Assoc **141**(11): 1365-70.

Grey, A. and Reid, I. R. (2006). "Differences between the bisphosphonates for the prevention and treatment of osteoporosis." Ther Clin Risk Manag **2**(1): 77-86.

Guldberg, R. E., Hollister, S. J., et al. (1998). "The accuracy of digital image-based finite element models." J Biomech Eng **120**(2): 289-95.

Guo, X. E., McMahon, T. A., et al. (1994). "Finite element modeling of damage accumulation in trabecular bone under cyclic loading." J Biomech **27**(2): 145-55.

Harrigan, T. P., Jasty, M., et al. (1988). "Limitations of the continuum assumption in cancellous bone." J Biomech **21**(4): 269-75.

Hayes, W. C. and Carter, D. R. (1976). "Postyield behavior of subchondral trabecular bone." J Biomed Mater Res **10**(4): 537-44.

Hazenberg, J. G., Taylor, D., et al. (2006). "Mechanisms of short crack growth at constant stress in bone." Biomaterials **27**(9): 2114-22.

Heaney, R. (2003). "Is the paradigm shifting?" Bone **33**: 457-465.

Hildebrand, T., Laib, A., et al. (1999). "Direct three-dimensional morphometric analysis of human cancellous bone: microstructural data from spine, femur, iliac crest, and calcaneus." J Bone Miner Res **14**(7): 1167-74.

Hill, P. A. (1998). "Bone remodelling." Br J Orthod **25**(2): 101-7.

Hodgskinson, R. and Currey, J. D. (1990). "The effect of variation in structure on the Young's modulus of cancellous bone: a comparison of human and non-human material." Proc Inst Mech Eng H **204**(2): 115-21.

Hoshaw, S. J., Cody, D. D., et al. (1997). "Decrease in canine proximal femoral ultimate strength and stiffness due to fatigue damage." J Biomech **30**(4): 323-9.

Hou, F. J., Lang, S. M., et al. (1998). "Human vertebral body apparent and hard tissue stiffness." J Biomech **31**(11): 1009-15.

Hu, J. H., Ding, M., et al. (2002). "Effects of short-term alendronate treatment on the three-dimensional microstructural, physical, and mechanical properties of dog trabecular bone." Bone **31**(5): 591-7.

Hui, S. L., Slemenda, C. W., et al. (1988). "Age and bone mass as predictors of fracture in a prospective study." J Clin Invest **81**(6): 1804-9.

Huja, S. S., Hasan, M. S., et al. (1999). "Development of a fluorescent light technique for evaluating microdamage in bone subjected to fatigue loading." J Biomech **32**(11): 1243-9.

Iwamoto, J., Sato, Y., et al. (2008). "Hip fracture protection by alendronate treatment in postmenopausal women with osteoporosis: a review of the literature." Clin Interv Aging **3**(3): 483-9.

Kameda, T., Mano, H., et al. (1997). "Estrogen inhibits bone resorption by directly inducing apoptosis of the bone-resorbing osteoclasts." J Exp Med **186**(4): 489-95.

Keaveny, T. M., Guo, X. E., et al. (1994). "Trabecular bone exhibits fully linear elastic behavior and yields at low strains." J Biomech **27**(9): 1127-36.

Keaveny, T. M., Pinilla, T. P., et al. (1997). "Systematic and random errors in compression testing of trabecular bone." J Orthop Res **15**(1): 101-10.

Keaveny, T. M., Wachtel, E. F., et al. (1994). "Differences between the tensile and compressive strengths of bovine tibial trabecular bone depend on modulus." J Biomech **27**(9): 1137-46.

Keaveny, T. M. and Yeh, O. C. (2002). "Architecture and trabecular bone - toward an improved understanding of the biomechanical effects of age, sex and osteoporosis." J Musculoskelet Neuronal Interact **2**(3): 205-8.

Keaveny, T. M. M., Elise F.; Neibur, Glen L.; Yeh, Oscar C. (2001). "Biomechanics of Trabecular Bone." Annu. Rev. Biomed. Eng. **3**: 307-33.

Keene, G. S., Parker, M. J., et al. (1993). "Mortality and morbidity after hip fractures." BMJ **307**(6914): 1248-50.

Kennedy, O. D., Brennan, O., et al. (2008). "The effects of increased intracortical remodeling on microcrack behaviour in compact bone." Bone **43**(5): 889-93.

Khosla, S., Melton, L. J., 3rd, et al. (1998). "Relationship of serum sex steroid levels and bone turnover markers with bone mineral density in men and women: a key role for bioavailable estrogen." J Clin Endocrinol Metab **83**(7): 2266-74.

Kimmel, D. B., Recker, R. R., et al. (1990). "A comparison of iliac bone histomorphometric data in post-menopausal osteoporotic and normal subjects." Bone Miner **11**(2): 217-35.

Kopperdahl, D. L. and Keaveny, T. M. (1998). "Yield strain behavior of trabecular bone." J Biomech **31**(7): 601-8.

Kosmopoulos, V., Schizas, C., et al. (2008). "Modeling the onset and propagation of trabecular bone microdamage during low-cycle fatigue." J Biomech **41**(3): 515-22.

Kuhn, J. L., Goldstein, S. A., et al. (1989). "Comparison of the trabecular and cortical tissue moduli from human iliac crests." J Orthop Res **7**(6): 876-84.

Kulin, R. M., Jiang, F., et al. (2008). "Aging and loading rate effects on the mechanical behavior of equine bone." Jom **60**(6): 39-44.

Landrigan, M. D., Li, J., et al. (2011). "Contrast-enhanced micro-computed tomography of fatigue microdamage accumulation in human cortical bone." Bone **48**(3): 443-50.

Lane, N. E., Sanchez, S., et al. (1998). "Parathyroid hormone treatment can reverse corticosteroid-induced osteoporosis. Results of a randomized controlled clinical trial." J Clin Invest **102**(8): 1627-33.

Lee, T. C., Arthur, T. L., et al. (2000). "Sequential labelling of microdamage in bone using chelating agents." J Orthop Res **18**(2): 322-5.

Lee, T. C., Mohsin, S., et al. (2003). "Detecting microdamage in bone." J Anat **203**(2): 161-72.

Leng, H., Wang, X., et al. (2008). "Micro-computed tomography of fatigue microdamage in cortical bone using a barium sulfate contrast agent." J Mech Behav Biomed Mater **1**(1): 68-75.

Liberman, U. A., Weiss, S. R., et al. (1995). "Effect of oral alendronate on bone mineral density and the incidence of fractures in postmenopausal osteoporosis. The

Alendronate Phase III Osteoporosis Treatment Study Group." N Engl J Med **333**(22): 1437-43.

Linde, F. (1994). "Elastic and Viscoelastic Properties of Trabecular Bone by a Compression Testing Approach." Danish Medical Bulletin **41**(2): 119-138.

Linde, F. and Hvid, I. (1987). "Stiffness behaviour of trabecular bone specimens." J Biomech **20**(1): 83-9.

Linde, F., Hvid, I., et al. (1992). "The effect of specimen geometry on the mechanical behaviour of trabecular bone specimens." J Biomech **25**(4): 359-68.

Linde, F., Pongsoipetch, B., et al. (1990). "Three-axial strain controlled testing applied to bone specimens from the proximal tibial epiphysis." J Biomech **23**(11): 1167-72.

Linde, F. and Sorensen, H. C. (1993). "The effect of different storage methods on the mechanical properties of trabecular bone." J Biomech **26**(10): 1249-52.

Lotz, J. C., Cheal, E. J., et al. (1991). "Fracture prediction for the proximal femur using finite element models: Part I--Linear analysis." J Biomech Eng **113**(4): 353-60.

Lotz, J. C., Cheal, E. J., et al. (1991). "Fracture prediction for the proximal femur using finite element models: Part II--Nonlinear analysis." J Biomech Eng **113**(4): 361-5.

Luckman, S. P., Hughes, D. E., et al. (1998). "Nitrogen-containing bisphosphonates inhibit the mevalonate pathway and prevent post-translational prenylation of GTP-binding proteins, including Ras." J Bone Miner Res **13**(4): 581-9.

Ma, Y. L., Zeng, Q. Q., et al. (2011). "Teriparatide [rhPTH (1-34)], But Not Strontium Ranelate, Demonstrated Bone Anabolic Efficacy in Mature, Osteopenic, Ovariectomized Rats." Endocrinology.

Mashiba, T., Turner, C. H., et al. (2001). "Effects of suppressed bone turnover by bisphosphonates on microdamage accumulation and biomechanical properties in clinically relevant skeletal sites in beagles." Bone **28**(5): 524-31.

McCalden, R. W., McGeough, J. A., et al. (1997). "Age-related changes in the compressive strength of cancellous bone. The relative importance of changes in density and trabecular architecture." J Bone Joint Surg Am **79**(3): 421-7.

McCreadie, B. R. and Goldstein, S. A. (2000). "Biomechanics of fracture: is bone mineral density sufficient to assess risk?" J Bone Miner Res **15**(12): 2305-8.

McNamara, L. M. and Prendergast, P. J. (2005). "Perforation of cancellous bone trabeculae by damage-stimulated remodelling at resorption pits: a computational analysis." Eur J Morphol **42**(1-2): 99-109.

Meunier, P. J., Roux, C., et al. (2004). "The effects of strontium ranelate on the risk of vertebral fracture in women with postmenopausal osteoporosis." N Engl J Med **350**(5): 459-68.

Michel, M. C., Guo, X. D., et al. (1993). "Compressive fatigue behavior of bovine trabecular bone." J Biomech **26**(4-5): 453-63.

Moore, T. L. and Gibson, L. J. (2003). "Fatigue microdamage in bovine trabecular bone." J Biomech Eng **125**(6): 769-76.

Moore, T. L. and Gibson, L. J. (2003). "Fatigue of bovine trabecular bone." J Biomech Eng **125**(6): 761-8.

Moore, T. L., O'Brien, F. J., et al. (2004). "Creep does not contribute to fatigue in bovine trabecular bone." J Biomech Eng **126**(3): 321-9.

Morgan, E. F. and Keaveny, T. M. (2001). "Dependence of yield strain of human trabecular bone on anatomic site." J Biomech **34**(5): 569-77.

Mori, S. and Burr, D. B. (1993). "Increased intracortical remodeling following fatigue damage." Bone **14**(2): 103-9.

Mori, S., Harruff, R., et al. (1997). "Trabecular bone volume and microdamage accumulation in the femoral heads of women with and without femoral neck fractures." Bone **21**(6): 521-6.

Mosekilde, L. (1989). "Sex differences in age-related loss of vertebral trabecular bone mass and structure--biomechanical consequences." Bone **10**(6): 425-32.

Mueller, T. L., van Lenthe, G. H., et al. (2009). "Regional, age and gender differences in architectural measures of bone quality and their correlation to bone mechanical competence in the human radius of an elderly population." Bone **45**(5): 882-91.

Nagaraja, S. (2006). "Microstructural Stresses and Strains Associated with Trabecular Bone Microdamage." Georgia Institute of Technology **Dissertation**.

Nagaraja, S., Couse, T. L., et al. (2005). "Trabecular bone microdamage and microstructural stresses under uniaxial compression." J Biomech **38**(4): 707-16.

Nagaraja, S., Lin, A. S., et al. (2007). "Age-related changes in trabecular bone microdamage initiation." Bone **40**(4): 973-80.

Nagaraja, S. O. N., JM; Boskey, A; Guldberg, RE (2009). "Age-Related Alterations in Mineral/Matrix Ratio in Test-induced Microdamaged Trabeculae." ORS 55th Annual Meeting.

Nalla, R. K., Kinney, J. H., et al. (2003). "Mechanistic fracture criteria for the failure of human cortical bone." Nat Mater **2**(3): 164-8.

Neviaser, A. S., Lane, J. M., et al. (2008). "Low-energy femoral shaft fractures associated with alendronate use." J Orthop Trauma **22**(5): 346-50.

Niebur, G. L., Feldstein, M. J., et al. (2000). "High-resolution finite element models with tissue strength asymmetry accurately predict failure of trabecular bone." J Biomech **33**(12): 1575-83.

Niebur, G. L., Yuen, J. C., et al. (2001). "Sensitivity of damage predictions to tissue level yield properties and apparent loading conditions." J Biomech **34**(5): 699-706.

Noble, B. (2005). "Microdamage and apoptosis." Eur J Morphol **42**(1-2): 91-8.

Norman, T. L., Vashishth, D., et al. (1995). "Fracture toughness of human bone under tension." J Biomech **28**(3): 309-20.

Norman, T. L., Yeni, Y. N., et al. (1998). "Influence of microdamage on fracture toughness of the human femur and tibia." Bone **23**(3): 303-6.

Nyman, J. S., Roy, A., et al. (2006). "Age-related effect on the concentration of collagen crosslinks in human osteonal and interstitial bone tissue." Bone **39**(6): 1210-7.

O'Brien, F. J., Taylor, D., et al. (2002). "An improved labelling technique for monitoring microcrack growth in compact bone." J Biomech **35**(4): 523-6.

O'Brien, F. J., Taylor, D., et al. (2003). "Microcrack accumulation at different intervals during fatigue testing of compact bone." J Biomech **36**(7): 973-80.

O'Neal, J. M., Diab, T., et al. (2010). "One year of alendronate treatment lowers microstructural stresses associated with trabecular microdamage initiation." Bone **47**(2): 241-7.

O'Neal, J. M. N., S.; Vidakovic, B.; Guldberg, R.E. (2010). "Von Mises Stress Threshold for Microdamage Initiation Decreases in Post-menopausal Women." Transactions of the Orthopaedic Research Society Conference **35**.

Osugi, K., Miwa, S., et al. (2011). "Diaphyseal femoral fatigue fracture associated with bisphosphonate therapy - 3 more cases." Acta Orthop **82**(1): 112-3.

Parfitt, A. M., Mathews, C. H., et al. (1983). "Relationships between surface, volume, and thickness of iliac trabecular bone in aging and in osteoporosis. Implications for the microanatomic and cellular mechanisms of bone loss." J Clin Invest **72**(4): 1396-409.

Paschalis, E. P., Betts, F., et al. (1997). "FTIR microspectroscopic analysis of normal human cortical and trabecular bone." Calcif Tissue Int **61**(6): 480-6.

Paschalis, E. P., Shane, E., et al. (2004). "Bone fragility and collagen cross-links." J Bone Miner Res **19**(12): 2000-4.

Pattin, C. A., Caler, W. E., et al. (1996). "Cyclic mechanical property degradation during fatigue loading of cortical bone." J Biomech **29**(1): 69-79.

Pistoia, W., van Rietbergen, B., et al. (2002). "Estimation of distal radius failure load with micro-finite element analysis models based on three-dimensional peripheral quantitative computed tomography images." Bone **30**(6): 842-8.

Recker, R., Lappe, J., et al. (2004). "Bone remodeling increases substantially in the years after menopause and remains increased in older osteoporosis patients." J Bone Miner Res **19**(10): 1628-33.

Recker, R., Masarachia, P., et al. (2005). "Trabecular bone microarchitecture after alendronate treatment of osteoporotic women." Curr Med Res Opin **21**(2): 185-94.

Reginster, J. Y. (2011). "Antifracture efficacy of currently available therapies for postmenopausal osteoporosis." Drugs **71**(1): 65-78.

Reginster, J. Y., Sarlet, N., et al. (2005). "Strontium ranelate: a new treatment for postmenopausal osteoporosis with a dual mode of action." Curr Osteoporos Rep **3**(1): 30-4.

Reginster, J. Y., Seeman, E., et al. (2005). "Strontium ranelate reduces the risk of nonvertebral fractures in postmenopausal women with osteoporosis: Treatment of Peripheral Osteoporosis (TROPOS) study." J Clin Endocrinol Metab **90**(5): 2816-22.

Reilly, G. C. and Currey, J. D. (2000). "The effects of damage and microcracking on the impact strength of bone." J Biomech **33**(3): 337-43.

Rho, J. Y., Ashman, R. B., et al. (1993). "Young's modulus of trabecular and cortical bone material: ultrasonic and microtensile measurements." J Biomech **26**(2): 111-9.

Riggs, B. L., Khosla, S., et al. (1998). "A unitary model for involutional osteoporosis: estrogen deficiency causes both type I and type II osteoporosis in postmenopausal women and contributes to bone loss in aging men." J Bone Miner Res **13**(5): 763-73.

Robling, A. G., Castillo, A. B., et al. (2006). "Biomechanical and molecular regulation of bone remodeling." Annu Rev Biomed Eng **8**: 455-98.

Rodan, G. A. and Martin, T. J. (2000). "Therapeutic approaches to bone diseases." Science **289**(5484): 1508-14.

Rodan, G. A. and Reszka, A. A. (2002). "Bisphosphonate mechanism of action." Curr Mol Med **2**(6): 571-7.

Roschger, P., Rinnerthaler, S., et al. (2001). "Alendronate increases degree and uniformity of mineralization in cancellous bone and decreases the porosity in cortical bone of osteoporotic women." Bone **29**(2): 185-91.

Roux, C., Reginster, J. Y., et al. (2006). "Vertebral fracture risk reduction with strontium ranelate in women with postmenopausal osteoporosis is independent of baseline risk factors." J Bone Miner Res **21**(4): 536-42.

Ruppel, M. E., Burr, D. B., et al. (2006). "Chemical makeup of microdamaged bone differs from undamaged bone." Bone **39**(2): 318-24.

Russell, R. G., Croucher, P. I., et al. (1999). "Bisphosphonates: pharmacology, mechanisms of action and clinical uses." Osteoporos Int **9 Suppl 2**: S66-80.

Ryan, S. D. and Williams, J. L. (1989). "Tensile testing of rodlike trabeculae excised from bovine femoral bone." J Biomech **22**(4): 351-5.

Schaffler, M. B., Choi, K., et al. (1995). "Aging and matrix microdamage accumulation in human compact bone." Bone **17**(6): 521-25.

Schaffler, M. B., Radin, E. L., et al. (1989). "Mechanical and morphological effects of strain rate on fatigue of compact bone." Bone **10**(3): 207-14.

Schaffler, M. B., Radin, E. L., et al. (1990). "Long-term fatigue behavior of compact bone at low strain magnitude and rate." Bone **11**(5): 321-6.

Schindeler, A., McDonald, M. M., et al. (2008). "Bone remodeling during fracture repair: The cellular picture." Semin Cell Dev Biol **19**(5): 459-66.

Seeman, E. (1999). "The antifracture efficacy of alendronate." Int J Clin Pract Suppl **101**: 40-5.

Seeman, E. (2003). "Reduced bone formation and increased bone resorption: rational targets for the treatment of osteoporosis." Osteoporos Int **14 Suppl 3**: S2-8.

Seeman, E. (2007). "Is a change in bone mineral density a sensitive and specific surrogate of anti-fracture efficacy?" Bone **41**(3): 308-17.

Seeman, E. and Delmas, P. D. (2006). "Bone quality--the material and structural basis of bone strength and fragility." N Engl J Med **354**(21): 2250-61.

Shane, E. (2010). "Evolving data about subtrochanteric fractures and bisphosphonates." N Engl J Med **362**(19): 1825-7.

Shane, E., Burr, D., et al. (2010). "Atypical subtrochanteric and diaphyseal femoral fractures: report of a task force of the American Society for Bone and Mineral Research." J Bone Miner Res **25**(11): 2267-94.

Shaw, J. A. W., Scott C.; Bruno, Anthony; Paul, Emmanuel M. (2005). "Comparison of primate and canine models for bone ingrowth experimentation, with reference to the effect of ovarian function on bone ingrowth potential." Journal of Orthopaedic Research **12**(2): 268-273.

Shi, X., Liu, X. S., et al. (2010) "Effects of trabecular type and orientation on microdamage susceptibility in trabecular bone." Bone **46**(5): 1260-6.

Sobelman, O. S., Gibeling, J. C., et al. (2004). "Do microcracks decrease or increase fatigue resistance in cortical bone?" J Biomech **37**(9): 1295-303.

Stepan, J. J., Burr, D. B., et al. (2007). "Low bone mineral density is associated with bone microdamage accumulation in postmenopausal women with osteoporosis." Bone **41**(3): 378-85.

Tang, S. Y., Allen, M. R., et al. (2009). "Changes in non-enzymatic glycation and its association with altered mechanical properties following 1-year treatment with risedronate or alendronate." Osteoporos Int **20**(6): 887-94.

Taylor, D. (1998). "Microcrack growth parameters for compact bone deduced from stiffness variations." J Biomech **31**(7): 587-92.

Teitelbaum, S. L. (2000). "Bone resorption by osteoclasts." Science **289**(5484): 1504-8.

Thomsen, J. S., Ebbesen, E. N., et al. (2000). "A new method of comprehensive static histomorphometry applied on human lumbar vertebral cancellous bone." Bone **27**(1): 129-38.

Thurner, P. E., Blake; Jungmann, R; Schriock, Zachary; Weaver, James; Fantner, Georg; Schitter, Georg; Morse, Daniel; Hansma, Paul (2007). "High-speed photography of compressed human trabecular bone correlates whitening to microscopic damage." Engineering Fracture Mechanics **74**: 1928-1941.

Thurner, P. E., Blake; Schriock, Zachary; Langan, John; Scott, Jeff; Zhao, Maria; Weaver, James; Fantner, Georg; Turner, Patricia; Kindt, Johannes; Schitter, Georg; Morse, Daniel; Hansma, Paul (2006). "High-speed photography of the development of microdamage in trabecular bone during compression." Journal of Materials Research **21**(5): 1093-1100.

Turner, C. H. (1989). "Yield behavior of bovine cancellous bone." J Biomech Eng **111**(3): 256-60.

Turner, C. H. (2002). "Biomechanics of bone: determinants of skeletal fragility and bone quality." Osteoporos Int **13**(2): 97-104.

Van Rietbergen, B., Weinans, H., et al. (1996). "Computational strategies for iterative solutions of large FEM spplications employing voxel data." Int. J. Numer Methods Eng. **39**: 2743-67.

Van Rietbergen, B., Weinans, H., et al. (1995). "A new method to determine trabecular bone elastic properties and loading using micromechanical finite-element models." J Biomech **28**(1): 69-81.

van Rietbergen B, W. H., Huiskes R (1996). "Computational Strategies for Iterative Solutions of Large FEM Applications Employing Voxel Data." International Journal for Numerical Methods in Engineering **39**: 2743-2767.

van Rietbergen B, W. H., Huiskes R, Odgaard A (1995). "A new method to determine trabecular bone elastic properties and loading using micromechanical finite-element models." J Biomech **28**(1): 69-81.

Vashishth, D., Behiri, J. C., et al. (1997). "Crack growth resistance in cortical bone: concept of microcrack toughening." J Biomech **30**(8): 763-9.

Vashishth D, J. C., Clovis N, Tanner KE, Bonfield W. (1994). "Double staining technique for histological evaluation of microcracks in cortical bone." Proc. 2nd World Cong. Biomech. **I:44**.

Vashishth, D., Koontz, J., et al. (2000). "In vivo diffuse damage in human vertebral trabecular bone." Bone **26**(2): 147-52.

Vashishth, D., Tanner, K. E., et al. (2000). "Contribution, development and morphology of microcracking in cortical bone during crack propagation." J Biomech **33**(9): 1169-74.

Vashishth, D., Verborgt, O., et al. (2000). "Decline in osteocyte lacunar density in human cortical bone is associated with accumulation of microcracks with age." Bone **26**(4): 375-80.

Verborgt, O., Gibson, G. J., et al. (2000). "Loss of osteocyte integrity in association with microdamage and bone remodeling after fatigue in vivo." J Bone Miner Res **15**(1): 60-7.

Verborgt, O., Tatton, N. A., et al. (2002). "Spatial distribution of Bax and Bcl-2 in osteocytes after bone fatigue: complementary roles in bone remodeling regulation?" J Bone Miner Res **17**(5): 907-14.

Wang, X., Guyette, J., et al. (2005). "Axial-shear interaction effects on microdamage in bovine tibial trabecular bone." Eur J Morphol **42**(1-2): 61-70.

Wang, X. and Niebur, G. L. (2006). "Microdamage propagation in trabecular bone due to changes in loading mode." J Biomech **39**(5): 781-90.

Wang, X. and Puram, S. (2004). "The toughness of cortical bone and its relationship with age." Ann Biomed Eng **32**(1): 123-35.

Wang, X., Shen, X., et al. (2002). "Age-related changes in the collagen network and toughness of bone." Bone **31**(1): 1-7.

Wenzel, T. E., Schaffler, M. B., et al. (1996). "In vivo trabecular microcracks in human vertebral bone." Bone **19**(2): 89-95.

Wynn, R. L. (2007). "Are there any alternatives to alendronate (Fosamax) for osteoporosis to avoid the risk of osteonecrosis of the jaw?" Gen Dent **55**(6): 495-8.

Yang, P. F., Bruggemann, G. P., et al. (2011). "What do we currently know from in vivo bone strain measurements in humans?" J Musculoskelet Neuronal Interact **11**(1): 8-20.

Yeh, O. C. and Keaveny, T. M. (2001). "Relative roles of microdamage and microfracture in the mechanical behavior of trabecular bone." J Orthop Res **19**(6): 1001-7.

Yeni, Y. N., Hou, F. J., et al. (2003). "Trabecular shear stresses predict in vivo linear microcrack density but not diffuse damage in human vertebral cancellous bone." Ann Biomed Eng **31**(6): 726-32.

Yeni, Y. N., Zelman, E. A., et al. (2008). "Trabecular shear stress amplification and variability in human vertebral cancellous bone: relationship with age, gender, spine level and trabecular architecture." Bone **42**(3): 591-6.

Zarrinkalam, K. H., Kuliwaba, J. S., et al. (2005). "New insights into the propagation of fatigue damage in cortical bone using confocal microscopy and chelating fluorochromes." Eur J Morphol **42**(1-2): 81-90.

Zilch, H., Rohlmann, A., et al. (1980). "Material properties of femoral cancellous bone in axial loading. Part II: Time dependent properties." Arch Orthop Trauma Surg **97**(4): 257-62.

Zioupos, P. (2001). "Accumulation of in-vivo fatigue microdamage and its relation to biomechanical properties in ageing human cortical bone." J Microsc **201**(Pt 2): 270-8.

Zioupos, P. (2001). "Ageing human bone: factors affecting its biomechanical properties and the role of collagen." J Biomater Appl **15**(3): 187-229.